technische universität
dortmund

Thesis to obtain the academic degree
Master of Science

Dynamics in the central spin model employing the Born approximation

Philipp Schering
born in Coesfeld

2016

Lehrstuhl für Theoretische Physik I
Fakultät Physik
Technische Universität Dortmund

First corrector:	Prof. Dr. Götz S. Uhrig
Second corrector:	Prof. Dr. Frithjof B. Anders
Submission date:	October 26th, 2016

Abstract

This thesis primarily consists of developing an approach, based on the Born approximation for the central spin model, to describe the dynamics of a central electron spin coupling to a nuclear spin bath due to the hyperfine interaction. Mainly the limit of a vanishing or small external magnetic field, coupling to the central spin, is discussed. Such calculations are hard to deal with, but they are relevant for spin noise measurements in semiconductor quantum dots.

As a starting point, the first quantum mechanical corrections to the classical equations of motion are derived using the Born approximation. The classical equations of motion only describe the precession of the spins. An error analysis proofs the correctness of these corrections up to second order in the hyperfine couplings. However, an improvement over the classical equations of motion is only visible on a small timescale. Afterwards, the corrections are used in different approaches of improving the full simulation of the classical equivalent for Gaussian bath ensembles. It appears that the contribution of the corrections is either too large, shows a bad scaling for larger bath sizes, or leads to an unpredictable behavior of the central spin dynamics. This renders the general approach useless in the low field limit. Lastly, an approach to calculate estimates for persisting spin correlations in the central spin model is developed. It uses the generalized Gibbs ensemble as a basis to approximately describe the equilibrium state at infinite times. This leads to improvements of recently calculated rigorous lower bounds for small bath sizes. The full persisting part is still not captured, though. It remains unclear if this changes significantly for the physically relevant large spin baths.

Kurzfassung

Das zentrale Thema dieser Arbeit ist die Entwicklung einer Methode, basierend auf der Born-Näherung für des Zentralspinmodell, zur Beschreibung der Dynamik eines zentralen Elektronenspins, der an ein Bad aus Kernspins über die Hyperfeinwechselwirkung koppelt. Hierbei wird hauptsächlich der Limes verschwindender und kleiner Feldstärken eines magnetischen Feldes, welches an den Zentralspin koppelt, diskutiert. Berechnungen hierzu sind schwierig durchzuführen, jedoch relevant für Messungen von Spinrauschen in Halbleiterquantenpunkten.

Zu Beginn wird die erste quantenmechanische Korrektur zu den klassischen Bewegungsgleichungen, welche lediglich die Präzessionsbewegung der einzelnen Spins beschreiben, mittels der Born-Näherung hergeleitet. Fehleranalysen bestätigen die Richtigkeit der Korrekturen bis zur zweiten Ordnung in den Kopplungskonstanten. Eine Verbesserung gegenüber den klassischen Bewegungsgleichungen ist jedoch nur auf kurzen Zeitskalen ersichtbar. Die Korrekturen werden in verschiedenen Ansätzen verwendet, um eine Verbesserung der vollen Simulation des klassischen Analogons für ein Ensemble gaußverteilter Spinbäder zu erzielen. Es stellt sich heraus, dass der Beitrag der hergeleiteten Korrekturen entweder zu groß ist, ein schlechtes Skalierungsverhalten für große Spinbäder zeigt oder zu einem unvorhersehbaren Verhalten der Zentralspindynamik für lange Zeiten führt. Deshalb muss der Ansatz, zumindest zur

Beschreibung des Limes kleiner Felder, als unbrauchbar deklariert werden. Zuletzt wird eine Methode zur Berechnung von Abschätzungen für persistente Spinkorrelationen entwickelt. Sie basiert auf dem verallgemeinerten Gibbs Ensemble, um den den Gleichgewichtszustand im Limes unendlicher Zeiten approximativ zu beschreiben. Für den Fall kleiner Badgrößen liefert diese Methode eine Verbesserungen gegenüber kürzlich berechneten rigorosen unteren Schranken, wobei der exakte persistente Anteil weiterhin nicht vollständig erfasst wird. Es bleibt unklar, ob sich dieses Verhalten für die physikalisch relevanten großen Spinbäder signifikant ändert.

Contents

1 Introduction

Throughout the last two decades, quantum information processing has emerged to be one of the most active research fields in physics. By exploiting the quantum mechanical features of superposition and entanglement, it is possible to develop quantum algorithms which can deal with specific problems much more efficiently than a classical computer.

The probably most famous example is the Shor algorithm [1, 2], allowing to find the prime decomposition of a given number in polynomial time. In contrast, classical algorithms require a non-polynomial runtime for this task. Nowadays within cryptography, finding such prime decompositions is the main task to decipher an encrypted message. Another famous example is the Grover algorithm [3] which enables a faster search in an unstructured database. Classical computers have to search through all entries so that the runtime scales linearly with this number. On a quantum computer, this effort scales with the square root of the number of entries, meaning very large databases can be searched on a much shorter timescale.

While many different approaches exist for the physical realization of a qubit (quantum bit), it is not clear if all of the well-known DiVincenzo criteria [4] for an implementation of a quantum computer can be fulfilled. Different approaches satisfy various but not all criteria and therefore, each possible candidate has its own advantages and disadvantages.

An electron or a hole in a quantum dot is a very promising system for the realization of a qubit [5, 6]. Realizations are not only studied theoretically [5, 7] but also experimentally [8–10]. The electron or the hole is confined in all three spatial dimensions within this low-dimensional semiconducting nanostructure. For example, the spin of an electron confined in a quantum dot defines a two level system which can be exploited as a qubit for quantum computation. Another example is given by nitrogen vacancy centers in diamond which can be described by an effective two-level system [11, 12].

In both physical systems, the qubit is confined in some environment. For a quantum dot, this environment consists of the nuclear spins of the semiconductor substrate, for example GaAs [6, 10, 13]. The nitrogen vacancy center in diamond couples to the surrounding ^{13}C nuclear spins [11, 12, 14]. This coupling of the qubit to an environment leads to decoherence, meaning the qubit loses its initially prepared state within the coherence time. In order to be able to perform a certain number of logical operations, the coherence time has to be long enough. If the mechanisms of decoherence were understood, strategies could be developed and applied to suppress it and therefore extend the eventual computation times. This is possible by, e. g., using optimized pulse sequences [15] which extend the coherence time.

The most important coupling to consider theoretically is the relativistic hyperfine interaction between a central spin (the qubit) and the nuclear spin bath. The description of such a two-level system, coupling to a spin bath, can be based on the central spin model (CSM) [6, 7,

16–18]. Many different approaches have been developed to analyze the CSM theoretically. Its classical simulation [16, 19, 20] allows dealing with an easy set of differential equations. This renders calculations for a very large number of nuclear spins, even in the thermodynamical limit [20], and for long times possible. Mean-field-based [21] and semiclassical approaches [18, 19] have been subject of research as well. The amount of relevant nuclear spins in quantum dot is given by the number of nuclear spins within the localization volume of the electronic wave function. Typically, $10^4 - 10^6$ spins have to be considered, corresponding to a very huge Hilbert space, so that exact quantum mechanical calculations for the relevant large bath sizes are out of reach. It is possible, though, to calculate rigorous lower bounds but also estimates for persisting correlations in the central spin model in the thermodynamical limit of infinite bath sizes [22, 23]. By employing heavy numerical approaches, a bath of about 20 spins can be simulated for long times based on a Chebychev polynomial expansion [24–27]. Calculations based on the time dependent density matrix renormalization group (DMRG) can be performed for up to 1000 bath spins but only for limited times [28, 29]. Analytical exact solutions are available for the unphysical uniform coupling distribution by using the algebraic Bethe ansatz [29, 30]. Moreover, by resorting to the Bethe ansatz for inhomogeneous couplings [31], calculations for up to 48 bath spins are feasible through statistical evaluation using Monte Carlo sampling [32, 33]. Other approaches are based on master equations with systematically controlled approximations [7, 34–41], exact equations of motion [42], or diagrammatic [43, 44] and cluster techniques [45, 46].

In principle, analytical results as those based on master equations are not limited in system size or time. Yet, approximations or expansions are usually justified by, e. g., a small parameter such as the ratio J_i/B of the hyperfine coupling J_i over the magnetic field strength B which is applied to the central spin externally. This ratio is small if a strong external magnetic field is applied, which is the case in many typical experimental setups [8–10]. However, for small or even vanishing magnetic fields, such calculations are no longer systematically controllable. Though, the description and understanding of this region is experimentally relevant for spin noise measurements in semiconductor quantum dots [47–50].

Therefore, the intention of the present thesis consists of trying to develop a method which allows for the description of the central spin model in the limit of a vanishing magnetic field while maintaining its advantages for finite field strengths. The present approach is based on the Born approximation [51], which is used to derive the first quantum mechanical corrections to the classical equations of motion for a central spin coupling to a nuclear spin bath. Since the simulation of the classical central spin model as discussed by Stanek et al. [19] and improved by Hüdepohl [20] leads to good but not exact results, the derived quantum mechanical corrections shall function as a small adjustment to this simulation for large bath sizes.

The thesis is set up as follows. First of all, in chapter 2, the central spin model is introduced. In chapter 3, the Born approximation is used to derive a differential equation system for the expectation value of the central spin. It includes the classical equations of motion but also the first quantum mechanical corrections in second order of the hyperfine couplings. A numerical analysis is performed in chapter 4 to proof the correctness of the derived differential equation system through various error analyses. First results are presented which are compared

to exact and DMRG calculations. The case of a vanishing and a finite external magnetic field, which couples to the central spin, is also studied. In chapter 5, an introduction to the classical simulation is given. It is used as a basis for various simulations including the derived quantum mechanical corrections. They are all performed by calculating an Gaussian ensemble average for a large number of individual simulations, but differ in the way the Gaussian distributed bath is sampled. Their accuracy is determined by comparing the results to the classical simulation and DMRG calculations. This concludes the discussion of the Born approximation for the central spin model. In chapter 6, an approach to calculate estimates for persisting spin correlations in the central spin model is developed. This approach is based on the generalized Gibbs ensemble [52] to approximately describe an equilibrium state at infinite times. Lastly, the thesis concludes in chapter 7 with a summary of the results and an outlook for potential further research.

2 The central spin model

The *central spin model* (CSM) is used to describe a qubit which is confined in a nuclear spin environment, for example in a quantum dot [6, 7, 16–18]. The electron spin $S = 1/2$, which is a two-level system, can be used for the physical realization of such a qubit.

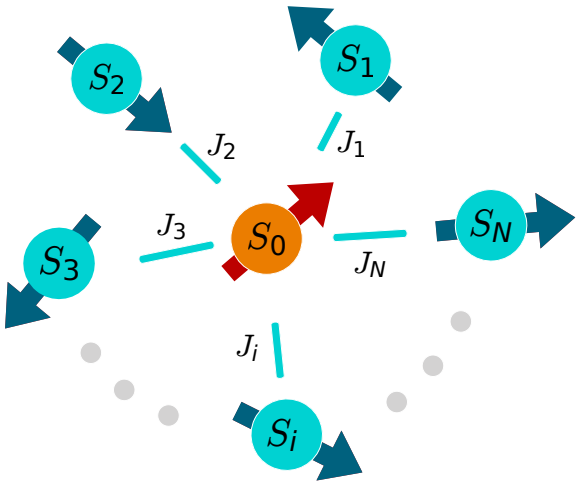

Figure 2.1: Sketch of the central spin model (2.1) and its star topology. The central spin $\vec{S}_0$ is coupled to the N surrounding bath spins $\vec{S}_i$ through the hyperfine interaction J_i.

The Hamiltonian of the central spin model, also known as Gaudin model [53, 54], is given by

$$H = \sum_{i=1}^{N} J_i \vec{S}_0 \cdot \vec{S}_i \,. \tag{2.1}$$

It describes the interaction of a central spin $\vec{S}_0$ with the N surrounding nuclear bath spins $\vec{S}_i$ through the relativistic hyperfine couplings J_i. Its star topology is sketched in Figure 2.1. Representing the nuclear spin bath by the *Overhauser field* operator

$$\vec{A} = \sum_{i=1}^{N} J_i \vec{S}_i \tag{2.2}$$

is going to be convenient later in this thesis. It can be considered as an effective magnetic field which couples to the central spin $\vec{S}_0$. Throughout this thesis, the CSM is be studied only for spins $S = 1/2$ for simplicity while establishing the main approach.

The application of an external magnetic field $\vec{B}$ can be studied by using the extended Hamiltonian

$$H = \sum_{i=1}^{N} J_i \vec{S}_0 \cdot \vec{S}_i \; - \vec{B} \cdot \vec{S}_0 \, . \tag{2.3}$$

Here, the external field acts only on the central spin operator $\vec{S}_0$. Note that in principle, the magnetic field can be time dependent, too. The coupling to the nuclear bath spins $\vec{S}_i$ is neglected because their magnetic moments are very small, leading to a very small Zeemann splitting. This becomes clear when looking at their nuclear magneton, which is proportional to the inverse mass of the nucleus. In contrast, the Bohr magneton of the electron is about three orders of magnitude larger, leading to a much larger Zeemann splitting. Note that the interaction of the external magnetic field with the nuclear spins could be included easily in the following approach. It is refrained from including this extension for further simplicity while developing the approach.

The CSM is a very simplistic but useful model to describe the electron spin decoherence in a quantum dot, only considering the most important hyperfine interaction with the surrounding nuclear spins. Typically, the hyperfine couplings J_i are in the range of μeV [16, 55, 56]. In the real physical system, other kind of interactions occur, too. Their influence usually appears on a longer timescale which is beyond the scope of this thesis. Therefore, they are neglected for further simplicity. One additional interaction is the dipole-dipole exchange coupling between the nuclear spins [6]. It only affects the decoherence of the central electron spin on a timescale which is approximately one to two orders of magnitude larger than the timescale induced by the hyperfine interaction, which is in the order of 1 ns [57]. Another interaction which can be considered is the nuclear electric quadrupolar interaction [58]. Its influence on the coherence time of hole and electron spins in semiconductor quantum dots is studied by Hackmann et al. [59].

In a quantum dot, the hyperfine interaction is inhomogeneous. In general, the coupling constants J_i are defined through the probability

$$J_i \propto |\Psi(\vec{r}_i)|^2 \propto \exp\left[-\left(\frac{r_i}{R}\right)^k\right] , \tag{2.4}$$

This definition is based on the isotropic envelope wave function of a localized electron in its orbital ground state [18, 35]. The radius R determines the number of strongly coupled nuclear spins which are relevant for the central spin dynamics. The amount of relevant nuclear spins is in the order of $10^4 - 10^6$. The parameter $k = 1$ leads to an exponential wave function while $k = 2$ corresponds to a Gaussian one.

Throughout this thesis, mainly the case of *exponentially* distributed couplings

$$J_i = \mathcal{N} \exp\left[-i\frac{x}{N}\right] , \qquad i \in \{1, \dots, N\} , \tag{2.5}$$

is studied (see Figure 2.2). The parameter $x := {}^{N}/_{N_0}$ indicates the ratio of the total number of bath spins N compared to the number of bath spins N_0 within the localization radius of the wave function [23]. Choosing a larger value for x increases the amount of weakly

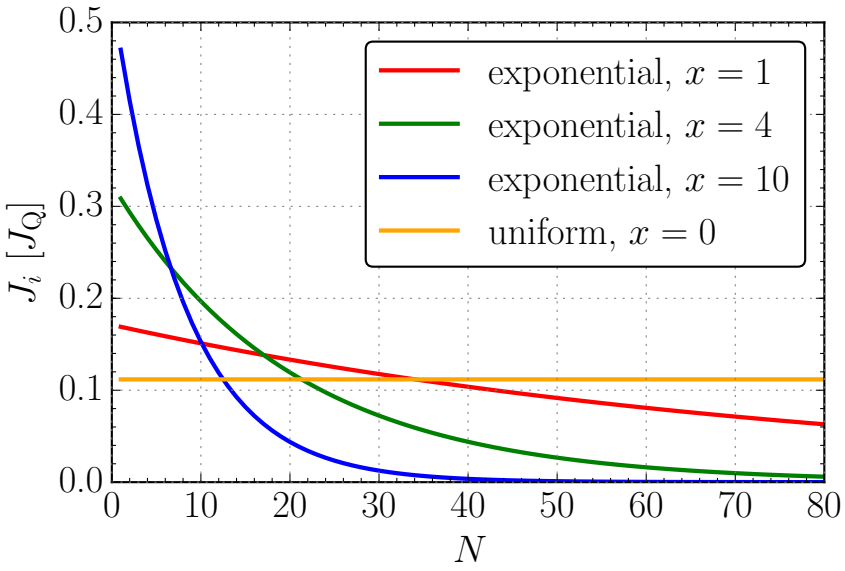

Figure 2.2: Illustration of the exponential and uniform coupling distributions defined in equations (2.5) and (2.7) for $N = 80$ bath spins. The distributions are normalized numerically so that $J_Q^2 = 1$ holds. The parameter x is responsible for the amount bath spins with a small coupling constant.

coupling bath spins, which have been identified to be responsible for the long-time behavior of the central spin dynamics [18, 23]. The distribution is normalized so that $\mathcal{N}$, which has the unit of an energy, is chosen such that

$$J_Q^2 := \sum_{i=1}^{N} J_i^2 = 1 \tag{2.6}$$

holds numerically. This is simply performed by normalizing the vector of coupling constants $\vec{J} = (J_1, J_2, \dots, J_N)^T$. Note that in this thesis, natural units ($\hbar = 1$) are used. Therefore, J_Q defines an energy scale which determines the timescale for the short time dynamics of the central spin [16].

This is because mainly completely disordered initial bath states are studied throughout this thesis so that the first moment of the coupling distribution does not contribute [57]. Consequently, the time t is specified in units of J_Q^{-1} in this thesis.

Additionally, the unphysical *uniform* coupling distribution

$$J_i = \frac{J_Q}{\sqrt{N}}, \qquad i \in \{1, \dots, N\}\ , \tag{2.7}$$

is studied (see Figure 2.2) because exact solutions for large bath sizes exist for this particular case [29, 30]. The exact results can function as a testbed for the new approach. Note that this distribution is also obtained from the exponential one (2.5) by simply inserting $x = 0$.

3 Born approximation for the central spin model

Due to the nature of the exponential growing Hilbert space in the central spin model for each additional bath spin, appropriate approximations have to be identified in order to deal with large bath sizes.

In this chapter, the general concept of the Born approximation [51] is introduced at first. Afterwards, it is shown that assuming the total density operator $\rho(t)$ of the whole system to be in a product state for all times leads to the classical equations of motion for the central spin model. These classical precession terms shall be included in the new approach as well. It is achieved by splitting the CSM Hamiltonian (2.3) into a free and an interacting part. In the interaction picture, the free part is solved exactly using the Heisenberg equation of motion. This leads to the classical equations of motion. The Born approximation is used to deal with the interacting part up to second order in the coupling constants. As a starting point, the easy case $N = 1$ is studied to establish the main approach. After checking the obtained differential equation system for its correctness by error analyses, a generalization to an arbitrary number of bath spins N is performed.

3.1 Born approximation

The present approach shall be based on the Born approximation as discussed in Reference [51]. The Hamiltonian of a *general* total system is assumed to have the form

$$H = H_{\mathrm{S}} + H_{\mathrm{B}} + H_{\mathrm{I}} \,. \tag{3.1}$$

The free Hamiltonians of the system H_{S} and the bath H_{B} can be treated exactly in the interaction picture by shifting their contribution using the Heisenberg equation of motion into the system and bath operators, respectively. The interacting part H_{I} is the problematic one. The starting point for its description is the interaction picture von Neumann equation

$$\frac{\mathrm{d}}{\mathrm{d}t}\rho(t) = -i\,[H_{\mathrm{I}},\, \rho(t)] \tag{3.2}$$

for the total density matrix $\rho(t)$. Note that natural units ($\hbar = 1$) are used throughout this thesis. Mathematically, it can be rewritten in its integral form

$$\rho(t) = \rho(0) - i \int_0^t \mathrm{d}s\, [H_{\mathrm{I}}(s),\, \rho(s)] \,. \tag{3.3}$$

Reinserting into equation (3.2) leads to the expression

$$\frac{\mathrm{d}}{\mathrm{d}t}\rho(t) = -i\,[H_{\mathrm{I}}(t),\, \rho(0)] - \int_0^t \mathrm{d}s\, [H_{\mathrm{I}}(t),\, [H_{\mathrm{I}}(s),\, \rho(s)]] \,, \tag{3.4}$$

which is a second order expansion in the differential equation for the total density matrix $\rho(t)$.

By calculating the trace over the bath, a differential equation for the reduced density matrix $\rho_{\mathrm{S}}(t)$ can be obtained. It would still include the total density matrix $\rho(t)$ on the right-hand side, though. Therefore, a *weak-coupling approximation* is performed. It assumes the interacting part H_{I} of the Hamiltonian H to be small compared to the contribution of the free Hamiltonians H_{S} and H_{B}, meaning the influence of the system on the bath is small. This means that its influence on the reduced density matrix of the bath ρ_{B} can be neglected. Then, the state of the total system can be described approximately by a tensor product

$$\rho(t) \approx \rho_{\mathrm{S}}(t) \otimes \rho_{\mathrm{B}}(t) \tag{3.5}$$

for all times t. Note that in this thesis and in contrast to Reference [51], it is refrained from neglecting the complete time dependency of the bath density matrix ρ_{B} because the slow intrinsic bath dynamics are responsible for the long-time dynamics of the central spin in the CSM. This ansatz leads to the so called *Born approximation*

$$\frac{\mathrm{d}}{\mathrm{d}t}\rho(t) = -i\left[H_{\mathrm{I}}(t),\, \rho_{\mathrm{S}}(0) \otimes \rho_{\mathrm{B}}(0)\right] - \int_0^t \mathrm{d}s\, \left[H_{\mathrm{I}}(t),\, \left[H_{\mathrm{I}}(s),\, \rho_{\mathrm{S}}(s) \otimes \rho_{\mathrm{B}}(s)\right]\right] \tag{3.6}$$

$$= -i\left[H_{\mathrm{I}}(t),\, \rho_{\mathrm{S}}(0) \otimes \rho_{\mathrm{B}}(0)\right] - \left[H_{\mathrm{I}}(t),\, \int_0^t \mathrm{d}s\, \left[H_{\mathrm{I}}(s),\, \rho_{\mathrm{S}}(s) \otimes \rho_{\mathrm{B}}(s)\right]\right] \tag{3.7}$$

which is an integro-differential equation. Now, the differential equation for the reduced density matrix $\rho_{\mathrm{S}}(t)$ of the system can be simply obtained by calculating the partial trace over the full bath on both sides of equation (3.7).

For the central spin model, the free Hamiltonians H_{S} and H_{B} will lead to classical precession terms. When using natural units ($\hbar = 1$), the inverse coupling constants J_i^{-1} define the timescale of the classical precession. This is the fast part of the dynamics in the system. The second order corrections obtained through the Born approximation will be of second order in the couplings J_i. Assuming uniformly distributed couplings $J_i \propto 1/\sqrt{N}$, this corresponds to $J_i^2 \propto 1/N$, meaning these quantum mechanical corrections introduce much slower and suppressed dynamics for large baths. Therefore, the weak-coupling approximation (3.5) is valid for the central spin model in the limit of large bath sizes N, even without a strong external magnetic field.

The application of an magnetic field to the central spin can only enhance this approach because its interaction can be considered as a part of the free Hamiltonian H_{S}, which is dealt with exactly. Now for very large field strengths $|\vec{B}|$, the weak-coupling approximation (3.5) which is used in the Born approximation (3.7) should work even better because then, the magnetic field strength determines the fast central spin dynamic.

A further Markovian approximation [51] should not be applied to the central spin model because it shows a non-Markovian behavior as discussed by Breuer et al. [60] and Coish and Loss [35].

3.2 Classical equations of motion

As a first step, the weak-coupling approximation (3.5) is applied to the von Neumann equation in order to show that this leads to the classical equations of motion with no quantum mechanical effects remaining.

The time evolution of the density operator in the Schrödinger picture is described by the von Neumann equation ($\hbar = 1$)

$$\frac{\mathrm{d}}{\mathrm{d}t}\rho(t) = -i\,[H,\,\rho(t)]\;. \tag{3.8}$$

The Hamiltonian of the central spin model reads

$$H = \sum_{i=1}^{N} J_i \vec{S}_0 \cdot \vec{S}_i - \vec{B} \cdot \vec{S}_0\,. \tag{3.9}$$

It describes a central spin $\vec{S}_0$ coupling to N bath spins with coupling constants J_i. Additionally, an external magnetic field $\vec{B}$ is applied to the central spin $\vec{S}_0$.

Applying the weak-coupling approximation (3.5) requires parameterizing the density operator $\rho(t) \approx \rho_0(t) \otimes \rho_\mathrm{B}(t)$. Since no direct interactions between the different nuclear spins $\vec{S}_i$ exist, the density operator of the spin bath $\rho_\mathrm{B}(t)$ is also assumed to be in a product state

$$\rho_\mathrm{B}(t) \approx \bigotimes_{i=1}^{N} \rho_i(t) \tag{3.10}$$

for all times t. Each reduced density operator $\rho_i(t)$ belongs to the individual bath spin i. This is an extension of the weak-coupling approximation (3.5) for the non-interacting bath of the central spin model. The total density operator of the whole system in weak-coupling approximation is therefore assumed to be

$$\rho(t) \approx \bigotimes_{i=0}^{N} \rho_i(t)\,. \tag{3.11}$$

Each density operator $\rho_i(t)$ can be represented by a 2×2-matrix using the Pauli matrices σ^α, with $\alpha \in \{x, y, z\}$. A possible parameterization is given by

$$\rho_i(t) = \frac{1}{2}\mathbb{1} + \vec{v}_i(t) \cdot \vec{\sigma}\,. \tag{3.12}$$

with $|\vec{v}_i(0)| \leq 1/2$ to ensure that $\rho_i(t)$ is positive semidefinite. This means that $2\vec{v}_i(0)$ is the Bloch vector. The central spin is in a pure state for $|\vec{v}_i(0)| = 1/2$, corresponding to the surface of the Bloch sphere.

Using this parameterization leads to the rather complicated expression for the total density matrix

$$\rho(t) = \sum_{j=0}^{N} \frac{1}{2^{N-1}} \vec{v}_j(t) \cdot \vec{S}_j + \sum_{k=1}^{N} \frac{1}{2^{N-3}} \left(\vec{v}_0(t) \cdot \vec{S}_0\right) \left(\vec{v}_k(t) \cdot \vec{S}_k\right) + \ldots\,, \tag{3.13}$$

with the spin operators

$$\vec{S}_i = \mathbb{1} \otimes \cdots \otimes \underbrace{\vec{\sigma}/2}_{i\text{th place}} \otimes \cdots \otimes \mathbb{1}\,. \tag{3.14}$$

However, not all terms are relevant as explained below.

In the extended weak-coupling approximation (3.11), $\rho(t)$ is fully described by the N reduced density operators $\rho_i(t)$ which are again fully described by the three-dimensional vectors $\vec{v}_i(t)$. It is therefore sufficient to rewrite the whole differential equation system (3.8) as a $3 \times N$-system of the vectors $\vec{v}_i(t)$.

As a first step, the differential equation for $\rho_0(t)$ is derived using the partial trace over the spin bath, denoted as $\mathrm{Tr_B}$. This leads to

$$\frac{\mathrm{d}}{\mathrm{d}t}\rho_0(t) = -i\,\mathrm{Tr_B}\left[H, \bigotimes_{i=0}^{N} \rho_i(t)\right] \tag{3.15a}$$

$$= -i\,\mathrm{Tr_B}\left[H, \sum_{j=0}^{N} \frac{1}{2^{N-1}} \vec{v}_j(t) \cdot \vec{S}_j + \sum_{k=1}^{N} \frac{1}{2^{N-3}} \left(\vec{v}_0(t) \cdot \vec{S}_0\right)\left(\vec{v}_k(t) \cdot \vec{S}_k\right)\right]\,. \tag{3.15b}$$

Since the trace of a Pauli matrix is zero, many terms within the commutator vanish and have been therefore omitted a priori. The strategy calculating the expression above consists of using the well known spin algebra to identify those terms that vanish anyway after tracing due to remaining spin operators. A useful compilation of spin and vector algebra used throughout this thesis can be found in Appendix A. Note that the time dependence of the vectors $\vec{v}_i$ is omitted as well for a better readability. Sums over Greek indices run over $\{x, y, z\}$.

As the next step, the commutator in equation (3.15b) has to be evaluated. Note that when tracing over the full bath, denoted by $\mathrm{Tr_B}$, any term proportional to a single bath spin operator $\vec{S}_i$ vanishes. This renders the calculations much easier a priori.

$$\mathrm{Tr_B}\left\{\frac{1}{2^{N-1}}\left[\sum_{i=1}^{N} J_i \vec{S}_0 \cdot \vec{S}_i - \vec{S}_0 \cdot \vec{B}, \sum_{j=0}^{N} \vec{v}_j \cdot \vec{S}_j\right]\right.$$
$$\left. + \frac{1}{2^{N-3}}\left[\sum_{i=1}^{N} J_i \vec{S}_0 \cdot \vec{S}_i - \vec{S}_0 \cdot \vec{B}, \sum_{k=1}^{N} \left(\vec{v}_0 \cdot \vec{S}_0\right)\left(\vec{v}_k \cdot \vec{S}_k\right)\right]\right\} \tag{3.16a}$$

$$= i\,\mathrm{Tr_B}\left\{-\frac{1}{2^{N-1}} \underbrace{\sum_{\alpha\beta\gamma} B^\alpha v_0^\beta S_0^\gamma \epsilon_{\alpha\beta\gamma}}_{=\left(\vec{B}\times\vec{v}_0\right)\cdot\vec{S}_0} + \frac{1}{2^{N-1}} \sum_{i=1}^{N} \underbrace{\sum_{\alpha\beta\delta} J_i v_i^\alpha v_0^\beta S_0^\delta \epsilon_{\alpha\beta\delta}}_{=J_i(\vec{v}_i\times\vec{v}_0)\cdot\vec{S}_0}\right\} \tag{3.16b}$$

Evaluating the trace $\mathrm{Tr_B}$ yields the differential equation for the partial density matrix $\rho_0(t)$,

$$\frac{\mathrm{d}}{\mathrm{d}t}\rho_0(t) = \left(-\vec{B} \times \vec{v}_0(t) + \sum_{i=1}^{N} J_i \vec{v}_i(t) \times \vec{v}_0(t)\right) \cdot \vec{\sigma} \tag{3.17}$$

$$= \left(\vec{B}_{\mathrm{eff}}(t) \times \vec{v}_0(t)\right) \cdot \vec{\sigma}\,. \tag{3.18}$$

In the latter step, the effective time dependent magnetic field

$$\vec{B}_{\text{eff}}(t) := -\vec{B} + \sum_{i=1}^{N} J_i \langle \vec{S}_i \rangle(t) \tag{3.19}$$

is introduced, consisting of the external magnetic field and the Overhauser field.

Equation (3.18) can be rewritten in terms of the expectation values $\langle \vec{S}_i \rangle$(t). In the following, the trace over the whole Hilbert space is denoted by Tr while Tr_i denotes the partial trace over the degrees of freedom of the ith bath spin. The vector $\vec{e}_\alpha$ is the unit vector in α-direction. Then, the following relation holds for the weak-coupling approximation (3.11).

$$\langle \vec{S}_i \rangle(t) = \text{Tr}\left\{ \vec{S}_i \rho(t) \right\} = \text{Tr}_i \left\{ \frac{1}{2} \vec{\sigma} \rho_i(t) \right\} = \text{Tr}_i \left\{ \frac{1}{2} \vec{\sigma} \left(\frac{1}{2} \mathbb{1} + \vec{v}_i(t) \cdot \vec{\sigma} \right) \right\} \tag{3.20a}$$

$$= \text{Tr}_i \left\{ \sum_{\alpha\beta} \frac{1}{2} \vec{e}_\alpha \sigma^\alpha \sigma^\beta v_i^\beta(t) \right\} = \text{Tr}_i \left\{ \sum_{\alpha\beta} \frac{1}{2} \delta_{\alpha\beta} v_i^\beta(t) \right\} = \vec{v}_i(t) \tag{3.20b}$$

This allows for the direct replacement of the vectors $\vec{v}_i(t)$ with the expectation values $\langle \vec{S}_i \rangle(t)$ in equation (3.18). Obviously, the same relation holds for $\vec{v}_0(t)$.

It is now easy to derive the differential equation for $\langle \vec{S}_0 \rangle(t)$.

$$\frac{\mathrm{d}}{\mathrm{d}t} \langle \vec{S}_0 \rangle(t) = \frac{\mathrm{d}}{\mathrm{d}t} \text{Tr}_0 \left\{ \frac{1}{2} \vec{\sigma} \rho_0(t) \right\} = \text{Tr}_0 \left\{ \frac{1}{2} \vec{\sigma} \underbrace{\frac{\mathrm{d}}{\mathrm{d}t} \rho_0(t)}_{(3.18)} \right\} \tag{3.21a}$$

$$= \vec{B}_{\text{eff}}(t) \times \langle \vec{S}_0 \rangle(t) \,. \tag{3.21b}$$

The differential equation for the expectation value of each bath spin $\langle \vec{S}_i \rangle(t)$ is derived in an analogous way, but with more vanishing terms. For example, the terms including the magnetic field $\vec{B}$ vanish because it couples only to the central spin operator $\vec{S}_0$. This leads to the full set of differential equations

$$\frac{\mathrm{d}}{\mathrm{d}t} \langle \vec{S}_0 \rangle(t) = \vec{B}_{\text{eff}}(t) \times \langle \vec{S}_0 \rangle(t) \tag{3.22a}$$

$$\frac{\mathrm{d}}{\mathrm{d}t} \langle \vec{S}_i \rangle(t) = J_i \langle \vec{S}_0 \rangle(t) \times \langle \vec{S}_i \rangle(t) \qquad \forall\, i \in \{1, \ldots, N\} \,. \tag{3.22b}$$

It describes the classical precession of the central spin around the effective magnetic field $\vec{B}_{\text{eff}}(t)$ while each bath spin precesses around the central spin. Therefore, this calculation can be considered as a simple mean-field approach. The precession frequencies of the bath spins are determined by their individual coupling constants J_i.

Throughout this thesis, the differential equation system (3.22) is referred to as the *classical equations of motion*. It can also be derived by simply treating the spin operators as classical vectors using the Heisenberg equation of motion. This mean-field approach does not describe the real quantum mechanics in the CSM, though. Hence, the Born approximation (3.7) is used in the following sections to include the quantum mechanical corrections to the classical equations of motion in second order of the couplings $\mathcal{O}\left(J_i^2\right)$.

3.3 Born approximation applied to the central spin model

In this section, the Born approximation as introduced in section 3.1 is applied to the central spin model. At first, an appropriate way to split the CSM Hamiltonian

$$H = \sum_{i=1}^{N} J_i \vec{S}_0 \cdot \vec{S}_i - \vec{B} \cdot \vec{S}_0 \,. \tag{3.23}$$

into a part H_0 which leads to the classical precession terms, and an interacting part H_I which is dealt with using the Born approximation, has to be found.

Interpreting spin operators as classical vectors leads to the classical equations of motion. Since this is very similar to replacing the spin operators $\vec{S}_{0/i}(t)$ by their expectation values $\langle \vec{S}_{0/i}(t) \rangle =: \vec{v}_{0/i}(t)$, it is convenient to introduce the splitting

$$\begin{aligned} H(t) = & \underbrace{\left(\sum_{i=1}^{N} J_i \vec{v}_i(t) - \vec{B} \right) \cdot \vec{S}_0(t) + \sum_{i=1}^{N} J_i \vec{v}_0(t) \cdot \vec{S}_i(t) + \sum_{i=1}^{N} J_i \vec{v}_0(t) \cdot \vec{v}_i(t)}_{=: H_0(t)} \\ & + \underbrace{\sum_{i=1}^{N} J_i \left(\vec{S}_0(t) - \vec{v}_0(t) \right) \cdot \left(\vec{S}_i(t) - \vec{v}_i(t) \right)}_{=: H_\mathrm{I}(t)} \,. \end{aligned} \tag{3.24}$$

The solvable part $H_0(t)$ leads to the classical precession of the central spin around the effective magnetic field $\vec{B}_\mathrm{eff}(t) := \sum_{i=1}^{N} J_i \vec{v}_i(t) - \vec{B}$ while the bath spins precess around the central spin expectation value $\vec{v}_0(t)$. This classical behavior is shifted into the the operators $\vec{S}_0(t)$ and $\vec{S}_i(t)$ using the Heisenberg equations of motion.

The interacting part $H_\mathrm{I}(t)$ can be interpreted as the interaction between the fluctuations from the expectation values $\vec{v}_0(t)$ and $\vec{v}_i(t)$. This term is dealt with using the Born approximation (3.7).

In the following subsection and as a starting point, the Hamiltonian (3.24) is discussed using this approach for the easier case $N = 1$. After checking the obtained differential equation system for correctness and completeness through an extensive error analysis, an extension to the full central spin model with arbitrary amount of bath spins N is performed.

3.3.1 Derivation for one bath spin

As a starting point, the split Hamiltonian (3.24) is discussed for the easier case $N = 1$ using the Born approximation.

As a first step, the dynamics provided by $H_0(t)$ is shifted into $\vec{S}_0(t)$ and $\vec{S}_i(t)$ by solving the corresponding Heisenberg equation of motion.

$$\frac{\mathrm{d}}{\mathrm{d}t}\vec{S}_0(t) = i\left[H_0(t),\, \vec{S}_0(t)\right] = i\left[\vec{B}_{\mathrm{eff}}(t)\cdot\vec{S}_0(t),\, \vec{S}_0(t)\right] \tag{3.25a}$$

$$= \vec{B}_{\mathrm{eff}}(t)\times\vec{S}_0(t) = V_{\mathrm{eff}}(t)\vec{S}_0(t) \tag{3.25b}$$

$$\frac{\mathrm{d}}{\mathrm{d}t}\vec{S}_i(t) = i\left[H_0(t),\, \vec{S}_i(t)\right] \tag{3.25c}$$

$$= J_i\vec{v}_0(t)\times\vec{S}_i(t) = J_iV_0(t)\vec{S}_i(t) \tag{3.25d}$$

In each latter step, the cross product is rewritten as a matrix-vector multiplication with the skew-symmetric matrices $V_{\mathrm{eff}}(t)$ and $V_0(t)$, respectively. As an illustration, the matrix $V_0(t)$ takes the form

$$V_0(t) = \begin{pmatrix} 0 & -v_0^z(t) & v_0^y(t) \\ v_0^z(t) & 0 & -v_0^x(t) \\ -v_0^y(t) & v_0^x(t) & 0 \end{pmatrix}. \tag{3.26}$$

Note that a skew-symmetric matrix V fulfills the useful relation $V = -V^T$.

In order to solve the differential equations (3.25b) and (3.25d), the ansatz

$$\vec{S}_{0/i}(t) = D_{0/i}(t)\vec{S}_{0,i} \tag{3.27}$$

is used. Inserting this ansatz into (3.25b) and (3.25d) yields differential equations for the matrices $D_{0/i}(t)$,

$$\frac{\mathrm{d}}{\mathrm{d}t}D_0(t) = V_{\mathrm{eff}}(t)D_0(t) \tag{3.28a}$$

$$\frac{\mathrm{d}}{\mathrm{d}t}D_i(t) = J_iV_0(t)D_i(t)\,. \tag{3.28b}$$

These matrices describe orthogonal rotations of the initial operator $\vec{S}_{0/i}(0) = \vec{S}_{0/i}$. In particular, these rotations are equal to the classical precession of the spins. The initial conditions are obviously given by an identity operation, meaning $D_{0/i}(t=0) = \mathbb{1}$. Therefore, if $D_{0/i}(t)$ is an orthogonal matrix, the relation $\det D_{0/i}(t) = 1$ has to hold. This is one of the two properties of a rotation matrix. The second one is the orthogonality which can be proven easily. The property to show is $D_{0/i}^T(t)D_{0/i}(t) = \mathbb{1}$ which is equal to the requirement $D_{0/i}^T(t) = D_{0/i}^{-1}(t)$. Since both differential equations (3.28a) and (3.28b) have the same structure, it is sufficient to proof this relation only for $D_i(t)$.

When assuming $D_i(t)$ to be orthogonal, the derivative

$$\frac{\mathrm{d}}{\mathrm{d}t}\left(D_i^T(t)D_i(t)\right) = 0 \tag{3.29}$$

is known. Using the product rule and then inserting equation (3.28b) leads to

$$\underbrace{\left(\frac{\mathrm{d}}{\mathrm{d}t}D_i^T(t)\right)}_{=J_iD_i^T(t)V_0^T(t)=-J_iD_i^T(t)V_0(t)} D_i(t) + D_i^T(t)\underbrace{\left(\frac{\mathrm{d}}{\mathrm{d}t}D_i(t)\right)}_{=J_iV_0(t)D_i(t)} = 0 \tag{3.30a}$$

$$\Leftrightarrow -J_iD_i^T(t)V_0(t)D_i(t) + J_iD_i^T(t)V_0(t)D_i(t) = 0\,. \tag{3.30b}$$

This proofs the orthogonality of $D_i(t)$ and therefore also of $D_0(t)$.

The parameterizations of the reduced density operators use a slightly different notation compared to section 3.2. The weak-coupling approximation (3.11) is still used, though.

$$\rho_0(t) = \frac{1}{2}\mathbb{1} + \vec{c}(t)\cdot\vec{\sigma} \tag{3.31a}$$

$$\rho_i(t) = \frac{1}{2}\mathbb{1} + \vec{b}_i(t)\cdot\vec{\sigma} \tag{3.31b}$$

$$\Rightarrow \rho(t) = \rho_0(t)\otimes\rho_i(t) = \frac{1}{4}\mathbb{1} + \vec{c}(t)\cdot\vec{S}_0 + \vec{b}_i(t)\cdot\vec{S}_i + 4\left(\vec{c}(t)\cdot\vec{S}_0\right)\left(\vec{b}_i(t)\cdot\vec{S}_i\right) \tag{3.31c}$$

Once again, the initial conditions $|\vec{c}(0)| \leq 1/2$ and $|\vec{b}_i(0)| \leq 1/2$ have to be fulfilled to ensure that the density matrices are positive semidefinite.

Calculating the expectation values $\langle\vec{S}_{0/i}(t)\rangle =: \vec{v}_{0/i}(t)$ yields the useful relations

$$\vec{v}_0(t) = \langle\vec{S}_0(t)\rangle = \operatorname{Tr}\left[D_0(t)\vec{S}_0\rho(t)\right] \tag{3.32a}$$

$$= \operatorname{Tr}\left[\sum_{\alpha\beta} D_0^{\alpha\beta} S_0^\beta \vec{e}_\alpha \left(\frac{1}{4}\mathbb{1} + \left(\vec{b}_i\cdot\vec{S}_i + \vec{c}\cdot\vec{S}_0\right) + 4\left(\vec{b}_i\cdot\vec{S}_i\right)\left(\vec{c}\cdot\vec{S}_0\right)\right)\right] \tag{3.32b}$$

$$= \operatorname{Tr}\left[\sum_{\alpha\beta} D_0^{\alpha\beta} S_0^\beta \vec{e}_\alpha \left(\vec{c}\cdot\vec{S}_0\right)\right] = \frac{1}{2}\operatorname{Tr}\left[\sum_{\alpha\beta\gamma} D_0^{\alpha\beta} S_0^\beta \vec{e}_\alpha c^\gamma S_0^\gamma\right] \tag{3.32c}$$

$$= D_0(t)\vec{c}(t) \tag{3.32d}$$

$$\vec{v}_i(t) = \langle\vec{S}_i(t)\rangle = D_i(t)\vec{b}_i(t)\,. \tag{3.32e}$$

These relations allow for the parameterization of $\rho(t)$ by making use of these expectation values if the rotation matrices $D_{0/i}(t)$ are known. As of now, the notation $\vec{v}_{0/i} = \langle\vec{S}_{0/i}\rangle$ is used throughout this thesis to describe the expectation value of spin operators.

The remaining task consists of deriving a system of differential equations for either $\vec{c}(t)$ and $\vec{b}_i(t)$ or for $\vec{v}_0(t)$ and $\vec{v}_i(t)$. In this thesis, the latter case is chosen because it allows for a direct calculation of the expectation values later on.

Despite the additional coupling of the central spin to the external field which is shifted into $D_0(t)$, the dynamics provided by interacting part $H_I(t)$ for $\vec{v}_0(t)$ only differs from $\vec{v}_i(t)$ by switching some indices due to the symmetric structure of the Hamiltonian. Therefore, the differential equation for $\vec{v}_i(t)$ is derived at first.

In the interaction picture, the derivative of the expectation value $\vec{v}_i(t)$ can be written as

$$\frac{\mathrm{d}}{\mathrm{d}t}\vec{v}_i(t) = \frac{\mathrm{d}}{\mathrm{d}t}\operatorname{Tr}\left[\vec{S}_i(t)\rho(t)\right] = \frac{\mathrm{d}}{\mathrm{d}t}\operatorname{Tr}_i\left[\vec{s}_i(t)\rho_i(t)\right] \tag{3.33a}$$

$$= \operatorname{Tr}_i\left[\underbrace{\left(\frac{\mathrm{d}}{\mathrm{d}t}\vec{s}_i(t)\right)}_{=J_i V_0(t)\vec{s}_i(t)}\rho_i(t) + \vec{s}_i(t)\underbrace{\left(\frac{\mathrm{d}}{\mathrm{d}t}\rho_i(t)\right)}_{\text{Bornapproximation}}\right]. \tag{3.33b}$$

The vector $\vec{s}_i(t) = D_i(t)\vec{s}_i$ is the time dependent vector of the 2×2 spin operators $s_i^\alpha = \sigma^\alpha/2$. The first term on the right-hand side will describe the classical precession around $\vec{v}_0(t)$ while the second term will include the second order $\mathcal{O}\left(J_i^2\right)$ quantum mechanical corrections to the classical dynamics which are derived in the following.

The Born approximation (3.7) for the reduced density operator of the bath spin reads

$$\frac{\mathrm{d}}{\mathrm{d}t}\rho_i(t) = -i\,\mathrm{Tr}_0\left[H_\mathrm{I}(t),\, \rho_0(0)\otimes\rho_i(0)\right] - \mathrm{Tr}_0\left[H_\mathrm{I}(t),\, \int_0^t \mathrm{d}s\left[H_\mathrm{I}(s),\, \rho_0(s)\otimes\rho_i(s)\right]\right]. \tag{3.34}$$

Despite the different time dependencies, the first commutator is almost equal to the inner commutator of the second term, $[H_\mathrm{I}(s),\, \rho_0(s)\otimes\rho_i(s)]$. Hence, the first commutator can be calculated by evaluating the correct terms of the inner commutator at $s=0$, namely $\vec{c}(s=0)$ and $\vec{b}_i(s=0)$ which have their origin in the parameterization of $\rho(0) = \rho_0(0)\otimes\rho_i(0)$. For a better readability throughout the following calculation, the time dependencies are omitted.

$$[H_\mathrm{I}(s),\, \rho_0(s)\otimes\rho_i(s)] = \left[J_i\left(\vec{S}_0(s) - \vec{v}_0(s)\right)\cdot\left(\vec{S}_i(s) - \vec{v}_i(s)\right),\, \rho_0(s)\otimes\rho_i(s)\right] \tag{3.35a}$$

$$= J_i\left[(D_0\vec{S}_0)\cdot(D_i\vec{S}_i) - (D_0\vec{S}_0)\cdot\vec{v}_i - (D_i\vec{S}_i)\cdot\vec{v}_0,\, \vec{c}\cdot\vec{S}_0 + \vec{b}_i\cdot\vec{S}_i + 4\left(\vec{c}\cdot\vec{S}_0\right)\left(\vec{b}_i\cdot\vec{S}_i\right)\right] \tag{3.35b}$$

Due to the linearity of commutators, this commutator splits into nine distinct commutators $\mathcal{C}_i$ where most of them are very similar, though. It is therefore refrained from giving the detailed calculation for each individual commutator. Only the two most important ones, $\mathcal{C}_1$ and $\mathcal{C}_3$, are discussed in detail. Mainly some vector algebra, the orthogonality of the rotation matrices $D_{0/i}(t)$, and the relations (3.32d) and (3.32e) are required to write the other commutators in the appropriate form.

The intention is to write the evaluated inner commutator of equation (3.34) in the form

$$[H_i(s),\, \rho_0(s)\otimes\rho_i(s)] = iJ_i\left[\vec{p}_i(t)\cdot\vec{S}_i + \vec{q}_i(s)\cdot\vec{S}_0 + \left(m_i(s)\vec{S}_i\right)\cdot\vec{S}_0\right]. \tag{3.36}$$

This notation allows for replacing the integral of the integro-differential equation (3.34) by additional differential equations later on. Note that a compilation of the required spin and vector algebra for the following evaluation of the commutators $\mathcal{C}_i$ can be found in Appendix A.

$$\mathcal{C}_1 := \left[(D_0\vec{S}_0)\cdot(D_i\vec{S}_i),\, \vec{b}_i\cdot\vec{S}_i\right] = \sum_{\alpha\beta\gamma\delta} D_0^{\alpha\beta}S_0^\beta D_i^{\alpha\gamma}b_i^\delta\left[S_i^\gamma,\, S_i^\delta\right] \tag{3.37a}$$

$$= i\sum_{\alpha\gamma\delta\epsilon}\left(D_0\vec{S}_0\right)^\alpha D_i^{\alpha\gamma}b_i^\delta S_i^\epsilon\epsilon_{\gamma\delta\epsilon} = i\sum_\alpha\left(D_0\vec{S}_0\right)^\alpha\left[D_i\left(\vec{b}_i\times\vec{S}_i\right)\right]^\alpha \tag{3.37b}$$

$$= i\left(D_0\vec{S}_0\right)\cdot\left[D_i\left(\vec{b}_i\times\vec{S}_i\right)\right] = i\left[D_0^T\underbrace{D_i\left(\vec{b}_i\times\vec{S}_i\right)}_{=\vec{v}_i\times\left(D_i\vec{S}_i\right)=V_iD_i\vec{S}_i}\right]\cdot\vec{S}_0 \tag{3.37c}$$

$$= i\left(D_0^TV_iD_i\vec{S}_i\right)\cdot\vec{S}_0 \tag{3.37d}$$

$$\mathcal{C}_2 := \left[(D_0\vec{S}_0)\cdot(D_i\vec{S}_i),\, \vec{c}\cdot\vec{S}_0\right] = -i\left(D_0^T V_0 D_i \vec{S}_i\right)\cdot\vec{S}_0 \tag{3.38}$$

$$\begin{aligned}
\mathcal{C}_3 &:= \left[(D_0\vec{S}_0)\cdot(D_i\vec{S}_i),\, 4\left(\vec{b}_i\cdot\vec{S}_i\right)\left(\vec{c}\cdot\vec{S}_0\right)\right] && \text{(3.39a)}\\
&= 4\sum_{\alpha\beta\gamma\delta\epsilon} D_0^{\alpha\beta} D_i^{\alpha\gamma} b_i^\delta c^\epsilon \underbrace{\left[S_0^\beta S_i^\gamma,\, S_i^\delta S_0^\epsilon\right]}_{=S_0^\beta\left[S_i^\gamma, S_i^\delta\right]S_0^\epsilon + S_i^\delta\left[S_0^\beta, S_0^\epsilon\right]S_i^\gamma} && \text{(3.39b)}\\
&= 4i\sum_{\beta\gamma\delta\epsilon\kappa} \left(D_0^T D_i\right)^{\beta\gamma} b_i^\delta c^\epsilon \left(\frac{1}{4}\delta_{\beta\epsilon} S_i^\kappa \epsilon_{\gamma\delta\kappa} + \frac{1}{4}\delta_{\delta\gamma} S_0^\kappa \epsilon_{\beta\epsilon\kappa}\right) && \text{(3.39c)}\\
&\quad + 4i\sum_{\beta\gamma\delta\epsilon\kappa\tau} \left(D_0^T D_i\right)^{\beta\gamma} b_i^\delta c^\epsilon \left(\underbrace{S_0^\tau S_i^\kappa \epsilon_{\gamma\delta\kappa}\epsilon_{\beta\epsilon\tau} - S_0^\kappa S_i^\tau \epsilon_{\gamma\delta\tau}\epsilon_{\beta\epsilon\kappa}}_{=0,\ \text{rename } \kappa\leftrightarrow\tau \text{ in 2nd term}}\right) && \text{(3.39d)}\\
&= i\sum_{\beta\gamma\delta\kappa} \left(D_0^T D_i\right)^{\beta\gamma} b_i^\delta c^\beta S_i^\kappa \epsilon_{\gamma\delta\kappa} + i\sum_{\beta\gamma\epsilon\kappa} \left(D_0^T D_i\right)^{\beta\gamma} b_i^\gamma c^\epsilon S_0^\kappa \epsilon_{\beta\epsilon\kappa} && \text{(3.39e)}\\
&= \underbrace{i\left[\left(D_i^T D_0 \vec{c}\right)\times\vec{b}_i\right]\cdot\vec{S}_i}_{=:\mathcal{C}_{3.1}} + \underbrace{i\left[\left(D_0^T D_i \vec{b}_i\right)\times\vec{c}\right]\cdot\vec{S}_0}_{=:\mathcal{C}_{3.2}} && \text{(3.39f)}
\end{aligned}$$

$$\mathcal{C}_4 := \left[-(D_0\vec{S}_0)\cdot\vec{v}_i,\, \vec{b}_i\cdot\vec{S}_i\right] = 0 \tag{3.40}$$

$$\mathcal{C}_5 := \left[-(D_0\vec{S}_0)\cdot\vec{v}_i,\, \vec{c}\cdot\vec{S}_0\right] = -i\left[(D_0^T\vec{v}_i)\times\vec{c}\right]\cdot\vec{S}_0 = -i\left[\left(D_0^T D_i\vec{b}\right)\times\vec{c}\right]\cdot\vec{S}_0 \tag{3.41}$$

$$\begin{aligned}
\mathcal{C}_6 &:= \left[-(D_0\vec{S}_0)\cdot\vec{v}_i,\, 4\left(\vec{c}\cdot\vec{S}_0\right)\left(\vec{b}_i\cdot\vec{S}_i\right)\right] && \text{(3.42a)}\\
&\underset{(3.41)}{=} -4i\left(\vec{b}_i\cdot\vec{S}_i\right)\left[(D_0^T\vec{v}_i)\times\vec{c}\right]\cdot\vec{S}_0 = 4i\left(D_0^T V_0 \vec{v}_i\vec{v}_i^T D_i\vec{S}_i\right)\cdot\vec{S}_0 && \text{(3.42b)}
\end{aligned}$$

$$\mathcal{C}_7 := \left[-\left(D_i\vec{S}_i\right)\cdot\vec{v}_0,\, \vec{b}_i\cdot\vec{S}_i\right] = -i\left[\left(D_i^T D_0\vec{c}\right)\times\vec{b}_i\right]\cdot\vec{S}_i \tag{3.43}$$

$$\mathcal{C}_8 := \left[-\left(D_i\vec{S}_i\right)\cdot\vec{v}_0,\, \vec{c}\cdot\vec{S}_0\right] = 0 \tag{3.44}$$

$$\mathcal{C}_9 := \left[-(D_i\vec{S}_i)\cdot\vec{v}_0,\, 4\left(\vec{b}_i\cdot\vec{S}_i\right)\left(\vec{c}\cdot\vec{S}_0\right)\right] = -4i\left(D_0^T\vec{v}_0\vec{v}_0^T V_i D_i\vec{S}_i\right)\cdot\vec{S}_0 \tag{3.45}$$

The first term of the right-hand side of the Born approximation (3.34) is evaluated using these nine commutators $\mathcal{C}_i$. It requires the calculation of the partial trace Tr_0 so that every term $\propto \vec{S}_0$ vanishes. Thus, the only contributing terms are $\mathcal{C}_{3.1}$ and $\mathcal{C}_7$. Note that the correct time dependencies are included again at this point.

$$\begin{aligned}
&-i\,\mathrm{Tr}_0\left[H_\mathrm{I}(t),\, \rho_0(0)\otimes\rho_i(0)\right] = -i^2 J_i\,\mathrm{Tr}_0\left\{\mathcal{C}_{3.1} + \mathcal{C}_7\right\} && \text{(3.46a)}\\
&= -i^2 J_i\,\mathrm{Tr}_0\left\{\left[\left(D_i^T(t)D_0(t)\vec{c}(0)\right)\times\vec{b}_i(0)\right]\cdot\vec{S}_i - \left[\left(D_i^T(t)\underbrace{D_0(t)\vec{c}(t)}_{=\vec{v}_0(t)}\right)\times\vec{b}_i(0)\right]\cdot\vec{S}_i\right\} && \text{(3.46b)}\\
&= J_i\left[\left(D_i^T(t)D_0(t)\vec{c}(0) - D_i^T(t)\vec{v}_0(t)\right)\times\vec{b}_i(0)\right]\cdot\vec{\sigma} && \text{(3.46c)}
\end{aligned}$$

Next, in order to write the inner commutator which appears in the Born approximation (3.34) in terms of equation (3.36), the commutators $\mathcal{C}_i$ have to be sorted in this regard. This leads to the following expressions for the coefficients $\vec{p}(s)$, $\vec{q}(s)$ and $m(s)$, defined in equation (3.36).

$$\vec{p}_i(s) = (\mathcal{C}_{3.1} + \mathcal{C}_7)/i = 0 \tag{3.47a}$$
$$\vec{q}_i(s) = (\mathcal{C}_{3.2} + \mathcal{C}_5)/i = 0 \tag{3.47b}$$
$$m_i(s) = (\mathcal{C}_1 + \mathcal{C}_2 + \mathcal{C}_6 + \mathcal{C}_9)/i \tag{3.47c}$$
$$= D_0^T(s)\left[V_i(s) - V_0(s)\right] D_i(s) + 4D_0^T(s)\left[V_0(s)\vec{v}_i(s)\vec{v}_i^T(s) - \vec{v}_0(s)\vec{v}_0^T(s)V_i(s)\right] D_i(s)\,. \tag{3.47d}$$

Thus, the inner commutator of the Born approximation (3.34) simply takes the form

$$\left[H_\mathrm{I}(s),\, \rho_0(s)\otimes\rho_i(s)\right] = iJ_i\left(m_i(s)\vec{S}_i\right)\cdot\vec{S}_0\,. \tag{3.48}$$

As already mentioned, this notation helps dealing with the integral in the integro-differential equation (3.34), but it leads to an additional differential equation due to

$$\int_0^t \mathrm{d}s\left[H_\mathrm{I}(s),\, \rho_i(s)\otimes\rho_0(s)\right] = iJ_i\int_0^t \mathrm{d}s\left(m_i(s)\vec{S}_i\right)\cdot\vec{S}_0 = iJ_i\left(M_i(t)\vec{S}_i\right)\cdot\vec{S}_0\,. \tag{3.49}$$

The additional differential equation to solve is given by

$$\frac{\mathrm{d}}{\mathrm{d}t}M_i(t) = m_i(t)\,, \tag{3.50}$$

with the arbitrary chosen initial condition $M_i(0) = 0$.

The remaining task is to calculate the outer commutator which appears in the Born approximation (3.34). According to the previous calculation, the commutator to evaluate is given by $\left[H_\mathrm{I}(t),\, iJ_i\left(M_i(t)\vec{S}_i\right)\cdot\vec{S}_0\right]$. By directly including the partial trace Tr_0, every term $\propto \vec{S}_0$ vanishes. This helps to handle the size of the following expressions. Note that the time dependencies are once again omitted for a better readability.

$$\mathrm{Tr}_0\left[H_\mathrm{I}(t),\, iJ_i\left(M_i(t)\vec{S}_i\right)\cdot\vec{S}_0\right] \tag{3.51a}$$
$$= iJ_i^2\,\mathrm{Tr}_0\left[\left(D_0\vec{S}_0\right)\cdot\left(D_i\vec{S}_i\right) - \left(D_0\vec{S}_0\right)\cdot\vec{v}_i - \left(D_i\vec{S}_i\right)\cdot\vec{v}_0,\, \left(M_i\vec{S}_i\right)\cdot\vec{S}_0\right] \tag{3.51b}$$
$$= iJ_i^2\,\mathrm{Tr}_0\left[\left(D_0\vec{S}_0\right)\cdot\left(D_i\vec{S}_i\right),\, \left(M_i\vec{S}_i\right)\cdot\vec{S}_0\right] \tag{3.51c}$$
$$= iJ_i^2\,\mathrm{Tr}_0\left\{\sum_{\alpha\beta\gamma\delta\epsilon} D_0^{\alpha\beta}D_i^{\alpha\gamma}M_i^{\delta\epsilon}\left[S_0^\beta S_i^\gamma,\, S_i^\epsilon S_0^\delta\right]\right\} \tag{3.51d}$$
$$= -\frac{J_i^2}{4}\,\mathrm{Tr}_0\left\{\sum_{\alpha\beta\gamma\epsilon\tau} D_0^{\alpha\beta}D_i^{\alpha\gamma}M_i^{\beta\epsilon}S_i^\tau\epsilon_{\gamma\epsilon\tau}\right\} \tag{3.51e}$$
$$= -\frac{J_i^2}{4}\sum_{\gamma\epsilon\tau}\left(D_i^TD_0M_i\right)^{\gamma\epsilon}\epsilon_{\gamma\epsilon\tau}\sigma^\tau \tag{3.51f}$$

By using this expression, the whole differential equation (3.34) for $\rho_i(t)$ takes the form

$$\begin{aligned}\frac{\mathrm{d}}{\mathrm{d}t}\rho_i(t) = J_i \left[\left(D_i^T(t)D_0(t)\vec{c}(0) - D_i^T(t)\vec{v}_0(t)\right) \times \vec{b}_i(0)\right] \cdot \vec{\sigma} \\ + \frac{J_i^2}{4} \sum_{\gamma\epsilon\tau} \left(D_i^T(t)D_0(t)M_i(t)\right)^{\gamma\epsilon} \epsilon_{\gamma\epsilon\tau}\sigma^\tau \,. \end{aligned} \tag{3.52}$$

In order to obtain the equation of motion for the expectation value $\vec{v}_i(t)$, equation (3.33b) is used, which reads

$$\frac{\mathrm{d}}{\mathrm{d}t}\vec{v}_i(t) = \mathrm{Tr}_i \left[\underbrace{\left(\frac{\mathrm{d}}{\mathrm{d}t}\vec{s}_i(t) \right)}_{=J_i V_0(t)\vec{s}_i(t)} \rho_i(t) + \vec{s}_i(t) \underbrace{\left(\frac{\mathrm{d}}{\mathrm{d}t}\rho_i(t) \right)}_{\text{Born approximation}} \right] . \tag{3.53}$$

It consists of two parts with both being known now. The first term is the classical precession term, given as

$$\mathrm{Tr}_i \left[J_i V_0(t)\vec{s}_i(t)\rho_i(t)\right] = J_i \,\mathrm{Tr}_i \left[\frac{1}{2}V_0(t)D_i(t)\vec{\sigma}\left(\frac{1}{2}\mathbb{1} + \vec{b}_i(t)\cdot\vec{\sigma}\right)\right] \tag{3.54a}$$

$$= J_i V_0(t) D_i(t)\vec{b}_i(t) = J_i V_0(t)\vec{v}_i(t) \tag{3.54b}$$

$$= J_i \vec{v}_0(t) \times \vec{v}_i(t) \,. \tag{3.54c}$$

The second term, which describes the second order quantum mechanical correction in Born approximation, reads

$$\mathrm{Tr}_i \left[\vec{s}_i(t)\left(\frac{\mathrm{d}}{\mathrm{d}t}\rho_i(t)\right)\right] \tag{3.55a}$$

$$\begin{aligned} = \mathrm{Tr}_i \Bigg[\sum_{\alpha\beta} \frac{1}{2} D_i^{\alpha\beta}(t)\sigma^\beta \vec{e}_\alpha \Big(J_i \left[\left(D_i^T(t)D_0(t)\vec{c}(0) - D_i^T(t)\vec{v}_0(t)\right) \times \vec{b}_i(0)\right] \cdot \vec{\sigma} \\ + \frac{J_i^2}{4} \sum_{\gamma\epsilon\tau} \left(D_i^T(t)D_0(t)M_i(t)\right)^{\gamma\epsilon} \sigma^\tau \epsilon_{\gamma\epsilon\tau} \Big) \Bigg] \end{aligned} \tag{3.55b}$$

$$\begin{aligned} = J_i \left(D_0(t)\vec{c}(0) - \vec{v}_0(t)\right) \times \left(D_i(t)\vec{b}_i(0)\right) \\ + \frac{J_i^2}{4} \sum_{\alpha\beta\gamma\epsilon} D_i^{\alpha\beta}(t) \left(D_i^T(t)D_0(t)M_i(t)\right)^{\gamma\epsilon} \vec{e}_\alpha \epsilon_{\gamma\epsilon\beta} \,. \end{aligned} \tag{3.55c}$$

In principle, it is possible to further rewrite the second order term. Since it will not be really beneficial, it is refrained from doing this, meaning the current form is kept.

Inserting the expressions (3.54c) and (3.55c) into (3.53) yields the final equation of motion for the expectation value $\vec{v}_i(t)$,

$$\begin{aligned}\frac{\mathrm{d}}{\mathrm{d}t}\vec{v}_i(t) = J_i \left[\vec{v}_0(t) \times \vec{v}_i(t) + \left(D_0(t)\vec{c}(0) - \vec{v}_0(t)\right) \times \left(D_i(t)\vec{b}_i(0)\right)\right] \\ + \frac{J_i^2}{4} \sum_{\alpha\beta\gamma\epsilon} D_i^{\alpha\beta}(t) \left(D_i^T(t)D_0(t)M(t)\right)^{\gamma\epsilon} \vec{e}_\alpha \epsilon_{\gamma\epsilon\beta} \,. \end{aligned} \tag{3.56}$$

Now due to symmetry, it is easy to derive the appropriate equation of motion for $\vec{v}_0(t)$,

$$\frac{\mathrm{d}}{\mathrm{d}t}\vec{v}_0(t) = \mathrm{Tr}_0\left[\underbrace{\left(\frac{\mathrm{d}}{\mathrm{d}t}\vec{s}_0(t)\right)}_{=V_{\mathrm{eff}}(t)\vec{s}_0(t)}\rho_0(t) + \vec{s}_0(t)\underbrace{\left(\frac{\mathrm{d}}{\mathrm{d}t}\rho_0(t)\right)}_{\text{Bornapproximation}}\right]. \tag{3.57}$$

Just as before, the first term of equation (3.57) reads

$$\mathrm{Tr}_0\left[V_{\mathrm{eff}}(t)\vec{s}_0(t)\rho_0(t)\right] = \vec{B}_{\mathrm{eff}}(t)\times\vec{v}_0(t)\,. \tag{3.58a}$$

The second term of equation (3.57) requires deriving the Born approximation for $\rho_0(t)$, which is again a very similar procedure.

Starting with the outer commutator (3.51a), but now with Tr_i instead of Tr_0, yields

$$\mathrm{Tr}_i\left[H_{\mathrm{I}}(t),\, iJ_i\left(M_i^T(t)\vec{S}_0\right)\cdot\vec{S}_i\right] = iJ_i^2\,\mathrm{Tr}_i\left[\left(D_0\vec{S}_0\right)\cdot\left(D_i\vec{S}_i\right),\,\left(M_i^T\vec{S}_0\right)\cdot\vec{S}_i\right] \tag{3.59a}$$

$$= -\frac{J_i^2}{4}\sum_{\gamma\epsilon\tau}\left(D_0^T D_i M_i^T\right)^{\gamma\epsilon}\epsilon_{\gamma\epsilon\tau}\sigma^\tau\,. \tag{3.59b}$$

Comparing this expression to equation (3.51f), only the indices of the rotation matrices $D_{0/i}(t)$ have switched and $M_i(t)$ has been replaced by its transpose $M_i^T(t)$. Hence, the differential equation for $M_i(t)$ has to be solved only once.

As a result, the Born approximation for $\rho_0(t)$ takes the form

$$\begin{aligned}\frac{\mathrm{d}}{\mathrm{d}t}\rho_0(t) = {}& J_i\left[\left(D_0^T(t)D_i(t)\vec{b}_i(0) - D_0^T(t)\vec{v}_i(t)\right)\times\vec{c}(0)\right]\cdot\vec{\sigma}(t)\\ &+\frac{J_i^2}{4}\sum_{\gamma\epsilon\tau}\left(D_0^T(t)D_i(t)M_i^T(t)\right)^{\gamma\epsilon}\epsilon_{\gamma\epsilon\tau}\sigma^\tau\,.\end{aligned} \tag{3.60}$$

Thus, the second term of equation (3.57) reads

$$\begin{aligned}\mathrm{Tr}_0\left[\vec{s}_0(t)\left(\frac{\mathrm{d}}{\mathrm{d}t}\rho_0(t)\right)\right] = {}& J_i\left(D_i(t)\vec{b}_i(0) - \vec{v}_i(t)\right)\times\left(D_0(t)\vec{c}(0)\right)\\ &+\frac{J_i^2}{4}\sum_{\alpha\beta\gamma\epsilon}D_0^{\alpha\beta}(t)\left(D_0^T(t)D_i(t)M_i^T(t)\right)^{\gamma\epsilon}\vec{e}_\alpha\epsilon_{\gamma\epsilon\beta}\,.\end{aligned} \tag{3.61}$$

As a result, the final equation of motion for the central spin expectation value $\vec{v}_0(t)$ is given by

$$\begin{aligned}\frac{\mathrm{d}}{\mathrm{d}t}\vec{v}_0(t) = {}& \vec{B}_{\mathrm{eff}}(t)\times\vec{v}_0(t) + J_i\left(D_i(t)\vec{b}_i(0) - \vec{v}_i(t)\right)\times\left(D_0(t)\vec{c}(0)\right)\\ &+\frac{J_i^2}{4}\sum_{\alpha\beta\gamma\epsilon}D_0^{\alpha\beta}(t)\left(D_0^T(t)D_i(t)M_i^T(t)\right)^{\gamma\epsilon}\vec{e}_\alpha\epsilon_{\gamma\epsilon\beta}\,,\end{aligned} \tag{3.62}$$

with the effective magnetic field $\vec{B}_{\mathrm{eff}}(t) = -\vec{B} + J_i\vec{v}_i(t)$.

In the following, a summary of the whole differential equation (DEQ) system is compiled.

$$\frac{\mathrm{d}}{\mathrm{d}t}D_0(t) = V_{\mathrm{eff}}(t)D_0(t) \tag{3.63a}$$

$$\frac{\mathrm{d}}{\mathrm{d}t}D_i(t) = J_i V_0(t)D_i(t) \tag{3.63b}$$

$$\begin{aligned}\frac{\mathrm{d}}{\mathrm{d}t}\vec{v}_0(t) = {}& \vec{B}_{\mathrm{eff}}(t) \times \vec{v}_0(t) + J_i \left(D_i(t)\vec{v}_i(0) - \vec{v}_i(t)\right) \times \left(D_0(t)\vec{v}_0(0)\right) \\ & + \frac{J_i^2}{4} \sum_{\alpha\beta\gamma\epsilon} D_0^{\alpha\beta}(t) \left(D_0^T(t)D_i(t)M^T(t)\right)^{\gamma\epsilon} \vec{e}_\alpha \epsilon_{\gamma\epsilon\beta}\end{aligned} \tag{3.63c}$$

$$\begin{aligned}\frac{\mathrm{d}}{\mathrm{d}t}\vec{v}_i(t) = {}& J_i\vec{v}_0(t) \times \vec{v}_i(t) + J_i \left(D_0(t)\vec{v}_0(0) - \vec{v}_0(t)\right) \times \left(D_i(t)\vec{v}_i(0)\right) \\ & + \frac{J_i^2}{4} \sum_{\alpha\beta\gamma\epsilon} D_i^{\alpha\beta}(t) \left(D_i^T(t)D_0(t)M(t)\right)^{\gamma\epsilon} \vec{e}_\alpha \epsilon_{\gamma\epsilon\beta}\end{aligned} \tag{3.63d}$$

$$\begin{aligned}\frac{\mathrm{d}}{\mathrm{d}t}M_i(t) = {}& D_0^T(t) \left[V_i(t) - V_0(t)\right] D_i(t) \\ & + 4D_0^T(t) \left[V_0(t)\vec{v}_i(t)\vec{v}_i^T(t) - \vec{v}_0(t)\vec{v}_0^T(t)V_i(t)\right] D_i(t)\end{aligned} \tag{3.63e}$$

Just as planned, the classical precession terms (3.22) appear directly in the equations (3.63c) and (3.63d) . The classical precession of the central spin around the effective magnetic field $\vec{B}_{\mathrm{eff}}(t) = -\vec{B} + J_i\vec{v}_i(t)$ is described by the first cross product which appears in equation (3.63c). The precession of the bath spin around the central spin is given through the first cross product in equation (3.63d). The remaining parts are required to calculate the second order quantum mechanical correction. It is not easy to give a meaningful physical interpretation for these terms. They mainly consist of various combinations of rotations.

The initial conditions are given by

$$D_{0/i}(0) = \mathbb{1}\,, \tag{3.64a}$$

$$\vec{v}_0(0) = D_0(0)\vec{c}(0) = \vec{c}(0)\,, \tag{3.64b}$$

$$\vec{v}_i(0) = D_i(0)\vec{b}_i(0) = \vec{b}_i(0)\,, \tag{3.64c}$$

$$M_i(0) = 0\,. \tag{3.64d}$$

The initial spin polarizations $\vec{v}_{0/i}(0)$ can be chosen almost freely. It only has to be ensured that the related density matrices are positive semidefinite. This is accomplished by the constraint $|\vec{v}_{0/i}(0)| \leq 1/2$.

In principle, it is possible to drastically simplify the DEQ system (3.63) for some special initial polarizations, for example if some components of the vectors $\vec{v}_{0/i}(0)$ are chosen to be zero. In such cases, many terms vanish so that they can be neglected a priori, which improves computation times.

Note that even third order terms occur in the DEQ system (3.63). They are not as obvious, though. This does not mean that the corrections are exact in third order of the coupling constant J_i. For example, the expression $J_i \left(D_i(t)\vec{v}_i(0) - \vec{v}_i(t)\right) \times \left(D_0(t)\vec{v}_0(0)\right)$, appearing in equation (3.63c), is of third order in the coupling constant J_i because the term

$(D_i(t)\vec{v}_i(0) - \vec{v}_i(t))$ is of second order itself. This is due to $D_i(t)\vec{v}_i(0)$ being exact in first order, since $D_i(t)$ only describes the classical precession of the bath spin around the central spin, while $\vec{v}_0(t)$ is being exact in second order. Physically, this third order term can be interpreted as a precession of the deviation from the classical bath spin expectation value around the classical central spin expectation value. Of course, the same argument is also valid for equation (3.63d).

3.3.2 Error analysis and first results

The Born approximation should yield a DEQ system which is correct up to second order in the coupling constant J_i. In order to study and confirm the correct error dependencies of the expectation values $\vec{v}_{0/i}$ in Born approximation, exact calculations are required as well. These are performed by solving the exact von Neumann equation in the Schrödinger picture

$$\frac{\mathrm{d}}{\mathrm{d}t}\rho(t) = -i\,[H,\,\rho(t)] \tag{3.65}$$

numerically. Since the CSM Hamiltonian H (2.3) describes a two spin system for $N = 1$, corresponding to a four dimensional Hilbert space, this differential equation is easily solved numerically using the classical Runge-Kutta method (RK4). The DEQ system (3.63) is solved using the same algorithm.

The orthogonality of $D_{0/i}(t)$ functions as an additional but very trivial check. This requires the calculation of $D^T_{0/i}(t)D_{0/i}(t) = \mathbb{1}$, which can be easily executed throughout the simulation. As a first result, this relation is fulfilled throughout all following calculations.

The initial spin polarizations are arbitrary chosen to be

$$\vec{v}_i(0) = \begin{pmatrix} 0.240525 \\ -0.144902 \\ 0.413704 \end{pmatrix}, \qquad \vec{v}_0(0) = \begin{pmatrix} -0.393780 \\ -0.290984 \\ 0.101283 \end{pmatrix}, \tag{3.66}$$

with $|\vec{v}_{0/i}(0)| = 1/2$.

For the case of a finite external magnetic field, the field is taken as

$$\vec{B} = \begin{pmatrix} \sqrt{1 - \cos^2\left(\frac{40}{180}\pi\right)} \\ 0 \\ \cos\left(\frac{40}{180}\pi\right) \end{pmatrix} = \begin{pmatrix} 0.642788 \\ 0 \\ 0.766044 \end{pmatrix}, \tag{3.67}$$

with $|\vec{B}| = 1$ and $\measuredangle\left(\vec{B},\, \vec{e}_z\right) = 40\,^\circ$.

The main error of interest is given by the deviation from the exact expectation value at a fixed time t,

$$|\Delta v^\alpha_{0/i}(J_i)| = |\vec{v}_{0/i}(J_i) - \vec{v}_{0/i,\mathrm{exact}}(J_i)|\,. \tag{3.68}$$

This error is expected to be at least of third order $\mathcal{O}\left(J_i^3\right)$ because in the Born approximation, all second order corrections are taken into account. If the derived DEQ system (3.63) showed an error of, e. g., $\mathcal{O}\left(J_i^2\right)$, this system would have to be considered as flawed. Note that for very small times t or coupling constant J_i, a possible power law is suppressed by the numerical accuracy. Additionally, once the error is in the order of the initial values, it cannot be described by a power law anymore.

Throughout this subsection, the energy J_U is defined to define the unit of the coupling J_i and the external magnetic field $\vec{B}$. Since natural units ($\hbar = 1$) are used, the inverse J_U^{-1} determines the unit of the time t. Explicitly, $J_\mathrm{U} = 1$ is used for the numerical calculations.

In the case of a vanishing magnetic field $|\vec{B}| = 0$, no other energy scale but the coupling constant J_i appears. Therefore, a dimensional analysis shows that the time depending error $|\Delta\vec{v}_{0/i}(t)|$ has to follow the same power law as $|\Delta\vec{v}_{0/i}(J_i)|$, meaning $\mathcal{O}\left(t^3\right)$. As shown in Figure 3.1a, this is clearly the case. Both errors follow the correct third order power law. Note that the calculated errors are plotted in a double logarithmic way. In this case, the power law $v_0^\alpha \propto J_i^m$ is reduced to a linear function with gradient m, which renders it easy to obtain the correct gradient from the plots without a fit.

As an additional check, the time t_tol, at which the observed error is equal to some tolerated error $|\Delta\vec{v}_{0/i}\left(t_\mathrm{tol}\right)| =: \Delta_\mathrm{tol}$, is introduced. This tolerated error is chosen as $\Delta_\mathrm{tol} = 10^{-4}$. Since natural units ($\hbar = 1$) are used, $|\Delta\vec{v}_{0/i}|$ has to be dimensionless. This means that the relation

$$|\Delta\vec{v}_{0/i}| \propto J_i^3 t^3 \tag{3.69}$$

has to hold because t has the unit of an inverse energy. As a consequence, the time t_tol has to follow the power law

$$t_\mathrm{tol} \propto J_i^{-3/3} = J_i^{-1}\,. \tag{3.70}$$

This behavior is confirmed in Figure 3.1a.

In contrast, the case of a finite magnetic field $|\vec{B}| = J_\mathrm{U}$ is a little bit more complicated due to an additional timescale introduced through $\vec{B}$. This leads to additional oscillations in the solution and therefore to crossings in the error of each component. By studying the absolute value of the error-vector $|\Delta\vec{v}_{0/i}|$, this effect is somewhat suppressed. Some artifacts will remain, though. While $|\Delta\vec{v}_{0/i}(J_i)|$ is still expected to be at least of order $\mathcal{O}\left(J_i^3\right)$, this must not be necessarily the case for $|\Delta\vec{v}_{0/i}(t)|$ anymore. As shown in Figure 3.1b, the error $\Delta\vec{v}_{0/i}(J)$ is proportional to J_i^3. This is the expected power law.

As mentioned before, the error dependency on the time t is not as obvious due to an additional energy scale introduced by the external field $\vec{B}$. However, Figure 3.1b suggests that $|\Delta\vec{v}_{0/i}(t)| \propto t^3$ is the adequate power law to describe this error. Then once again due to dimensional reasons, the time tol has to follow the power law

$$t_\mathrm{tol} \propto J_i^{-1}\,. \tag{3.71}$$

This is also confirmed in Figure 3.1b.

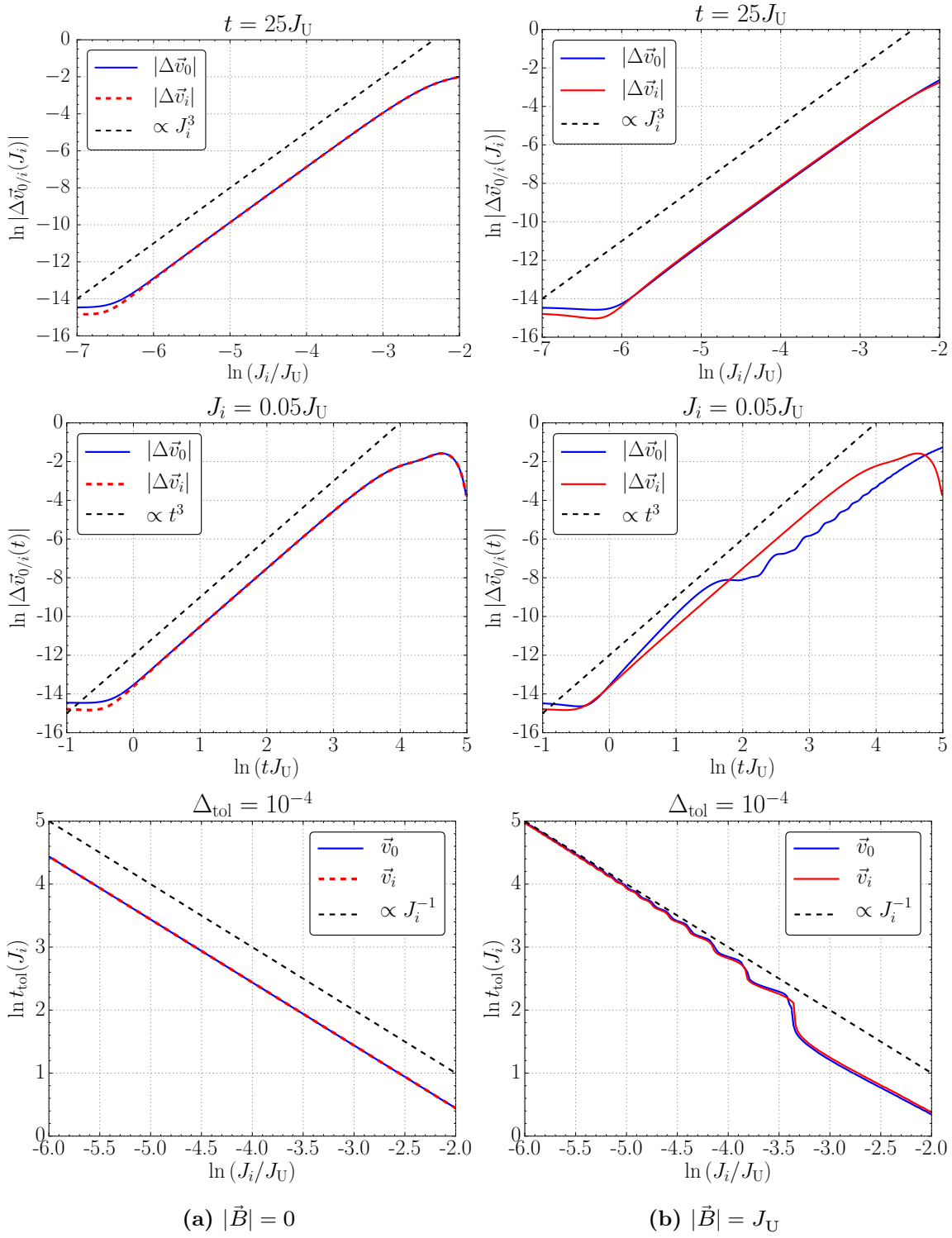

(a) $|\vec{B}| = 0$ **(b)** $|\vec{B}| = J_\mathrm{U}$

Figure 3.1: Various error analyses for the case of **(a)** a *vanishing* and **(b)** a *finite* external magnetic field $\vec{B}$. Depending on the studied error, the parameters t, J_i, and Δ_tol have to be kept constant. The constant values are given above each plot. The appropriate power laws are plotted as black dashed lines.

As a conclusion, the error $|\Delta\vec{v}_{0/i}(J_i)| \propto J_i^3$ follows the correct power law for (a) a vanishing and (b) a finite external field. This is confirmed by a dimensional analysis, which is very precise for the vanishing external field and within the expected accuracy for the finite external field. A check for each individual component has been performed as well. It leads to the same observations as before. As a result, the derived DEQ system (3.63) has to be considered as correct so that no term is wrong or missing.

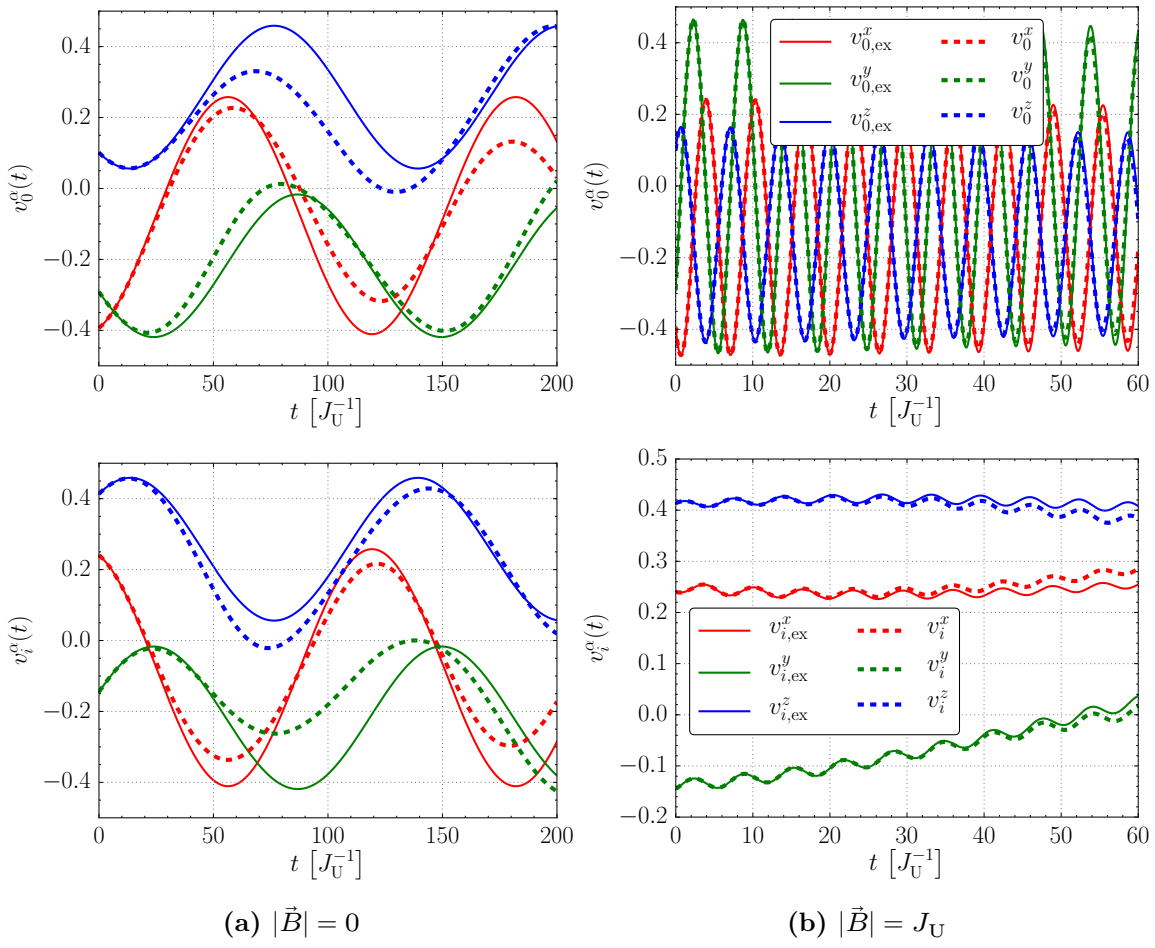

(a) $|\vec{B}| = 0$ **(b)** $|\vec{B}| = J_\mathrm{U}$

Figure 3.2: Comparison between the exact and the approximated dynamics of $\vec{v}_{0/i}(t)$ for the case of **(a)** a *vanishing* and **(b)** a *finite* external magnetic field $|\vec{B}|$. The coupling constant is chosen as $J_i = 0.05 J_\mathrm{U}$.

Examples for the explicit dynamics of $\vec{v}_{0/i}(t)$ for the above studied cases are given in Figure 3.2. The coupling constant is chosen as $J_i = 0.05 J_\mathrm{U}$. In case (a), meaning no external magnetic field is applied to the central spin, the only timescale is given trough the coupling between both spins, determined by the inverse coupling constant J_i^{-1}. While it can be argued that qualitative behavior of $\vec{v}_{0/i}(t)$ is similar to the exact solution, the quantitative deviation is clearly visible at $t \approx 25 J_\mathrm{U}^{-1}$. This is much earlier than the classical precession period $T = {}^{2\pi}/_{J_i} \approx 125.7 J_\mathrm{U}^{-1}$ promotes, meaning quantum mechanical effects play an important role already for short times.

In case (b), the dynamics are mostly driven by the oscillations induced through the finite external magnetic field $|\vec{B}| = J_\mathrm{U}$. This classical precession corresponds to the period $T_\mathrm{B} = {}^{2\pi}/_{J_\mathrm{U}} \approx 6.3 J_\mathrm{U}^{-1}$. It is included exactly in the Born approach and clearly visible in Figure 3.2b. First deviations appear at $t \approx 40 J_\mathrm{U}^{-1}$. They seem to increase slower in time compared to the case with vanishing external field. This is due to J_i being 20 times smaller than $|\vec{B}$, meaning the exact classical precession dominates the short time dynamics while quantum mechanical effects are mainly important for longer times $t \gg T_\mathrm{B}$.

Note that if the bath consists of only *one* bath spin, the used weak-coupling approximation (3.11) is only valid for $J_i \ll |\vec{B}|$. Otherwise, the argument of separated timescales for the classical and the interacting part is invalid. Remember that the weak-coupling approximation is valid for large bath sizes N when dealing with a vanishing or small external magnetic field. This leads to overall larger errors for the case of a vanishing magnetic field compared to the finite case with J_i being 20 times smaller than $|\vec{B}|$. Additionally, it is interesting to see that for $N = 1$, despite using the invalid weak-coupling approximation (3.11) for the case of a vanishing field, the discussed errors obey the correct power laws.

Later for the whole central spin model with large bath sizes and without an external field, the classical precession leads to much faster dynamics compared to the second order corrections. Thus, the present approach should yield better results for larger bath sizes N.

3.3.3 Extension to the full central spin model

Extending the previous results (3.63) for the simple two spin system to the whole central spin model mainly requires taking the additional sum over all N bath spins for the dynamics of $\vec{v}_0(t)$ and $D_0(t)$ into account.

The split Hamiltonian (3.24) is now studied for an arbitrary number of bath spins N. It is once again given by

$$H(t) = \sum_{i=1}^{N} J_i \vec{S}_0(t) \cdot \vec{S}_i(t) - \vec{B} \cdot \vec{S}_0(t) \tag{3.72a}$$

$$= \underbrace{\sum_{i=1}^{N} J_i \left(\vec{S}_0(t) - \vec{v}_0(t)\right) \cdot \left(\vec{S}_i(t) - \vec{v}_i(t)\right)}_{=:H_\mathrm{I}(t)}$$

$$\underbrace{+ \left(\sum_{i=1}^{N} J_i \vec{v}_i(t) - \vec{B}\right) \cdot \vec{S}_0(t) + \sum_{i=1}^{N} J_i \vec{v}_0(t) \cdot \vec{S}_i(t) - \sum_{i=1}^{N} J_i \vec{v}_0(t) \cdot \vec{v}_i(t)}_{=:H_0(t)} . \tag{3.72b}$$

Shifting the dynamics given through $H_0(t)$ into the spin operators $\vec{S}_{0/i}(t)$ is easy and works just as in subsection 3.3.1 for the case $N = 1$. Because all new terms in the Hamiltonian $H_0(t)$ commute within the Heisenberg equation of motion, the differential equation (3.63b) for $D_i(t)$ remains the same. A differential equation for each $i \in \{1, \dots, N\}$ has to be solved

now, though. For $D_0(t)$, an additional sum over all bath spins i with couplings J_i has to be included, meaning the effective magnetic field now takes the form

$$\vec{B}_{\text{eff}} = -\vec{B} + \sum_{i=1}^{N} J_i \vec{v}_i(t)\,. \tag{3.73}$$

The central spin precesses around this effective field, consisting of the external magnetic field (if applied) and the Overhauser field.

In second order, new terms that indirectly couple two different bath spins to each other could contribute to the dynamics of the expectation values $\vec{v}_{0/i}(t)$. Therefore, new features that might occur in Born approximation have to be identified.

Due to the larger Hilbert space for $N+1$ spins, the total density matrix in weak-coupling approximation (3.11) has the more complicated structure

$$\rho(t) = \left(\frac{1}{2}\mathbb{1} + \vec{c}(t)\cdot\vec{\sigma}\right) \otimes \left(\frac{1}{2}\mathbb{1} + \vec{b}_1(t)\cdot\vec{\sigma}\right) \otimes \cdots \otimes \left(\frac{1}{2}\mathbb{1} + \vec{b}_N(t)\cdot\vec{\sigma}_N\right)\,. \tag{3.74a}$$

However, only combinations of a maximal number of three spin operators can contribute to the dynamics in second order because a maximum of two commutators has to be evaluated for the Born approximation (3.7). Hence, most terms in equation (3.74a) will not yield a contribution and can therefore be neglected a priori.

The relevant part of $\rho(t)$ is represented by

$$\begin{aligned}\rho(t) = {} & \frac{1}{2^{N+1}}\mathbb{1} + \frac{1}{2^{N-1}}\vec{c}(t)\cdot\vec{S}_0 + \frac{1}{2^{N-1}}\sum_{i=1}^{N}\vec{b}_i(t)\cdot\vec{S}_i + \frac{1}{2^{N-3}}\sum_{i=1}^{N}\left(\vec{c}(t)\cdot\vec{S}_0\right)\left(\vec{b}_i(t)\cdot\vec{S}_i\right) \\ & + \frac{1}{2^{N-5}}\sum_{i=1}^{N-1}\sum_{j>i}\left(\vec{c}(t)\cdot\vec{S}_0\right)\left(\vec{b}_i(t)\cdot\vec{S}_i\right)\left(\vec{b}_j(t)\cdot\vec{S}_j\right) + \ldots\,.\end{aligned} \tag{3.75}$$

While calculating the whole nested commutator which appears in the Born approximation (3.7), only terms of the inner commutator that can be written as a part of

$$[H_{\text{I}}(s),\,\rho(s)] = \frac{i}{2^{N-1}}\sum_{i=1}^{N} J_i\left[\vec{p}_i(s)\cdot\vec{S}_i + \vec{q}_i(s)\cdot\vec{S}_0 + \left(m_i(s)\vec{S}_i\right]\cdot\vec{S}_0\right) \tag{3.76}$$

will contribute later after calculating the trace. The prefactor $\frac{1}{2^{N-1}}$ is included in order to obtain the same prefactors as in the final equations of motion as for the two spin system ($N=1$) discussed in subsection 3.3.1.

It is obvious that a sum over all bath spins i occurs for the differential equations describing $D_0(t)$ and $\vec{v}_0(t)$. Now, due to the more complex structure of the total density matrix $\rho(t)$ and the possibility of combining different bath spins, new terms which yield a non-vanishing contribution according to equation (3.76) have to be identified. The only new terms to consider are

$$\begin{aligned}&\left[-J_j\left(D_0(s)\vec{S}_0\right)\cdot\vec{v}_j(s),\,\frac{1}{2^{N-3}}\left(\vec{c}(s)\cdot\vec{S}_0\right)\left(\vec{b}_i(s)\cdot\vec{S}_i\right)\right] \\ &= \frac{i}{2^{N-3}}J_j\left[D_0^T(s)V_0(s)\vec{v}_j(s)\vec{v}_i^T(s)D_i(s)\vec{S}_i\right]\cdot\vec{S}_0\end{aligned} \tag{3.77}$$

and (for $i \neq j$)

$$\left[J_j\vec{S}_0(s)\cdot\vec{S}_j(s),\, \frac{1}{2^{N-5}}\left(\vec{c}(s)\cdot\vec{S}_0\right)\left(\vec{b}_i(s)\cdot\vec{S}_i\right)\left(\vec{b}_j(s)\cdot\vec{S}_j\right)\right] \tag{3.78}$$
$$= -\frac{i}{2^{N-3}}J_j\left[\left(D_0^T(s)V_0(s)\vec{v}_j(s)\vec{v}_i^T(s)D_i(s)\vec{S}_i\right)\cdot\vec{S}_0 + \left(D_j^T(s)V_j(s)\vec{v}_0(s)\vec{v}_i^T(s)D_i(s)\vec{S}_i\right)\cdot\vec{S}_j\right].$$

It is refrained from giving the detailed calculation because both commutators are very similar to the commutators $\mathcal{C}_i$ that are calculated in subsection 3.3.1. Note that the second term of the second commutator (3.78) is $\propto S_iS_j$, with $i \neq j$. Therefore, it is not contributing to the dynamics as it cannot be written in terms of equation (3.76) and thus, it would vanish anyway later while calculating the trace.

Interestingly, the remaining terms cancel out each other for all $i \neq j$. Therefore, no contributions of second order $\mathcal{O}\left(J_iJ_j\right)$, coupling different bath spins to each other, occur within Born approximation. It is best to convince oneself that this is really true, for instance for $N = 3$. In this case, the first commutator (3.77) contributes with six different combinations of i and j. The same amount of combinations appear for the second commutator (3.78). Hence, both cancel out each other for $i \neq j$. Moreover, for $i = j$, the second commutator (3.78) does not exist while the first commutator (3.77) remains because it already appears for $N = 1$ as discussed in subsection 3.3.1 (see equation (3.42)).

These thoughts combined lead to the final set of differential equations for the central spin model within Born approximation. Overall, not much has changed compared to the case $N = 1$. The main difference is an additional sum which runs over all bath spins for $\frac{\mathrm{d}}{\mathrm{d}t}\vec{v}_0(t)$. This sum also appears in the effective magnetic field $\vec{B}_{\mathrm{eff}}(t)$ (3.73) which appears in the DEQ for $D_0(t)$ as the skew-symmetric matrix $V_{\mathrm{eff}}(t)$. See equation (3.25b) for how $V_{\mathrm{eff}}(t)$ has been introduced. Additionally, differential equations have to be solved for all bath spins $i \in \{1, \dots, N\}$ for $D_i(t)$, $M_i(t)$ and $\vec{v}_i(t)$. No other new features appear.

A summary of the full differential equation system is given below.

$$\frac{\mathrm{d}}{\mathrm{d}t}D_0(t) = V_{\mathrm{eff}}(t)D_0(t) \tag{3.79a}$$

$$\frac{\mathrm{d}}{\mathrm{d}t}D_i(t) = J_iV_0(t)D_i(t) \tag{3.79b}$$

$$\begin{aligned}\frac{\mathrm{d}}{\mathrm{d}t}\vec{v}_0(t) &= \vec{B}_{\mathrm{eff}}(t)\times\vec{v}_0(t) + \sum_{i=1}^{N}J_i\left(D_i(t)\vec{v}_i(0) - \vec{v}_i(t)\right)\times\left(D_0(t)\vec{v}_0(0)\right)\\ &\quad + \sum_{i=1}^{N}\frac{J_i^2}{4}\sum_{\alpha\beta\gamma\epsilon}D_0^{\alpha\beta}(t)\left(D_0^T(t)D_i(t)M_i^T(t)\right)^{\gamma\epsilon}\vec{e}_\alpha\epsilon_{\gamma\epsilon\beta}\end{aligned} \tag{3.79c}$$

$$\begin{aligned}\frac{\mathrm{d}}{\mathrm{d}t}\vec{v}_i(t) &= J_i\vec{v}_0(t)\times\vec{v}_i(t) + J_i\left(D_0(t)\vec{v}_0(0) - \vec{v}_0(t)\right)\times\left(D_i(t)\vec{v}_i(0)\right)\\ &\quad + \frac{J_i^2}{4}\sum_{\alpha\beta\gamma\epsilon}D_i^{\alpha\beta}(t)\left(D_i^T(t)D_0(t)M_i(t)\right)^{\gamma\epsilon}\vec{e}_\alpha\epsilon_{\gamma\epsilon\beta}\end{aligned} \tag{3.79d}$$

$$\begin{aligned}\frac{\mathrm{d}}{\mathrm{d}t}M_i(t) &= D_0^T(t)\left[V_i(t) - V_0(t)\right]D_i(t)\\ &\quad + 4D_0^T(t)\left[V_0(t)\vec{v}_i(t)\vec{v}_i^T(t) - \vec{v}_0(t)\vec{v}_0^T(t)V_i(t)\right]D_i(t)\end{aligned} \tag{3.79e}$$

Note that the differential equations (3.79b) (3.79d) and (3.79e) have to be solved for $i \in \{1, \dots, N\}$, meaning for each individual bath spin. This also means that the size of the DEQ system scales linearly with the bath size N, which allows to deal with the physical relevant large baths. The initial conditions are the same as for $N = 1$. They are listed in equation (3.64), now just with a larger number of bath spins. Solving this DEQ system (3.79) numerically to calculate the expectation values $\vec{v}_{0/i}(t)$ will be referred to as the *Born approach*.

The interpretation of the DEQ system (3.79) is almost the same as for the the case $N = 1$, which is discussed in subsection 3.3.1. Most importantly, the classical precession terms (3.22) are directly included. This was the reason to use the split Hamiltonian (3.24) in the first place. The difference is that the central spin precesses around the effective magnetic field $\vec{B}_{\text{eff}}$, which now consists of the external magnetic field and the *whole* classical Overhauser field $\vec{A} = \sum_{i=1}^{N} J_i \vec{v}_i(t)$. This is the classical part which describes the fast dynamics in the system (see equation (3.22)). Now for the second order correction, each bath spin yields a contribution to the central spin dynamic. However, no terms of order $\mathcal{O}\left(J_i J_j\right)$, coupling different bath spins to each other, appear.

In principle, it is also possible to calculate the expectation value of other observables. This is due to the chosen parameterization, allowing the total density matrix of the system $\rho(t)$ in weak-coupling approximation (3.11) to be calculated if the matrices $D_{0/i}(t)$ and the expectation values $\vec{v}_{0/i}(t)$ were known. An example for an interesting alternative observable is the autocorrelation function $\langle \vec{S}_0(t) \vec{S}_0(0) \rangle$, which is often studied in other works [19, 20, 22, 23, 28]. In this thesis, though, the focus lies on the time evolution of the expectation values $\vec{v}_{0/i}(t)$.

4 Numerical analysis

In this chapter, a numerical analysis of the derived DEQ system (3.79) for the spin expectation values $\vec{v}_{0/i}(t)$ is performed in order to verify its correctness and completeness. This is performed by analyzing the power law of the time-dependent errors $\Delta\vec{v}_{0/i}(t)$ for the case of a vanishing external field. Additionally, first results for the dynamics of $\vec{v}_{0/i}(t)$ are studied and compared to exact or alternative approaches. Diverse coupling distributions and initial polarizations are considered, with and without an external field coupling to the central spin.

The numerical solution of the DEQ system (3.79) is calculated by the usage of the classical Runge-Kutta method (RK4), implemented in C++. No adaptive stepsize is used because the calculations can still be executed fast and accurate with the sufficiently small constant stepsize of $h = 0.001$.

4.1 Error analysis and results for a small bath

In order to verify the correctness and completeness of the DEQ system (3.79), an error analysis similar to subsection 3.3.2 is performed. Since the correct inclusion of the external magnetic field $\vec{B}$ is already confirmed there, it is sufficient to only study the case of a vanishing external field $|\vec{B}| = 0$. Due to the exponentially growing Hilbert space, the exact dynamics can be calculated numerically by solving the von Neumann equation only for a limited bath size of about $N = 8$. However, this size is sufficient to verify that all possible new terms have been taken into account in the correct manner.

In contrast to the case $N = 1$, different coupling distributions J_i can be studied here. For the test of correctness, it is convenient to discuss a uniform coupling distribution (also known as box model)

$$J_i = \frac{J_{\mathrm{Q}}}{\sqrt{N}} \qquad \forall\, i \in \{1, \dots, N\} \; . \tag{4.1}$$

It is normalized such that $J_{\mathrm{Q}}^2 = 1$ holds numerically. This way, the error is still expected to be of third order, meaning $\mathcal{O}\left(J_i^3\right)$. Because of the missing external field, the only energy scale is given through the coupling constants J_i. Hence, it is sufficient to study the time-dependent error $\Delta v_{0/i}^{\alpha}(t)$ which requires less calculations. Due to dimensional reasons, this dimensionless error has to follow the same power law as $\Delta v_{0/i}^{\alpha}(t)$, meaning $\Delta v_{0/i}^{\alpha}(t) \propto t^3$ if $\Delta v_{0/i}^{\alpha}(J) \propto J_i^3$.

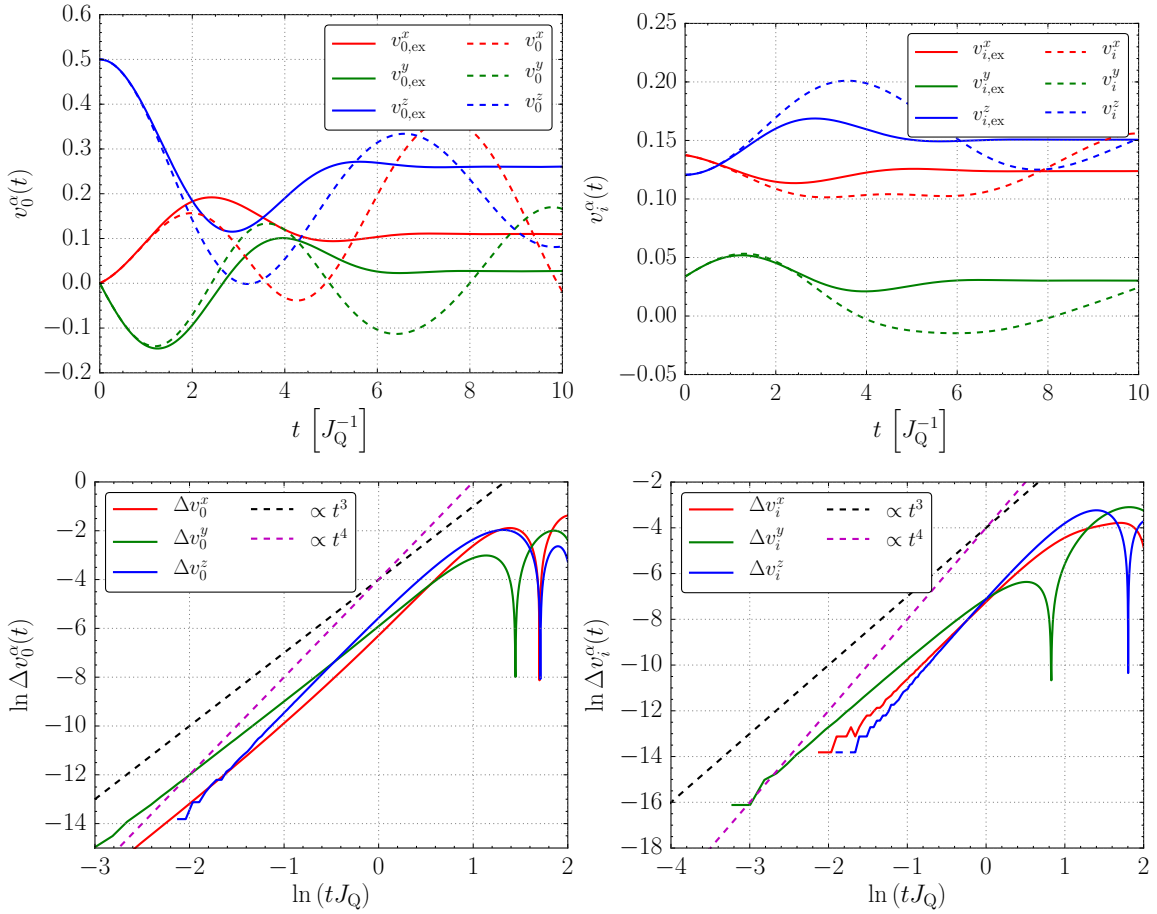

(a) $\vec{v}_0(t)$ **(b)** $\vec{v}_i(t)$

Figure 4.1: Realtime dynamics of the expectation values $\vec{v}_{0/i}(t)$ and time-dependent errors $\Delta\vec{v}_{0/i}(t)$ for a system of $N = 8$ bath spins and uniform coupling constants. No external magnetic field is applied. The central spin $\vec{v}_0(0)$ is fully polarized in $+z$ direction so that it is initially in a pure state. The dashed lines in the error plots indicate the appropriate third and fourth order power laws.

The initial polarization of the central spin is chosen as

$$\vec{v}_0(0) = \begin{pmatrix} 0 \\ 0 \\ \frac{1}{2} \end{pmatrix} \tag{4.2}$$

so that it is fully polarized in $+z$ direction. This is a pure state. The term *fully $+z$ polarized* is used to describe the central spin being initially in its up-state $|\uparrow\rangle$, corresponding to the density operator $\rho_0 = |\uparrow\rangle\langle\uparrow|$, which is the projector on the up-state.

Note that solving the classical equations of motion (3.22) for these initial polarizations would lead to no dynamics emerging at all because all cross products would simply vanish. This means that the Born approximation at least leads to an obvious improvement of the classical solution.

Each bath spin is chosen with $|\vec{v}_i(0)| \leq 1/2$ to ensure that the corresponding density matrix is positive semidefinite. The resulting errors $\Delta v^{\alpha}_{0/i}(t)$ and the related dynamics for the central spin and for one arbitrary bath spin i are shown in Figure 4.1. Obviously, the error shows the correct power law. For the x and y components of $\vec{v}_{0/i}(t)$, it is of third order $\mathcal{O}(t^3)$. For the z component, the error is even of fourth order $\mathcal{O}(t^4)$, meaning no third order corrections exist. This is due to the special initial polarization of the central spin with vanishing x and y component. Unfortunately, a noticeable difference of the Born from the exact solution is visible already at $t \approx J_{\mathrm{Q}}^{-1}$. The main characteristics of the exact solution are the almost constant values of $v^{\alpha}_{0/i}(t)$ for longer times t. This feature is not captured when using the Born approach.

An identical analysis is performed for the same initial polarizations of the bath spins but for an arbitrary chosen initial polarization of the central spin

$$\vec{v}_0(0) = \begin{pmatrix} 0.2 \\ -0.4 \\ -0.1 \end{pmatrix} . \tag{4.3}$$

This corresponds to a mixed state due to $|\vec{v}_0(0)| < 1/2$. The resulting errors and the related dynamics are shown in Figure 4.2. The errors still obey the correct power law. However, in contrast to the fully $+z$ polarized central spin in the previous analysis, the error of the z component is now of third instead of fourth order, meaning $\mathcal{O}(t^3)$. Additionally, the dynamics show a similar unfortunate behavior as in the previous case.

For further convenience, the physically relevant exponential coupling distribution

$$J_i = \mathcal{N} \exp\left[-i\frac{x}{N}\right] , \qquad i \in \{1, \dots, N\} , \tag{4.4}$$

with $x = 1$ and normalized by choosing $\mathcal{N}$ such that $J_{\mathrm{Q}}^2 = 1$ holds numerically, is studied. Note that for $x = 0$, this distribution is equal to the uniform case (2.7). Now in contrast to this case of uniformly distributed couplings, each bath spin evolves on a different timescale given by its individual coupling constant J_i. As an example, the first bath spin will have the strongest coupling to the central spin given by J_1, hence it will show the fastest dynamic. The last bath spin has the smallest coupling constant J_N and therefore shows the slowest dynamic. Now an interesting aspect arises from the conceptional possibility of two bath spins coupling to each other in second order indirectly, meaning terms that are proportional to $J_i J_j$ with $i \neq j$. No such terms appear in the DEQ system (3.79) for the central spin model because these terms cancel out each other during its derivation. In the case of uniformly distributed couplings, this is easier to confirm because all second order terms are proportional to the same $J_i^2 = {}^{J_{\mathrm{Q}}}/_{N}$. But for exponentially distributed couplings, errors during the derivation can occur easier due to the non-identical couplings J_i, leading to more complicated features that might have been overlooked. However, analyzing the time-dependent error $\Delta\vec{v}_{0/i}(t)$ for this coupling distribution leads to the same observation as before, meaning the error obeys the correct power law so that no additional features are missing in the DEQ system (3.79). Due to the lack of important differences in the error for this alternative coupling distribution, no additional plots are included.

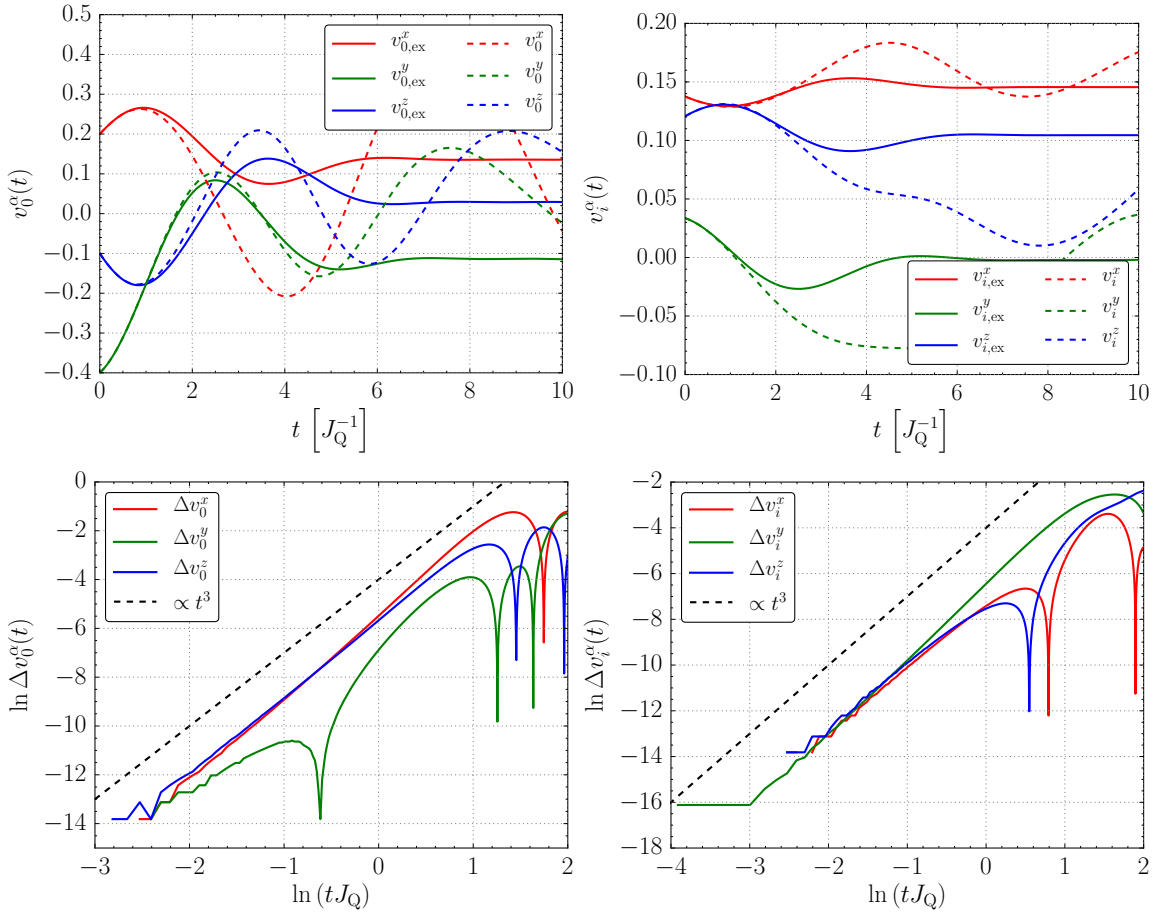

(a) $\vec{v}_0(t)$ **(b)** $\vec{v}_i(t)$

Figure 4.2: Realtime dynamics of the expectation values $\vec{v}_{0/i}(t)$ and time-dependent errors $\Delta\vec{v}_{0/i}(t)$ for a system of $N = 8$ bath spins and uniformly distributed couplings. No external magnetic field is applied. The central spin $\vec{v}_0(0)$ is polarized in an *arbitrary* direction with length $|\vec{v}_0(0)| < 1/2$ so that it is initially in a mixed state. The dashed lines in the error plots indicates the appropriate third order power law.

As a conclusion, the extension (3.79) of the DEQ system to the central spin model is considered as correct. All second order corrections are included correctly. There is no hint which might lead to a different conclusion. An interesting observation is the fact that for some specific initial conditions, for example a central spin being initially in its up-state $|\uparrow\rangle$, no third order corrections $\mathcal{O}\left(J_i^3\right)$ appear for the z components of the expectation values. However, even for this special case, the observed dynamics do not show the expected and anticipated accuracy. At least for a small bath size of $N = 8$, with uniformly or exponentially distributed couplings and a vanishing external field, this approach does not yield results that can be considered as a good approximation for the interesting physical phenomena. The timescale on which the approximate and exact solutions match is way too short.

4.2 Comparison between the exact, the Born, and the classical solution

Until now, it is not clear whether solving the DEQ system (3.79) leads to a better solution than solving the simple classical equations of motion (3.22). Therefore, a comparison between the exact solution, the Born approach and the classical solution for the expectation value $\vec{v}_0(t)$ is presented. The system parameters are same as used in Figure 4.1, meaning $N = 8$ bath spins with uniformly distributed couplings (2.7) and the central spin being initially in its up-state $|\uparrow\rangle$.

The solution of the classical equations of motion has an overall larger deviation from the exact solution than the Born result. This is already visible in the left plot showing the time evolution of $\vec{v}_0(t)$, but also by comparing the absolute errors in the right plot. The errors of the classical solution obey the power law $|\vec{v}_{0,\text{exact}} - \vec{v}_{0,\text{classical}}| \propto t^2$ and $|\vec{v}_{0,\text{classical}} - \vec{v}_{0,\text{Born}}| \propto t^2$. Due to dimensional reasons, this corresponds to an error $\propto J_i^2$. This is the expected power law for the errors of the classical solution because no second order corrections are included here. In contrast, the error of the Born approach is at least of order $\mathcal{O}\left(J_i^3\right)$, just as discussed in the previous section 4.1.

Even though the Born result shows a qualitative different behavior already on a short timescale, it leads to a slightly longer agreement with the exact solution than the classical result. Hence, the Born approach yields an improvement over the classical equations of motion.

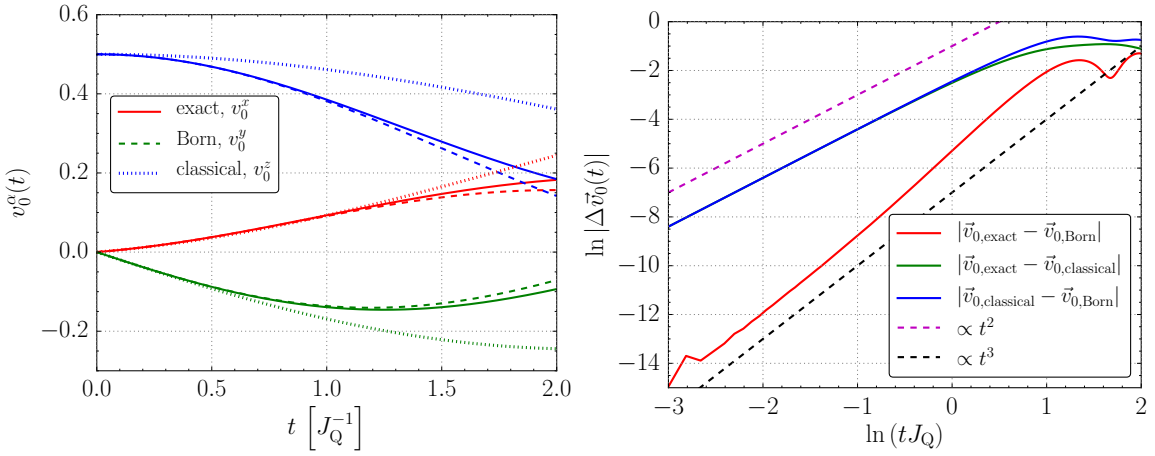

Figure 4.3: Left: Comparison between the exact solution (solid), the Born approximation (dashed), and the classical equations of motion (dots) for $\vec{v}_0(t)$. The system parameters are the same as used in Figure 4.1. **Right:** Various absolute errors (solid) with their appropriate power laws (dashed).

4.3 Comparison for large bath sizes with uniformly distributed couplings

For the unphysical uniform coupling distribution (2.7), analytically exact results based on the algebraic Bethe ansatz are available [29–31], even for very large bath sizes. The exact results used throughout this section have been provided by Lars Gravert [61].

The Born approach leads to a DEQ system with a dimension scaling linearly with the bath size N. This means that calculations for bath sizes of $\mathcal{O}(1000)$ spins are mostly limited by the computation time, independently of the coupling distribution. In principle, this is a very nice feature because many alternative approaches can only deal with a small number of bath spins while the real physical systems consist of $10^4 - 10^6$ spins.

As seen in the previous section, especially the results for a vanishing external magnetic field are not promising. But note that the Born approximation is only justified if the contribution of the interaction Hamiltonian is small compared to the classical precession. With absent external field, the central spin precesses only around the Overhauser field. Now assuming uniformly distributed couplings $J_i =\propto {}^1/\sqrt{N}$, the classical part of equation (3.79c) is proportional to $\sum_{i=1}^{N} J_i = \sqrt{N}$ while the second order correction is proportional to $\sum_{i=1}^{N} J_i^2 = 1$. Therefore, the system should show a classical behavior for large bath sizes while the second order correction should lead to an overall slower dynamic. Hence, the Born approximation should yield better results for larger bath sizes N. This has been the main argument to introduce the weak-coupling approximation (3.5) in the first place.

The comparison to the exact data for uniform couplings is performed for the experimentally motivated initial condition of a fully $+z$ polarized central spin, meaning it is initially in its up-state $|\uparrow\rangle$, and a completely disordered bath. This corresponds to the initial polarizations

$$\vec{v}_0(0) = \begin{pmatrix} 0 \\ 0 \\ \frac{1}{2} \end{pmatrix} , \qquad \vec{v}_i(0) = \begin{pmatrix} 0 \\ 0 \\ 0 \end{pmatrix} \qquad \forall\, i \in \{1, \dots, N\} \ . \tag{4.5}$$

The time-dependent error $\Delta v_0^z(t)$ is shown in Figure 4.4 for a vanishing external magnetic field. Additionally, a comparison of the central spin dynamics $\vec{v}_0(t)$ is given in Figure 4.5a for $N = 640$ bath spins. The x and y components are omitted because they show no dynamics at all. The time-dependent error is of fourth order $\mathcal{O}(t^4)$, just as observed in the previous section for the same initial polarization $\vec{v}_0(0)$. This confirms the correctness of the DEQ system (3.79) once again. Unfortunately, the exact time evolution of $\vec{v}_0(t)$ is only captured well for a very small timescale again. The Born solution only shows periodic oscillations but lacks dephasing. Varying the bath size significantly does not change this behavior either.

The inclusion of an external magnetic field

$$\vec{B} = \begin{pmatrix} 0 \\ 0 \\ -10 J_{\mathrm{Q}} \end{pmatrix} \tag{4.6}$$

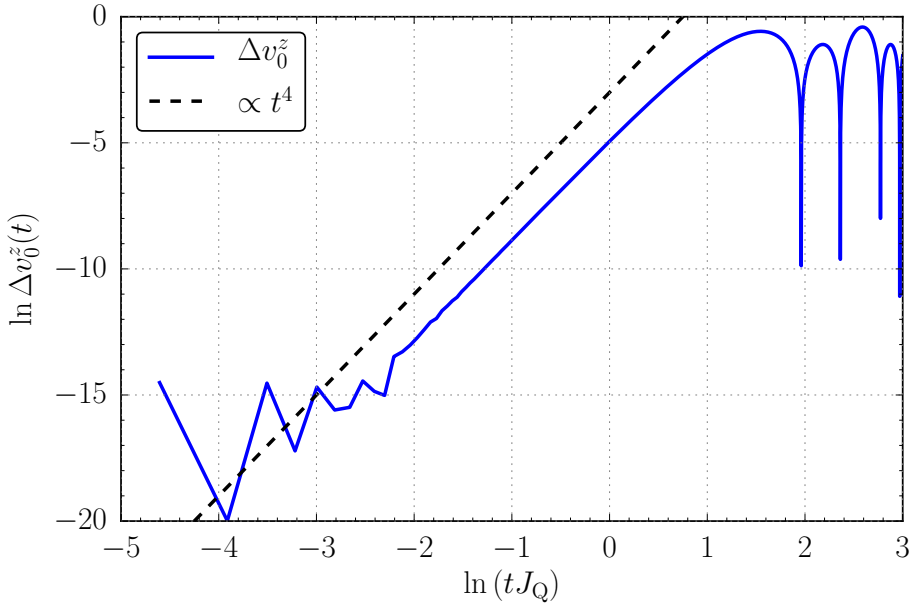

Figure 4.4: Realtime error $\Delta v_0^z(t) = |v_{0,\mathrm{exact}}^z(t) - v_{0,\mathrm{Born}}^z(t)|$ and its suitable power law $\mathcal{O}(t^4)$ (black dashed line) for the case of a *vanishing* external magnetic field, $N = 640$ bath spins, *uniformly* distributed couplings, and an initially unpolarized bath. The central spin $\vec{v}_0(0)$ is initially in its up-state $|\uparrow\rangle$.

leads to an improvement which is shown in Figure 4.5b. Note that the scale of the ordinate is completely different compared to the scale used in Figure 4.5a because otherwise, almost nothing would be visible. The most part of the initial central spin polarization persists for both the exact and the approximate (Born) calculation. This is due to the strong magnetic field coupling to the central spin. While the absolute error decreases significantly, the major feature of dephasing is still not captured at all. The amplitude stays constant for all time while the oscillation frequency seems to be captured correctly. Only the time-average of both solutions for $v_0^z(t)$ seems to match approximately.

All these observations do not change significantly when varying the bath size to $N = 320$, 160 or 80. This shows that the accuracy of the Born approach is almost independent of the bath size for the here studied initial polarizations, which is in contrast to the previous belief.

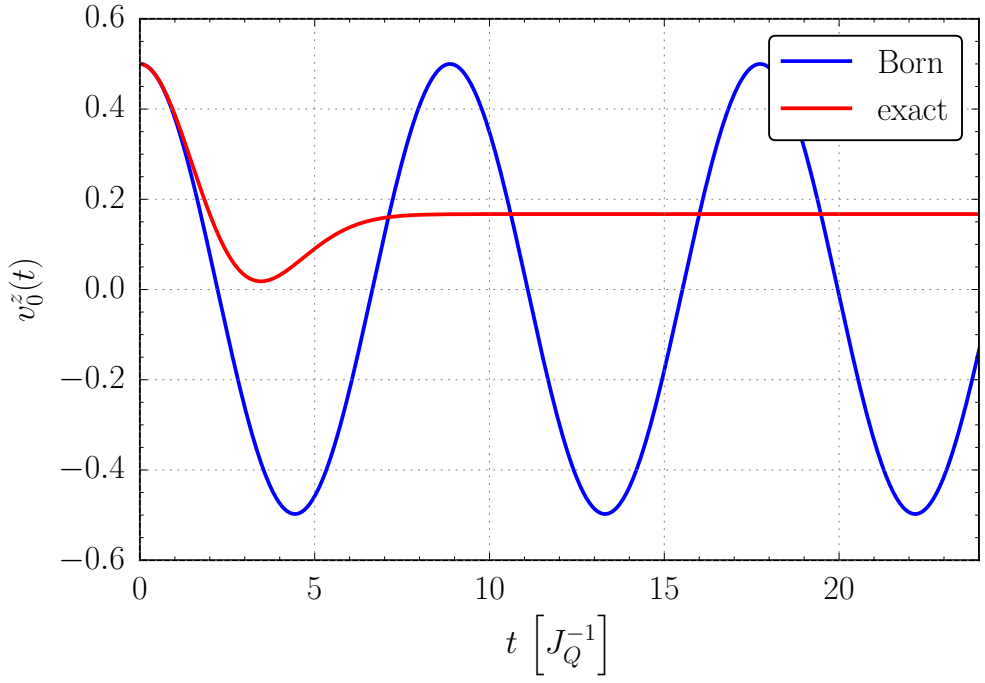

(a) $|\vec{B}| = 0$

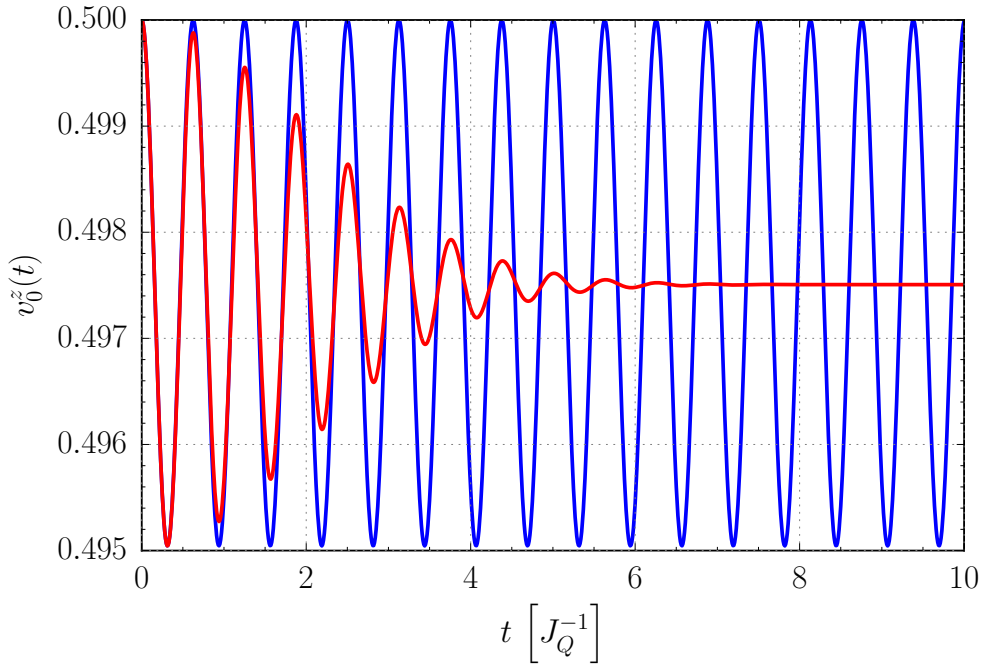

(b) $\vec{B} = \left(0, 0, -10J_{\mathrm{Q}}\right)^T$

Figure 4.5: Comparison between the exact and the Born solution for the central spin dynamics $v_0^z(t)$ with **(a)** vanishing external magnetic field and **(b)** $\vec{B} = \left(0, 0, -10J_{\mathrm{Q}}\right)^T$, $N = 640$ bath spins, *uniformly* distributed couplings, and an initially unpolarized bath. The central spin $\vec{v}_0(0)$ is initially in its up-state $|\uparrow\rangle$.

4.4 Comparison to DMRG for exponentially distributed couplings

For the physically motivated exponential coupling distribution (2.5), time dependent DMRG calculations were performed by Stanek et al. [28] and Gravert et al. [29] and have been provided by Lars Gravert [61]. This data is used to compare it to the Born approach. In contrast to the exact results for the uniform couplings in the previous section, this method is limited due to its truncation error which grows in time. This truncation error is smaller for larger external fields so that longer simulation times are feasible. Additionally, this approach is limited to intermediate bath sizes because it requires quite heavy numerical calculations.

The initial conditions are chosen as in the previous section, meaning a fully unpolarized bath and the central spin being in its up-state $|\uparrow\rangle$. The coupling distribution is given as

$$J_i = \mathcal{N} \exp\left[-i\frac{x}{N}\right] , \qquad i \in \{1, \dots, N\} , \tag{4.7}$$

with $x = 4$ and normalized by choosing $\mathcal{N}$ such that $J_Q^2 = 1$ holds numerically. The bath is chosen to consist of $N = 80$ spins.

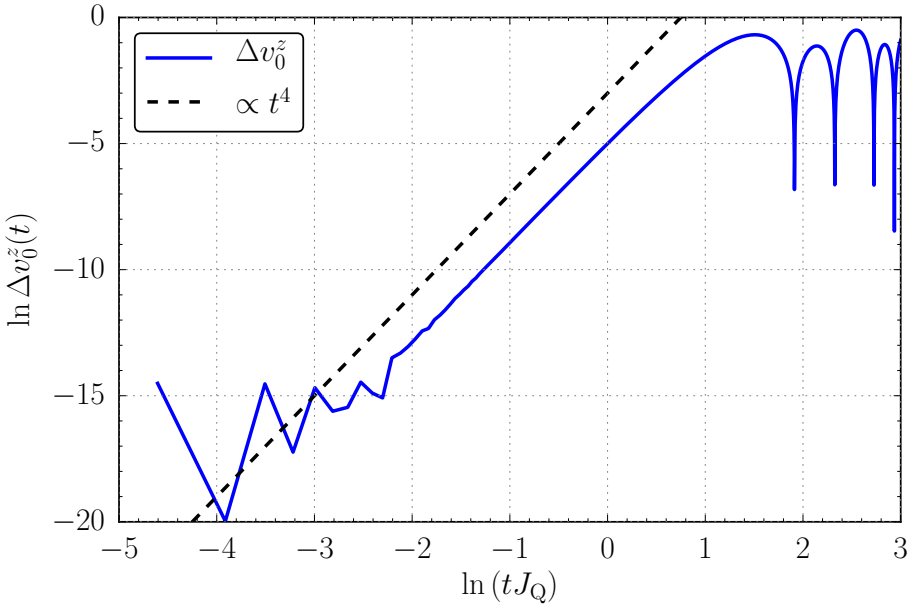

Figure 4.6: Realtime deviation $\Delta v_0^z(t) = |v_{0,\mathrm{DMRG}}^z(t) - v_{0,\mathrm{Born}}^z(t)|$ and its suitable power law $\mathcal{O}(t^4)$ (black dashed line) for the case of a *vanishing* external field, $N = 80$ bath spins, *exponentially* distributed couplings with $x = 4$, and an initially unpolarized bath. The central spin $\vec{v}_0(0)$ is initially in its up-state $|\uparrow\rangle$.

In the case of a vanishing external magnetic field, the time-dependent deviation $\Delta v_0^z(t)$ shown in Figure 4.6 shows the correct power law $\mathcal{O}(t^4)$. Note that the data obtained by DMRG calculations are considered as almost exact for the shown times $t < 25 J_Q^{-1}$. Once again, this proofs the correctness of the Born corrections in the DEQ system (3.79). The dynamics of $v_0^z(t)$ for both a vanishing and a finite external field are shown in Figure 4.7. For

a vanishing external field as shown in Figure 4.7a, only a very short timescale is captured. This behavior has been already observed during the error analysis for $N = 8$ in section 4.1 The feature of dephasing is still missing. Interestingly, a very small decay of the amplitude can be observed. In contrast for uniform couplings, it stays constant for all times. This behavior is more dominant for a finite external field as shown in Figure 4.7b. Again, the scale of the ordinate is chosen differently compared to Figure 4.7a. The decay of the amplitude is much faster as observed for no external field. Unfortunately, it cannot catch up with the accurate DMRG results, though. Only the oscillation frequency is captured almost correctly, just as in the uniform case.

As a conclusion, the Born approach seems to yield better but still not reliable results for large external magnetic fields. This is expected since the weak-coupling approximation is especially valid in this particular case because the classical precession around the external magnetic field leads to the fastest dynamics in the system. Additionally, this approach yields slightly better results for the more physical exponential coupling distribution because the amplitude does not stay constant for all times. This change of the amplitude occurs on a too long timescale, though. In general, the Born solution differs so much from the exact results that they cannot even function as an approximation of the quantum mechanical behavior of the central spin for the relevant long timescales.

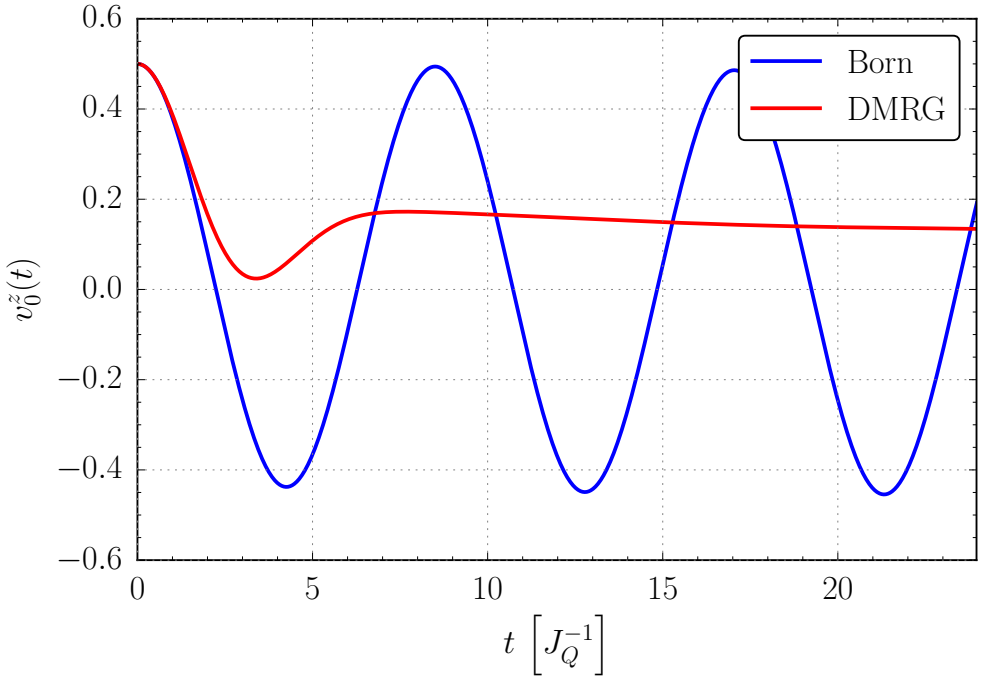

(a) $|\vec{B}| = 0$

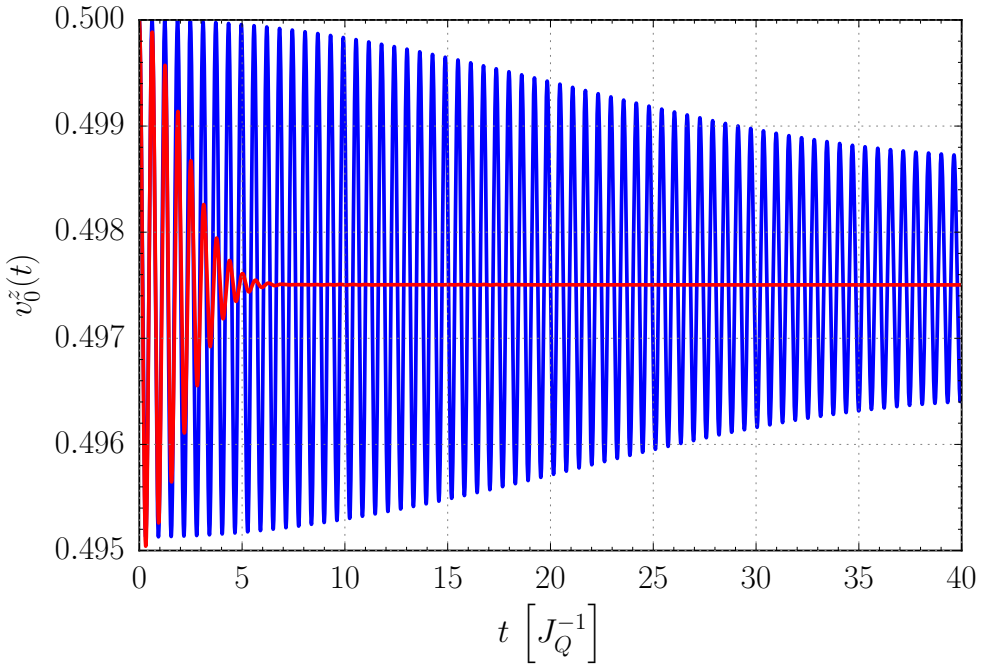

(b) $\vec{B} = (0, 0, -10J_{\mathrm{Q}})^T$

Figure 4.7: Comparison between the exact and Born solution for the central spin dynamics $v_0^z(t)$ with **(a)** absent external field and **(b)** $\vec{B} = (0, 0, -10J_{\mathrm{Q}})^T$, $N = 80$ bath spins, *exponentially* distributed couplings with $x = 4$, and an initially unpolarized bath. The central spin $\vec{v}_0(0)$ is initially in its up-state $|\uparrow\rangle$.

5 Simulations using Gaussian bath ensembles

The numerical analysis in the previous chapter shows the correctness and completeness of the derived DEQ system (3.79) for the expectation values $\vec{v}_{0/i}(t)$. The lack of dephasing is the main missing feature of the calculated dynamics. Throughout classical simulations for the central spin model [19, 20], dephasing is induced by calculating the average for an ensemble of Gaussian distributed baths. This requires solving classical equations of motion for each individual initial bath configuration.

The intention of this chapter is to enhance this idea by including the first quantum mechanical corrections to the classical equations of motion derived in chapter 3 by using the Born approximation. Remember that the classical equations of motion are directly included in the DEQ system (3.79) and thus, a straight comparison between classical and Born simulation is possible and desirable.

Because the classical simulation as introduced in the following section 5.1 already yields promising results without the inclusion of an external magnetic field and this is the harder case, no field is applied to the central spin in the approach of improving the classical simulation by using the Born corrections either.

In order to reduce the required computation time for the simulations, the adaptive Runge-Kutta-Fehlberg method (RKF45) is used to solve the DEQ systems numerically. It also enables to maintain a similar accuracy for both the classical simulations and the simulations including the Born corrections by using the same error tolerance for the stepsize adjustment. Additionally, the DEQ systems are solved on a finite grid to be able to calculate the ensemble average at the gridpoints. The grid spacing, which mainly determines the resolution of the plots, is typically much larger than the stepsize used in the RKF45 algorithm.

5.1 Classical simulations

In this section, different approaches for a classical simulation of the central spin model are presented. They all have their own advantages but also problems that have to be identified and understood to choose the right basis to build on for the inclusion of the Born corrections in section 5.2. A comparison and discussion of the different results is given in subsection 5.1.4.

In the classical simulation, the spin operators $\vec{S}_{0/i}$ are considered as classical vectors. In quantum mechanics, these vectors are represented by the expectation values $\vec{v}_{0/i}(t)$. In the following, this notation is kept to describe the classical vectors. After calculating the ensemble average, the resulting quantity is denoted as $\overline{\langle \vec{v}_0 \rangle}(t)$ to distinguish from quantum mechanical expectation values $\vec{v}_0(t)$.

5.1.1 Full classical simulation

Within the *full classical simulation*, the classical equations of motion

$$\frac{\mathrm{d}}{\mathrm{d}t}\vec{v}_0(t) = \sum_{i=1}^{N} J_i \vec{v}_i(t) \times \vec{v}_0(t) \tag{5.1a}$$

$$\frac{\mathrm{d}}{\mathrm{d}t}\vec{v}_i(t) = J_i \vec{v}_0(t) \times \vec{v}_i(t) \qquad \forall\, i \in \{1, \dots, N\} \tag{5.1b}$$

are solved numerically for various initial conditions. The central spin is always chosen such that it is fully polarized in $+z$ direction, meaning

$$\vec{v}_0(0) = \begin{pmatrix} 0 \\ 0 \\ \frac{1}{2} \end{pmatrix} \tag{5.2}$$

so that it is initially in its up-state $|\uparrow\rangle$. The initial bath spin polarization $\vec{v}_i(0)$ is taken from a Gaussian distribution with mean value $\mu_i = 0$, meaning the bath is completely disordered. This is a valid assumption since the hyperfine couplings J_i in the central spin model are in the range of μeV[16, 55, 56]. This corresponds to temperatures of about 10 mK which is small compared to the experimentally relevant temperature [13]. The choice of the variance is quantum mechanically motivated. For spin $S = 1/2$, it is initially given by

$$\sigma_i^2 := \langle S_i^\alpha(0) S_i^\alpha(0) \rangle = \frac{1}{4}\,. \tag{5.3}$$

As a consequence, the whole spin bath forms a Gaussian distribution with mean $\mu_A = 0$ and variance $\sigma_A^2 = J_\mathrm{Q}^2/4$.

The standard deviation of the simulation at a finite time t is proportional to $1/\sqrt{n}$, with n being the number of individual simulations. At least $n = 10^5$ is required to be able to neglect error bars. The solution obtained by calculating the average of $n = 10^6$ individual simulations for the initial central spin polarization $\vec{v}_0(0) = (0, 0, 1/2)^T$ is shown in Figure 5.2 (see subsection 5.1.4) for a system of $N = 80$ bath spins As of now, it is denoted as the full classical simulation (FCS). The couplings are chosen to be exponentially distributed according to

$$J_i = \mathcal{N} \exp\left[-i\frac{x}{N}\right], \qquad i \in \{1, \dots, N\}\,, \tag{5.4}$$

with $x = 1$ and normalized by choosing $\mathcal{N}$ such that $J_\mathrm{Q}^2 = 1$ holds numerically. A discussion and comparison to the other approaches can be found in subsection 5.1.4.

A more detailed discussion of this classical approach and its efficient simulation can be found in Reference [20]. The FCS is included here because the the intention of the present chapter consists of enhancing the results of this simulation by including the first quantum mechanical corrections, obtained by using the Born approximation, in section 5.2.

5.1.2 Frozen Overhauser field

In a work by Merkulov et al. [16], the bath is assumed to form the effective Overhauser field $\vec{A} = \sum_{i=1}^{N} J_i \vec{v}_i$ which is assumed to be frozen in time, meaning no dynamics is included for each individual bath spin. This approximation is justified for small times because for a large bath size, the central spin precesses around Overhauser field much faster than each bath spin around the central spin. Hence, the central spin is coupled to bath spins that are constant in a first zeroth-order approximation. This behavior is described by the differential equation

$$\frac{\mathrm{d}}{\mathrm{d}t}\vec{v}_0(t) = \vec{A} \times \vec{v}_0(t)\,. \tag{5.5}$$

A general solution is given by

$$\vec{v}_0(t) = (\vec{v}_0(0)\cdot\vec{m})\,\vec{m} + (\vec{m}\times\vec{v}_0(0))\sin\left(|\vec{A}|t\right) + [\vec{v}_0(0) - (\vec{m}\cdot\vec{v}_0(0))\,\vec{m}]\cos\left(|\vec{A}|t\right)\,, \tag{5.6}$$

with $\vec{m} = \vec{A}/|\vec{A}|$. The polarization of the frozen Overhauser field is taken from a Gaussian distribution with mean $\mu_A = 0$ and variance $\sigma_A^2 = J_\mathrm{Q}^2/4$. Now averaging the solution (5.6) over this distribution yields the well known analytical expression

$$\overline{\langle\vec{v}_0\rangle}(t) = \frac{\vec{v}_0(0)}{3}\left[1 + 2\left(1 - \frac{J_\mathrm{Q}^2}{4}t^2\right)\exp\left(-\frac{J_\mathrm{Q}^2}{8}t^2\right)\right]\,. \tag{5.7}$$

As of now, this solution is referred to as the *Merkulov-solution* (MS). [16] It is shown in figure Figure 5.2 (see subsection 5.1.4) for the initial central spin polarization $\vec{v}_0(0) = (0, 0, 1/2)^T$. The calculation is independent of the amount of bath spins and the distribution of their couplings J_i. It only depends on the parameter J_Q^2 which determines the short time dynamics of the central spin. A discussion and comparison to the other approaches is given in subsection 5.1.4.

5.1.3 Quantum mechanical sampling

In general, the Overhauser field $\vec{A}$ is not frozen but shows fluctuations due to the dynamics of the bath spins that have been neglected in the Merkulov-solution. As a next step, the precession of each bath spin around the central spin is included. Basically, the DEQ system to solve is the same as in subsection 5.1.1, namely the classical equations of motion (5.1). The difference is given through the choice of the initial bath polarization.

In this approach, the Overhauser field $\vec{A}$ is sampled directly from a Gaussian distribution with mean $\mu_A = 0$ and variance $\sigma_A^2 = J_\mathrm{Q}^2/4$, just as for the Merkulov-solution (5.7). The question is how this translates to the initial polarization of each individual bath spin. This approach is quantum mechanically motivated because the length of each bath spin should be treated in a quantum mechanical manner. Obviously, this is not the case if each initial bath spin polarization is sampled from a Gaussian distribution with mean value $\mu_i = 0$ and variance $\sigma_i^2 = 1/4$. Note that this constraint limits the maximal length $\vec{A}$ of the Overhauser field due to the limited length of each bath spin.

The approach starts with parameterizing the initial density operator ρ_B of the full bath as

$$\rho_\mathrm{B} = \frac{1}{Z_\mathrm{B}\left(\vec{\lambda}\right)} \exp\left(-\vec{\lambda}\cdot\vec{A}\right) , \tag{5.8}$$

with the partition function $Z_\mathrm{B}\left(\vec{\lambda}\right) = \mathrm{Tr}\left[\exp\left(-\vec{\lambda}\cdot\vec{A}\right)\right]$, the Overhauser field $\vec{A} = \sum_{i=1}^{N} J_i \vec{S}_i$, and the Lagrange multiplier $\vec{\lambda}$. This is the likeliest initial state of the bath because it maximizes the entropy when only the initial Overhauser field $\vec{A}$ is fixed. It is also a product state. Hence, the term $\exp\left(-\vec{\lambda}\cdot\vec{A}\right)$ factorizes into

$$\exp\left(-\vec{\lambda}\cdot\vec{A}\right) = \bigotimes_{i=1}^{N} \exp\left(-\frac{J_i}{2}\vec{\lambda}\cdot\vec{\sigma}\right) \tag{5.9}$$

and thus, it is possible to derive a relation between the parameter $\vec{\lambda}$ and the initial expectation values $\vec{v}_i(0)$ which are used to parameterize the bath in weak-coupling approximation (see subsection 3.3.1).

The term $\exp\left(\frac{J_i}{2}\lambda\cdot\vec{\sigma}\right)$ can be rewritten as a series expansion which splits into even and uneven powers. Note that the notation $\vec{n} = \vec{\lambda}/|\vec{\lambda}|$ is used to describe the normal vector of the parameter $\vec{\lambda}$.

$$\exp\left(\frac{J_i}{2}\lambda\cdot\vec{\sigma}\right) = \sum_{k=0}^{\infty} \frac{1}{(2k+1)\,!} \left(\frac{J_i}{2}|\vec{\lambda}|\right)^{2k+1} (\vec{n}\cdot\vec{\sigma})^{2k+1} + \sum_{k=0}^{\infty} \frac{1}{(2k)\,!} \left(\frac{J_i}{2}|\vec{\lambda}|\right)^{2k} (\vec{n}\cdot\vec{\sigma})^{2k} \tag{5.10a}$$

This expression can be evaluated by making use of the following relations.

$$(\vec{n}\cdot\vec{\sigma})^{2k} = \left[\underbrace{(\vec{n}\cdot\vec{\sigma})^2}_{=|\vec{n}|^2=1}\right]^k = \mathbb{1} \tag{5.11a}$$

$$(\vec{n}\cdot\vec{\sigma})^{2k+1} = \underbrace{(\vec{n}\cdot\vec{\sigma})^{2k}}_{=\mathbb{1}} (\vec{n}\cdot\vec{\sigma}) = \vec{n}\cdot\vec{\sigma} \tag{5.11b}$$

Inserting into equation (5.10a) yields

$$\exp\left(\frac{J_i}{2}\lambda\cdot\vec{\sigma}\right) = \sum_{k=0}^{\infty} \frac{1}{(2k+1)\,!} \left(\frac{J_i}{2}|\vec{\lambda}|\right)^{2k+1} (\vec{n}\cdot\vec{\sigma}) + \sum_{k=0}^{\infty} \frac{1}{(2k)\,!} \left(\frac{J_i}{2}|\vec{\lambda}|\right)^{2k} \mathbb{1} \tag{5.12a}$$

$$= \sinh\left(-\frac{J_i}{2}|\vec{\lambda}|\right)(\vec{n}\cdot\vec{\sigma}) + \cosh\left(-\frac{J_i}{2}|\vec{\lambda}|\right)\mathbb{1} \tag{5.12b}$$

$$= \cosh\left(\frac{J_i}{2}|\vec{\lambda}|\right)\mathbb{1} - \sinh\left(\frac{J_i}{2}|\vec{\lambda}|\right)(\vec{n}\cdot\vec{\sigma}) \ . \tag{5.12c}$$

This expression also enables to calculate the partition function $Z(\vec{\lambda})$.

$$Z(\vec{\lambda}) = \mathrm{Tr}\left[\exp\left(-\sum_{i=1}^{N}\frac{J_i}{2}\vec{\lambda}\cdot\vec{\sigma}\right)\right] \tag{5.13a}$$

$$= \mathrm{Tr}\left[\bigotimes_{i=1}^{N}\left\{\cosh\left(\frac{J_i}{2}|\vec{\lambda}|\right)\mathbb{1} - \sinh\left(\frac{J_i}{2}|\vec{\lambda}|\right)(\vec{n}\cdot\vec{\sigma})\right\}\right] \tag{5.13b}$$

$$= 2^N\prod_{i=1}^{N}\cosh\left(\frac{J_i}{2}|\vec{\lambda}|\right) \tag{5.13c}$$

Now, the density operator of the bath ρ_B takes the final form

$$\rho_\mathrm{B} = \frac{\bigotimes_{i=1}^{N}\left[\cosh\left(\frac{J_i}{2}|\vec{\lambda}|\right)\mathbb{1} - \sinh\left(\frac{J_i}{2}|\vec{\lambda}|\right)(\vec{n}\cdot\vec{\sigma})\right]}{2^N\prod_{i=1}^{N}\cosh\left(\frac{J_i}{2}|\vec{\lambda}|\right)} \tag{5.14a}$$

$$= \bigotimes_{i=1}^{N}\left[\frac{1}{2}\mathbb{1} - \frac{1}{2}\tanh\left(\frac{J_i}{2}|\vec{\lambda}|\right)(\vec{n}\cdot\vec{\sigma})\right]. \tag{5.14b}$$

A direct comparison of the coefficients to the original parameterization of the bath spin density operators in subsection 3.3.3, chosen as

$$\rho_i(0) = \frac{1}{2}\mathbb{1} + \vec{b}_i(0)\cdot\vec{\sigma} = \frac{1}{2}\mathbb{1} + \vec{v}_i(0)\cdot\vec{\sigma}\,, \tag{5.15}$$

shows that the initial polarization $\vec{v}_i(0)$ is determined by the choice of the parameter $\vec{\lambda}$ through the relation

$$\vec{v}_i(0) = -\frac{1}{2}\tanh\left(\frac{J_i}{2}|\vec{\lambda}|\right)\frac{\vec{\lambda}}{|\vec{\lambda}|}\,. \tag{5.16}$$

It only depends on the individual coupling constant J_i and the Lagrange multiplier $\vec{\lambda}$. Note that this relation limits the length $|\vec{v}_i(0)|$ to the interval $[-1/2, 1/2]$, meaning the length of each bath spin is treated in a quantum mechanical manner.

The parameter $\vec{\lambda}$ has to be calculated from the relation

$$\frac{\partial}{\partial\lambda^\alpha}\ln Z\left(\vec{\lambda}\right) = \frac{1}{Z\left(\vec{\lambda}\right)}\frac{\partial}{\partial\lambda^\alpha}Z\left(\vec{\lambda}\right) \tag{5.17a}$$

$$= \frac{1}{Z\left(\vec{\lambda}\right)}\frac{\partial}{\partial\lambda^\alpha}\mathrm{Tr}\left[\exp\left(-\vec{\lambda}\cdot\vec{A}\right)\right] \tag{5.17b}$$

$$= -A^\alpha\,. \tag{5.17c}$$

This expression is evaluated by using the derivative of $Z\left(\vec{\lambda}\right) = 2^N\prod_{i=1}^{N}\cosh\left(\frac{J_i}{2}|\vec{\lambda}|\right)$. Calculating this derivative requires using the product rule

$$f(x) = \prod_{i=1}^{N}f_i(x) \qquad \Rightarrow \qquad f'(x) = \sum_{i=1}^{N}f_i'(x)\prod_{k=1,\,k\neq i}^{N}f_k(x)\,. \tag{5.18}$$

Its application leads to

$$\frac{\partial}{\partial\lambda^\alpha}Z\left(\vec{\lambda}\right) = \frac{\partial}{\partial\lambda^\alpha}\prod_{i=1}^{N}\cosh\left(\frac{J_i}{2}|\vec{\lambda}|\right) \tag{5.19a}$$

$$= \sum_{i=1}^{N}\frac{J_i}{2}\frac{\lambda^\alpha}{|\vec{\lambda}|}\sinh\left(\frac{J_i}{2}|\vec{\lambda}|\right)\prod_{k=1,\,k\neq i}^{N}\cosh\left(\frac{J_k}{2}|\vec{\lambda}|\right). \tag{5.19b}$$

Inserting the derivative into (5.17a) yields

$$\frac{1}{Z\left(\vec{\lambda}\right)}\frac{\partial}{\partial\lambda^\alpha}Z\left(\vec{\lambda}\right) = \frac{\lambda^\alpha}{|\vec{\lambda}|}\frac{\sum_{i=1}^{N}\frac{J_i}{2}\sinh\left(\frac{J_i}{2}|\vec{\lambda}|\right)\prod_{k=1,\,k\neq i}^{N}\cosh\left(\frac{J_k}{2}|\vec{\lambda}|\right)}{\prod_{j=1}^{N}\cosh\left(\frac{J_i}{2}|\vec{\lambda}|\right)} \tag{5.20a}$$

$$= \frac{\lambda^\alpha}{|\vec{\lambda}|}\sum_{i=1}^{N}\frac{J_i}{2}\tanh\left(\frac{J_i}{2}|\vec{\lambda}|\right). \tag{5.20b}$$

Hence, the equation to solve with respect to $\vec{\lambda}$ takes the form

$$\frac{\lambda^\alpha}{|\vec{\lambda}|}\sum_{i=1}^{N}\frac{J_i}{2}\tanh\left(\frac{J_i}{2}|\vec{\lambda}|\right) = -A^\alpha. \tag{5.21}$$

This is a three-dimensional system of equations since it has to be solved for each component $\alpha \in \{x, y, z\}$.

Actually, an easier derivation is given by making use of equation (5.16). For a classically chosen Overhauser field component $A^\alpha := A^\alpha(0)$, the relation

$$A^\alpha = A^\alpha(0) = \sum_{i=1}^{N} J_i v_i^\alpha(0) \tag{5.22}$$

has to hold. This relation is obtained by replacing the quantum mechanical bath spin operators $\vec{S}_i$ in the Overhauser field operator by their expectation values $\vec{v}_i$. Now inserting $v_i^\alpha(0)$ as given through equation (5.16) leads to the same system of equations as given in equation (5.21).

It is difficult to solve such multi-dimensional systems numerically. However, it is possible to reduce it to a one-dimensional one. The left-hand side of equation (5.21) in the slightly rearranged form

$$\sum_{i=1}^{N}\frac{J_i}{2}\tanh\left(\frac{J_i}{2}|\vec{\lambda}|\right) = -A^\alpha\frac{|\vec{\lambda}|}{\lambda^\alpha} \tag{5.23}$$

is independent of α and therefore the same for all three equations. This means that the right-hand sides have to be equal, too. Therefore, the following useful relations emerge.

$$\frac{A^x}{\lambda^x} = \frac{A^y}{\lambda^y} = \frac{A^z}{\lambda^z} \tag{5.24a}$$

$$\Rightarrow \lambda^y = \frac{A^y}{A^x}\lambda^x, \qquad \lambda^z = \frac{A^z}{A^x}\lambda^x \tag{5.24b}$$

$$\Rightarrow |\vec{\lambda}| = \sqrt{(\lambda^x)^2 + (\lambda^y)^2 + (\lambda^z)^2} = \lambda^x\sqrt{1 + \left(\frac{A^y}{A^x}\right)^2 + \left(\frac{A^z}{A^x}\right)^2} = \lambda^x\frac{|\vec{A}|}{A^x} \tag{5.24c}$$

As a consequence, the final equation is obtained by replacing λ^y and λ^z through their relations (5.24b) with λ^x.

$$\sum_{i=1}^{N} \frac{J_i}{2} \tanh\left(\frac{J_i}{2}\frac{|\vec{A}|}{A^x}\lambda^x\right) + |\vec{A}| = 0 \tag{5.25}$$

It has to be solved numerically with respect to the Lagrange multiplier λ^x. In practice, this task is executed by interval bisection quite easily. The remaining Lagrange multipliers are then obtained by resorting to the relations (5.24b).

Note that the Overhauser field $\vec{A}$ is sampled from a Gaussian distribution with mean value $\mu_A = 0$ and variance $\sigma_A^2 = J_{\mathrm{Q}}^2/4$. Therefore, a solution does not necessarily exist for every sampled $\vec{A}$ because $\tanh(x)$ is limited to the interval $[-1, 1]$. As a consequence, a solution exists only for

$$|\vec{A}| \leq \frac{1}{2}\sum_{i=1}^{N} J_i \,. \tag{5.26}$$

In practice, this condition is almost always fulfilled. If no solution is found, a new $\vec{A}$ is sampled from the Gaussian distribution. This leads to a negligibly small cutoff in the resulting distribution.

In principle, the present approach also allows to discuss an initially polarized bath by chosing the mean value μ_A of the Gaussian distribution to be nonzero. This case is not studied in this thesis, though.

Resorting to equation (5.16) to calculate the initial bath spin expectation values $\vec{v}_i(0)$ results in all bath spins being polarized in the exact same direction $\vec{\lambda}$. This is also the direction of the Overhauser field $\vec{A}$. It can be argued that it is not really physical that *all* bath spins point in the same direction, but this approach solves the problem of dealing with bath spins with too long length $|\vec{v}_i(0)|$, which appear during the full classical simulation. Note that for a specific bath spin i, the initial length $|\vec{v}_i(0)|$ scales with the bath size N according to

$$|\vec{v}_i(0)| \propto \frac{1}{\sqrt{N}} \,. \tag{5.27}$$

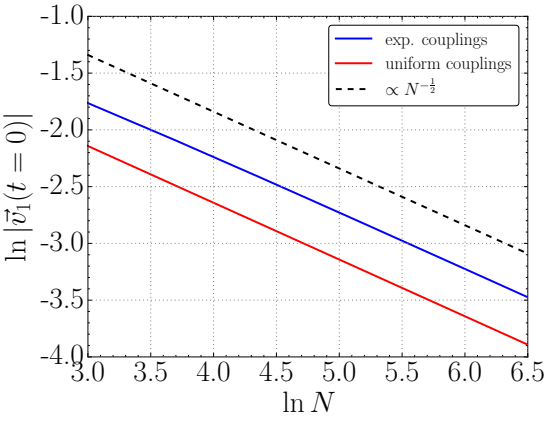

Figure 5.1: Quantum mechanical sampling: Scaling of the first bath spin $|\vec{v}_1(0)|$ for a given Overhauser field $\vec{A}(0)$, depending on the bath size N. The power law $|\vec{v}_1(0)| \propto N^{-\frac{1}{2}}$ is identical for the exponential and uniform coupling distribution.

An illustration for the scaling of the first bath spin $|\vec{v}_1(0)|$ is given in Figure 5.1 for an exponential but also an uniform coupling distribution. The scaling behavior is going to

be an important argument in the next section while studying the influence of the Born corrections. This approach of sampling the initial Overhauser field will be referred to as *quantum mechanical sampling* (QMS). The result of averaging the solution of the classical equations of motion (5.1) for $n = 10^6$ is given in Figure 5.2 (see subsection 5.1.4) for a system of $N = 80$ bath spins with exponentially distributed couplings ($x = 1$). A detailed discussion and comparison to the other approaches is given in the following subsection 5.1.4.

5.1.4 Results and comparison

The solutions $\overline{\langle v_0^z \rangle}(t)$ for the three different approaches discussed in the previous subsections are compiled in Figure 5.2. The x and y components vanish anyway for $n \to \infty$ and are therefore omitted. They only show small statistical fluctuations due to calculating the average of a finite ensemble.

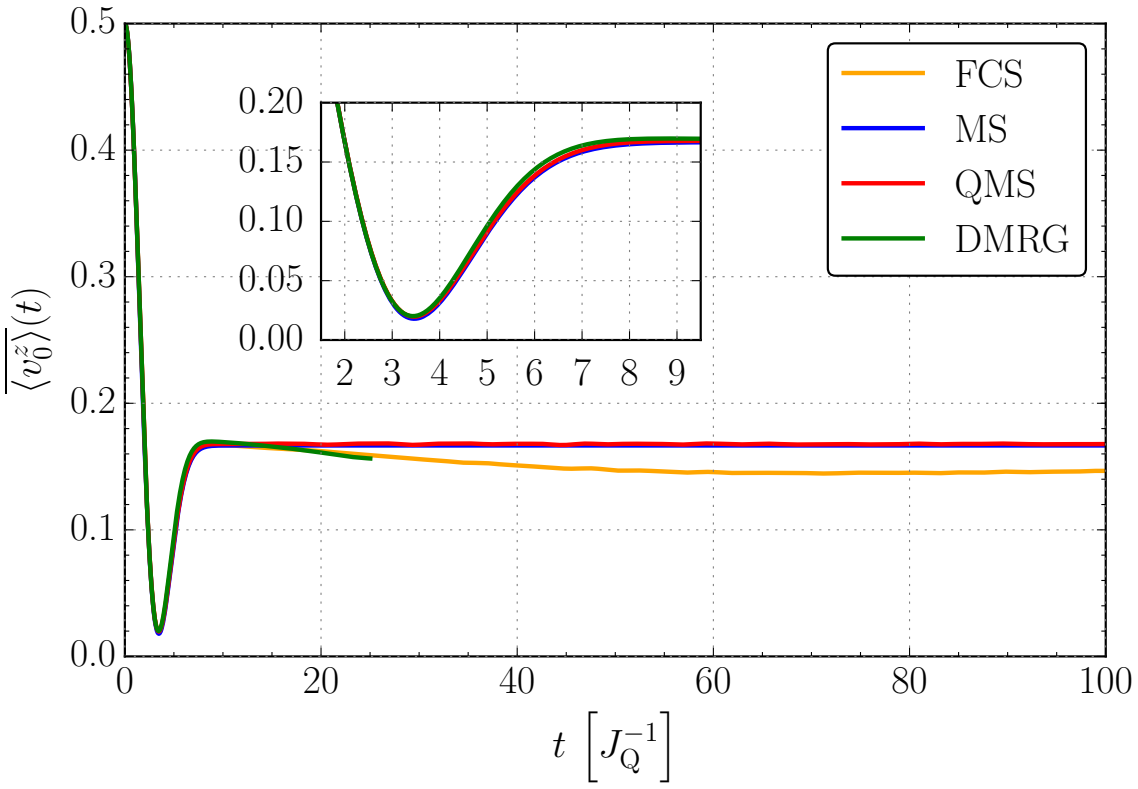

Figure 5.2: Three different approaches for a classical simulation of the central spin dynamics $\overline{\langle v_0^z \rangle}(t)$ (full classical simulation (FCS), Merkulov-solution (MS), quantum mechanical sampling (QMS)). The quantum mechanical expectation value $\langle \vec{S}_0 \rangle(t)$ calculated by DMRG is included for $t \leq 25 J_{\mathrm{Q}}^{-1}$. Despite small statistical fluctuations which result from calculating an average for a finite ensemble, the x and y components vanish and are therefore neglected. The calculations are performed for a system of $N = 80$ bath spins with exponential distributed couplings ($x = 1$) and averaging over $n = 10^6$ individual simulations.

The calculations are performed for $N = 80$ bath spins with exponential distributed couplings ($x = 1$) given through equation (5.4) while the parameter $J_Q^2 = 1$ determines the timescale. The average is calculated for $n = 10^6$ ensembles so that error bars can be neglected. The initial central spin polarization is chosen to be $\vec{v}_0 = (0, 0, 1/2)^T$. A DMRG calculation for the quantum mechanical expectation value $\langle \vec{S}_0(t) \rangle = \vec{v}_0(t)$ is included which is considered to be accurate for $t < 25 J_Q^{-1}$.

The characteristic minimum at $t \approx 3.5 J_Q^{-1}$ is captured well by all approaches (see inset of Figure 5.2). It is not really possible to tell which one describes the real quantum mechanical solution the best. Apparently, this minimum is mainly described by the central spin precessing around a frozen Overhauser field since even the Merkulov-solution describes the exact solution quite well on this timescale.

The full classical simulation (FCS) seems to be the best approach to describe the dephasing of the central spin after the characteristic minimum for $t > 9 J_Q^{-1}$. Since the DMRG results are only accurate for small times $t < 25 J_Q^{-1}$, it is not possible to give a detailed analysis for larger times. The analytical Merkulov-solution (MS) converges against the value $\lim_{t\to\infty} \overline{\langle v_0 \rangle}(t) = 1/6$. The same behavior occurs for the approach using the quantum mechanical sampling (QMS). Despite the small remaining statistical fluctuations, the results from QMS seem to match the Merkulov-solution.

Both the Merkulov and the QMS solution lack the dephasing of the central spin for $t \gtrsim 10 J_Q^{-1}$. However, since the characteristic minimum is described well, the hope is to obtain this missing feature by including the Born corrections during the QMS calculation in the following section 5.2. Since the FCS does not exactly match the DMRG results, it might be possible to enhance this directly simulation by including the Born corrections.

5.2 Simulations including the Born approximation

In the previous sections, the advantages of the full classical simulation (FCS) and the quantum mechanical sampling (QMS) have been discussed. All classical approaches capture the characteristic minimum at $t \approx 3.5 J_{\mathrm{Q}}^{-1}$. The main difference is that the FCS includes the dephasing for $t \gtrsim 10 J_{\mathrm{Q}}^{-1}$ while the QMS solution converges against the constant value $1/6$. The FCS is not completely accurate, though. Therefore, trying to enhance the FCS directly by including the Born corrections is the first approach to follow.

However, problems may arise when sampling the initial bath spin polarizations $\vec{v}_i(0)$ from the Gaussian distribution with mean value $\mu_i = 0$ and variance $\sigma_i^2 = 14$, just as in the FCS. This is due to the parameterization of the reduced density operator of the bath spins $\rho_i(0)$ which is chosen to be

$$\rho_i(0) = \frac{1}{2}\mathbb{1} + \vec{v}_i(0) \cdot \vec{\sigma}\,. \tag{5.28}$$

Now in quantum mechanics, it has to be ensured that such an operator has non-negative eigenvalues, meaning it is positive semidefinite. This is achieved by the constraint $|\vec{v}_i(0)| \leq 1/2$ which is not necessarily fulfilled in the FCS. Otherwise, exponentially growing terms may occur in the solution. In contrast, the QMS obeys this condition which is its main advantage over the FCS.

Until now, it is not clear if breaking this constraint leads to problems when adding the Born corrections to the FCS, for example due to exponential growing terms. For the classical equations of motion (5.1), no problems occur because the corresponding dynamics only consist of a spin precession which preserves the spin length. However, if such exponentially growing terms appear, attempting to the FCS by the inclusion of the Born corrections is pointless. Therefore, the DEQ system (3.79) is studied in the following subsection for invalid density operators due to $|\vec{v}_i(0)| > 1/2$.

5.2.1 Born approximation for invalid density operators

In general, a density operator

$$\rho_i(0) = \frac{1}{2}\mathbb{1} + \vec{v}_i(0) \cdot \vec{\sigma} \tag{5.29}$$

with $|\vec{v}_i(0)| > 1/2$ is not positive semidefinite, meaning it is an invalid density operator. In quantum mechanics, this usually results in exponentially growing terms over time. Until now, it is not clear if solving the Born DEQ system (3.79) really requires fulfilling this constraint, though. Additionally, it is not clear a priori at what time t a divergent behavior emerges.

At least for the FCS, breaking this constraint leads to no problems because the classical equations of motion only describe a spin precession which preserves the spin length. If no problems emerged, the FCS could be used as a basis for including the Born approximation.

Unfortunately, Figure 5.3 gives an example in which the solver fails due to a divergent behavior. These exponentially growing terms would also become dominant while trying to improve the FCS with the Born approximation. Hence, this is definitely the wrong route to follow. It is not discussed any further.

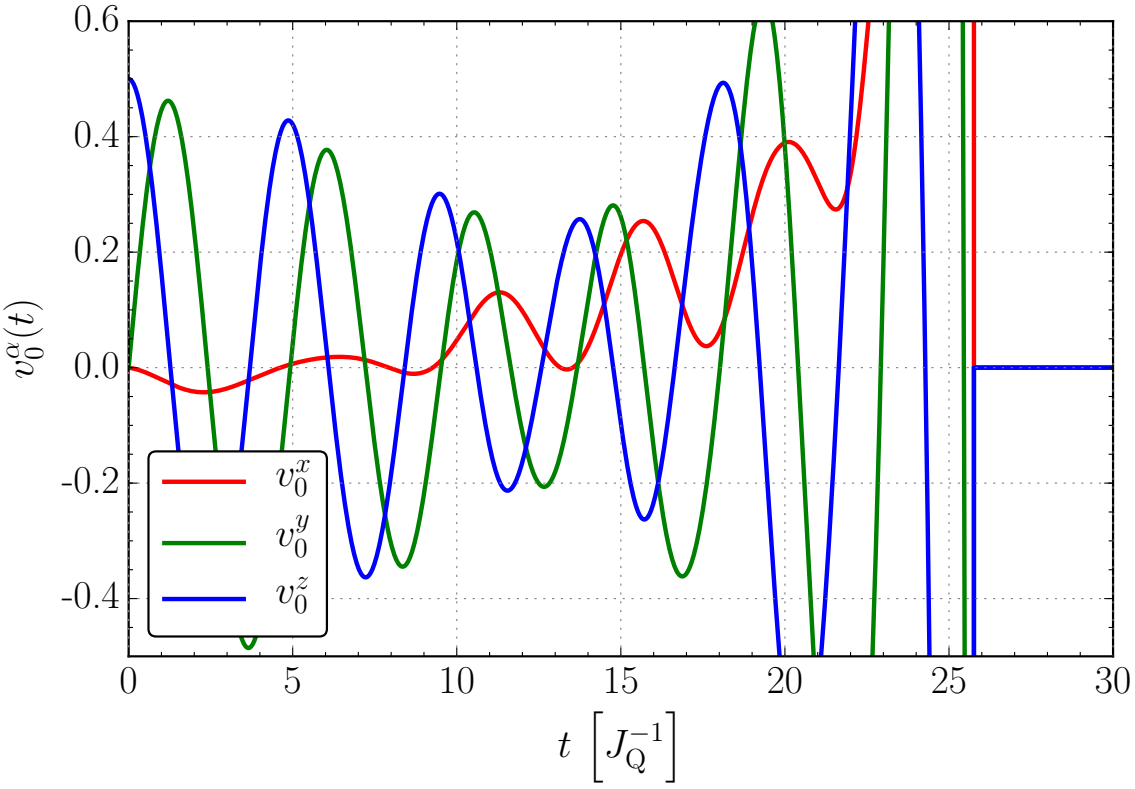

Figure 5.3: Example for the divergent behavior of the central spin expectation value $\vec{v}_0(t)$ when using the Born approximation (3.79) while allowing initial bath polarizations $|\vec{v}_i(0)| > 1/2$ which are not in agreement with quantum mechanics. This calculation is performed for $N = 20$ bath spins with exponentially distributed couplings ($x = 1$).

5.2.2 Quantum mechanical sampling including the Born approximation

In contrast to the FCS, the approach of quantum mechanical sampling as introduced in subsection 5.1.3 obeys the constraint $|\vec{v}_i(0)| \leq 1/2$. As a result, the simulation can be performed using the same algorithm by additionally including the Born corrections. The only difference in practice is solving the DEQ system (3.79) instead of (5.1). This approach is denoted as the Born QMS simulation.

The structure of this DEQ system is much more complicated and the dimension is larger due to the additional differential equations for the matrices $D_{0/i}(t)$ and $M_i(t)$. To maintain the same error tolerance as for the classical simulation, the advaptive RKF45 algorithm has to reduce its stepsize to an smaller value. This is mainly due to the more complex structure of the DEQ system (3.79) which requires the calculation of many matrix multiplications.

This means that additional computation time is required which results in calculations for an overall smaller number of individual simulations $n = 10^5$. This amount is still sufficiently large to neglect error bars and to study the qualitative behavior of this approach in order to judge whether it is reasonable to invest more work into it or not.

In order to compare this calculation to the previous classical simulations as well as the DMRG results, the same parameters as in subsection 5.1.4 are used. The resulting dynamics for $\overline{\langle v_0^z \rangle}(t)$ are shown in Figure 5.4. Obviously, it does not match the previous results at all. Not even the characteristic minimum at $t \approx 3.5 J_\mathrm{Q}^{-1}$ is captured correctly anymore. It appears that the contribution of the Born approximation is too large for all times t. Note that the remaining statistical fluctuations are too small to explain this deviation.

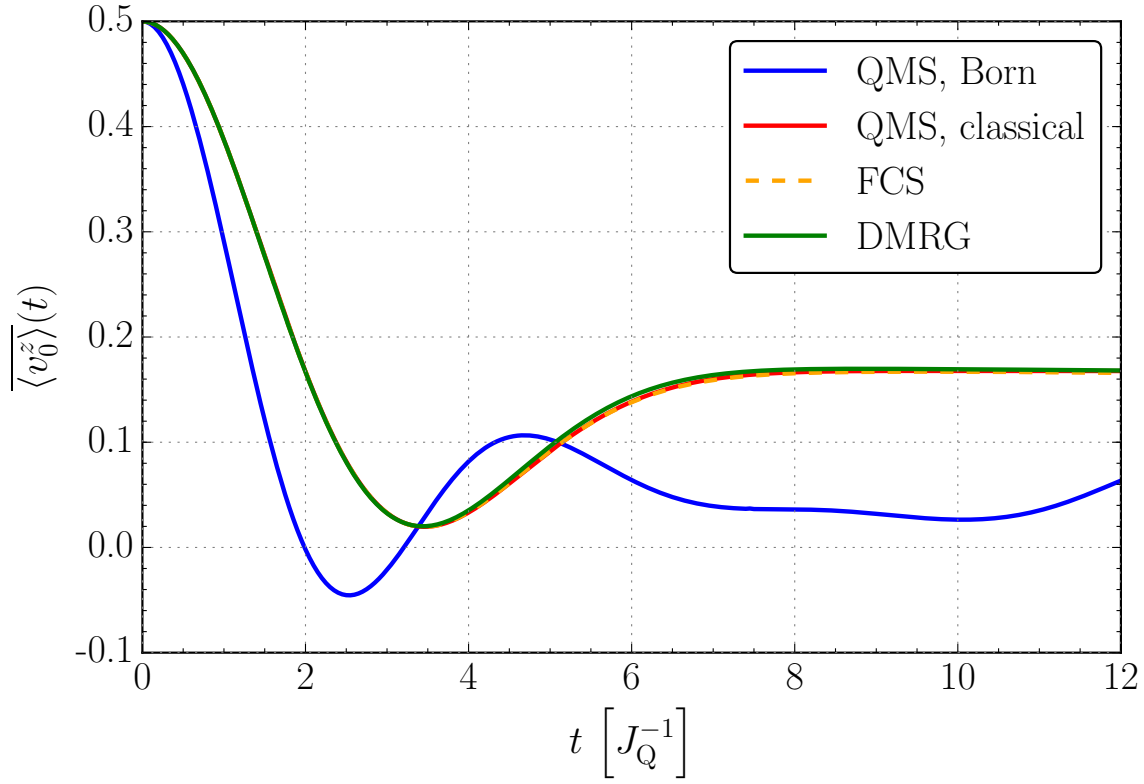

Figure 5.4: Quantum mechanical sampling (QMS) with (Born) and without (classical) Born corrections compared to the full classical simulation (FCS, $n = 10^6$) and DMRG results. The system parameters are the same as used for Figure 5.2, meaning $N = 80$ and $x = 1$. For the Born QMS calculation, the average $\overline{\langle v_0^z \rangle}(t)$ is obtained by averaging over $n = 10^5$ individual simulations.

There is still hope to obtain better results by increasing the bath size N. For larger bath sizes, the quantum mechanical corrections should be suppressed. Now imagine uniformly distributed couplings $J_i \propto 1/\sqrt{N}$. The classical precession term in the differential equation for $\vec{v}_0(t)$ is proportional to $\sum_{i=1}^{N} J_i = \sqrt{N}$. In contrast, the second order correction is proportional to $\sum_{i=1}^{N} J_i^2 = 1$. This means that the classical precession should dominate the dynamics of $\vec{v}_0(t)$ for large bath sizes N.

Fortunately, the size of the DEQ system (3.79) increases linearly with the bath size N. Therefore, a simulation for $N = 800$ bath spins can be performed by decreasing the number for individual simulations by approximately a factor of ten or simply by increasing the computation time by that amount. Of course, the former would lead to larger statistical fluctuations so that the second option is chosen.

A comparison between the Born QMS simulations for $N = 80$ and 800 bath spins is shown in Figure 5.5. No improvement is visible. Their deviation is of the same order as the statistical fluctuations. It appears that this simulation is almost independent of the bath size N, which is in contrast to the previous expectation.

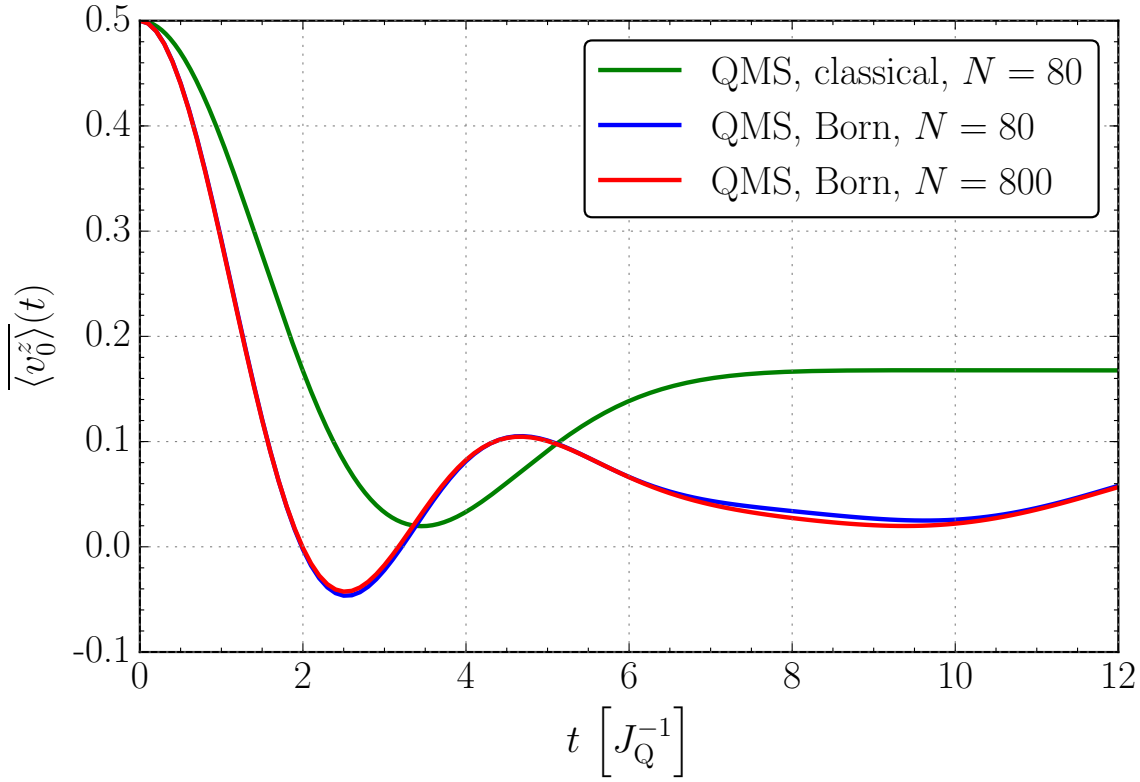

Figure 5.5: Comparison between the Born QMS simulations for $N = 80$ and 800 bath spins ($x = 1$). In both cases, the average $\overline{\langle v_0^z \rangle}(t)$ is calculated by averaging over $n = 10^5$ individual simulations. The classical QMS simulation for $N = 80$ is included as reference ($n = 10^6$).

As argued in subsection 5.1.3, the initial length $|\vec{v}_i(0)|$ is proportional to $1/\sqrt{N}$ (see Figure 5.1). Therefore, this relation has to be taken into account while studying the dependency on N of the DEQ system (3.79) obtained by using the Born approximation. The matrices $D_{0/i}(t)$ describe orthogonal rotations which are of order $\mathcal{O}(1)$, meaning they can be neglected for this analysis. The classical precession terms always include a cross product with $\vec{v}_i(t)$ which is of order $\mathcal{O}(1/\sqrt{N})$. For the second order correction, the N-dependency lies in the matrices $M_i(t)$. The differential equations for $M_i(t)$ contain a term that is independent of $\vec{v}_i$, namely $-D_0^T(t)V_0(t)D_i(t)$, meaning it is of order $\mathcal{O}(1)$. The other terms are of order $\mathcal{O}(1/\sqrt{N})$ or

$\mathcal{O}(1/N)$ so that they are suppressed for large bath sizes N.

For a qualitative argument, the coupling constants are taken from the uniform coupling distribution $J_i \propto 1/\sqrt{N}$ once again. As a result, the classical precession term of $\vec{v}_0(t)$ is now of order $\mathcal{O}(1)$. The second order correction is still of order $\mathcal{O}(1)$ because the matrix $M_i(t)$ is also of order $\mathcal{O}(1)$. Hence, both the classical and the second order correction terms are of the same order $\mathcal{O}(1)$. The same argument holds for the differential equation of each individual bath spin $\vec{v}_i(t)$. The only difference is the additional sum over all bath spins which results in an additional factor N for the differential equation of $\vec{v}_0(t)$. Therefore, both the classical and the second order correction terms are of the same order $\mathcal{O}(1/N)$ for each bath spin $\vec{v}_i(t)$.

As a conclusion, no real improvement can be expected by dealing with larger bath sizes N because the classical precession and the second order correction show the same scaling with N, just as confirmed in Figure 5.5. Unfortunately, this renders the Born QMS approach rather useless.

5.2.3 Alternative sampling approaches

The emerging challenge consists of treating the spin length quantum mechanically, meaning $|\vec{v}_i| < 1/2$, while also sampling the Overhauser field distribution with the correct variance $\sigma_A^2 = J_Q^2/4$. Additionally, each bath spin should be sampled independently so that their initial length $|\vec{v}_i(0)|$ does not scale with the bath size N or at least slower than $1/\sqrt{N}$. These three constraints have to be fulfilled at the same time.

In a first alternative approach, each individual bath spin $\vec{v}_i(0)$ is sampled directly from a Gaussian distribution with mean value $\mu_i = 0$ and variance $\sigma_i^2 = 1/4$, just as for the full classical simulation. In contrast, a cutoff at $|\vec{v}_i(0)| = 1/2$ is introduced so that the spin length is treated quantum mechanically while also also remaining independent of the bath size N. If a bath spin is sampled with $|\vec{v}_i(0)| > 1/2$, it is rescaled to the cutoff length $|\vec{v}_i(0)| = 1/2$. Note that this is an unphysical assumption, though. Obviously, this approach leads to a wrong effective variance $\sigma_{\text{cutoff}}^2 < \sigma_A^2$ for the Overhauser field distribution which is mainly responsible for the characteristic minimum in the classical simulations. This can already be seen when analyzing the Merkulov-solution (5.7) which depends on the variance $\sigma_A^2 = J_Q^2/4$ of the Gaussian distribution. Reducing the variance would mainly shift the characteristic minimum at $t \approx 3.5 J_Q^{-1}$ in Figure 5.2 to the right. This is also the case when using this cutoff approach for a classical simulation because it samples an effectively smaller variance of the Overhauser field.

Another alternative approach samples each individual bath spin $\vec{v}_i(0)$ on the Bloch sphere equidistantly. This fixes the spin length at $|\vec{v}_i(0)| = 1/2$ so that it is treated in a quantum mechanical manner while also remaining independent of the bath size N. Even though this samples a Gaussian distribution with mean value $\mu_{\text{Bloch}} = 0$, it leads to a wrong variance $\sigma_{\text{Bloch}}^2 \neq \sigma_A^2$.

The results of both sampling approaches are shown in Figure 5.6 for a bath of $N = 80$ spins with exponentially distributed couplings ($x = 1$), averaged over $n = 10^5$ individual

simulations. Interestingly, the characteristic minimum is shifted to the left and not to the right as previously assumed. But note that the argument which leads to this assumption is based on the classical Merkulov-solution. By including the Born approximation now, it is not a priori clear what impact it has. The contribution of Born corrections must be simply too large as already observed in the previous subsection 5.2.2. This behavior does not noticeably change when dealing with larger baths either, even though the bath spins are sampled independently of the bath size N in both approaches. This is a hint that the scaling behavior of $\vec{v}_i(0)$ is not the only reason for the Born QMS approach failing in the previous subsection 5.2.2

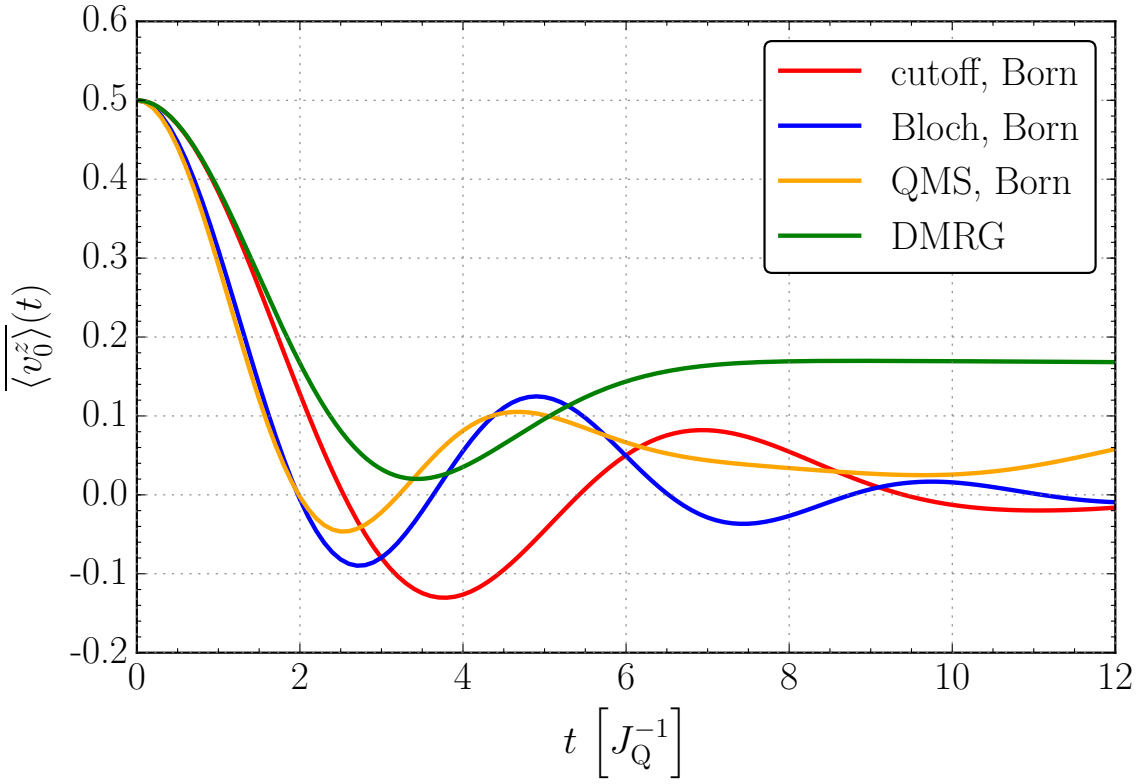

Figure 5.6: Comparison between the cutoff, the Bloch, and the QMS Born approach. The DMRG result functions as reference. The calculations are performed for a bath of $N = 80$ spins with exponentially distributed couplings ($x = 1$), averaged over $n = 10^5$ individual simulations.

So far, no approach fulfilling all three constraints has been found. Hence, the approach of enhancing the classical simulation by the first quantum mechanical corrections in Born approximation is considered as unsuccessful. While this does not necessarily mean that no appropriate solution for this problem exists, the current results rather promote studying the full classical simulation instead.

5.3 Semiclassical simulation

The main ingredient of all classical simulations is the central spin precession around a Gaussian distributed Overhauser field with mean value $\mu_A = 0$ and variance $\sigma_A^2 = {}^{J_Q^2}/_4$. Even the frozen Overhauser field approach which leads to the Merkulov-solution (5.7) can describe the characteristic minimum at $t \approx 3.5 J_Q^{-1}$ well (see Figure 5.2). Dephasing is induced within the full classical simulation by sampling each bath spin independently with variance $\sigma_i^2 = {}^1/_4$. It looks like the intrinsic bath dynamics are mainly responsible for the dephasing of the central spin after the first characteristic minimum.

A semiclassical approach consists of considering the Overhauser field as a classical field, just as in the classical simulation. Then, the central spin precesses around this classical field according to the classical equations of motion. The sampling of each bath spin is still performed by the QMS approach as introduced in subsection 5.1.3 so that the spin length is treated in a quantum mechanical manner. The difference to the classical QMS approach lies in considering each bath spin as a quantum mechanical object that is treated within Born approximation. The DEQ system to solve numerically is still given by (3.79), but without the Born corrections for the central spin $\vec{v}_0(t)$. In contrast to the DEQ system (3.79), the differential equation for the central spin expectation value $\vec{v}_0(t)$ simply reads

$$\frac{\mathrm{d}}{\mathrm{d}t}\vec{v}_0(t) = \sum_{i=1}^{N} J_i \vec{v}_i(t) \times \vec{v}_0(t)\,. \tag{5.30}$$

This is the classical equation of motion for the central spin precessing around a time-dependent Overhauser field.

The reasoning behind this semiclassical approach is based on the experience gained from the Born QMS approach as discussed in subsection 5.2.2. At first glance, the individual bath spin dynamics should not depend on the bath size N because the bath spins are only directly coupled to the central spin. This is clearly the case within Born approximation even in second order because no terms coupling different bath spins to each other occur. Hence, the Born corrections for the bath spins are unproblematic. They are included to understand the real bath dynamics quantum mechanically better by not only treating each bath spin as a classical vector which precesses around the central spin. In contrast, the central spin dynamics depend on the bath size to an important degree so that it can be considered as a classical system for very large bath sizes. Since this behavior does not appear for the Born QMS simulation, the second order corrections for the central spin are simply neglected here.

The result for the central spin dynamics $\overline{\langle v_0^z \rangle}(t)$ are shown in Figure 5.7 for a bath of $N = 80$ spins with exponentially distributed couplings ($x = 1$). The full classical simulation and the DMRG results are included for comparison. In contrast to subsection 5.2.2, the characteristic minimum at $t \approx 3.5 J_Q^{-1}$ is captured adequately. This behavior is expected because on this short timescale, the intrinsic bath spin dynamics do not play an important role. The semiclassical solution shows a sharp maximum at $t \approx 7.5 J_Q^{-1}$ which does not appear as clearly in the DMRG solution. For $t > 7.5 J_Q^{-1}$, a fast decrease of the solution is visible which could be interpreted as dephasing. Note that this decrease happens way too

fast compared to the dephasing appearing in the DMRG and FCS results. Additionally, the semiclassical results seem to be rather unpredictable because for $t > 17 J_{\mathrm{Q}}^{-1}$, the solution increases notably. For $t > 31 J_{\mathrm{Q}}^{-1}$, it decreases again. Since the calculation is performed for an ensemble of $n = 10^5$ individual simulations, the statistical fluctuations are by far too small to explain this behavior.

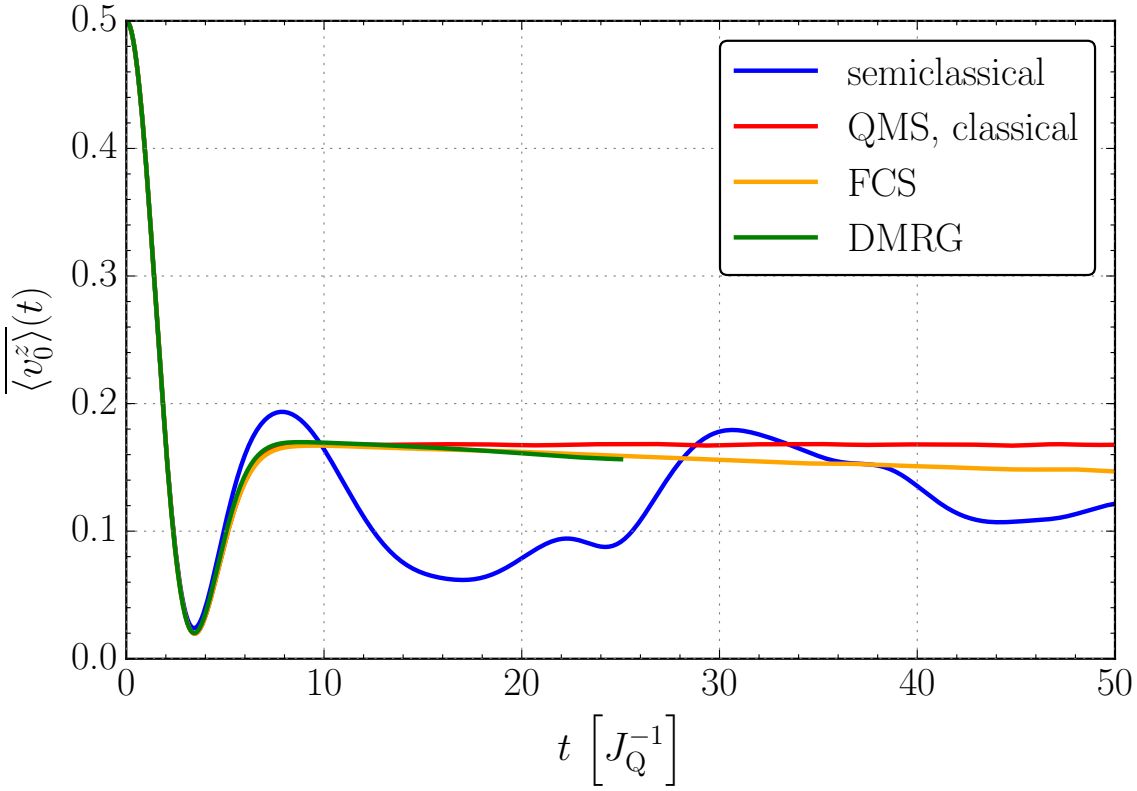

Figure 5.7: Semiclassical simulation for a bath of $N = 80$ spins with exponentially distributed couplings ($x = 1$). The ensemble average is calculated for $n = 10^5$ individual simulations. The classical QMS approach, the full classical simulation (FCS), and the DMRG results are included for comparison.

For a larger bath of $N = 800$ spins, the solution is following the Merkulov-solution for slightly longer times. However, a too fast decrease of the solution appears once again for $t > 7.5 J_{\mathrm{Q}}^{-1}$. No plot is included for this case due to the lack of a significant improvement.

Overall, this semiclassical approach leads to a better result compared to the full Born QMS approach which is discussed in subsection 5.2.2. Nevertheless, the result still cannot function as a good basis for further discussions and analyses of the interesting physical phenomena because its behavior is rather unpredictable and does not match the real longtime solution at all. The only benefit is the quantum mechanically treated spin length. This is not the case in the full classical simulation. However, the FCS is much closer to the DMRG solution, especially for long times and thus, it should be the route to follow for further analyses.

6 Estimates for persisting spin correlations in the central spin model

The present chapter does not deal with a further enhancement of simulations using the Born approximation, but a new approach to calculate estimates for *persisting correlations* in the central spin model is established.

In a previous work by Uhrig et al. [22], a method to calculate rigorous lower bounds for persisting correlations has been established. In particular, this method uses information provided by the constants of motion X_i of the central spin model, which allows the calculation of a rigorous lower bound S_{low} for the persisting part $S_\infty := \lim_{t\to\infty} S(t)$ of the central spin autocorrelation function $S(t) := \langle S_0^z(t) S_0^z(0)\rangle$ in the long-time limit $t \to \infty$.

If this limit does not exist, but $|S(t)| < \infty$ holds, for example due to small remaining oscillations, then the time-independent part of the autocorrelation function is given by the long-time average

$$S_\infty := \lim_{t\to\infty} \frac{1}{t} \int_0^t S(t')\, \mathrm{d}t' \,. \quad (6.1)$$

In general, S_∞ describes the non-decaying fraction of $S(t)$ (see Figure 6.1).

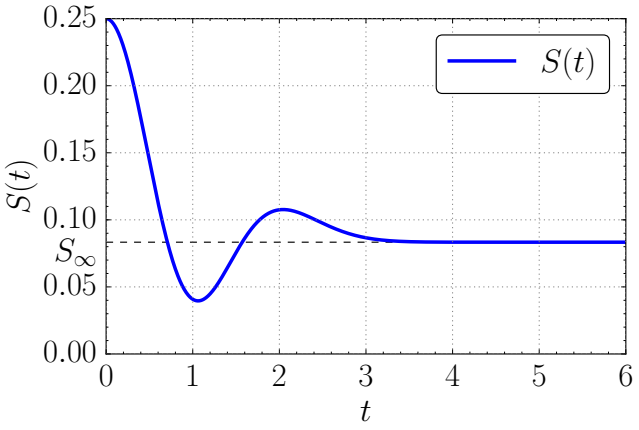

Figure 6.1: Exemplary autocorrelation function $S(t)$ with well-defined long-time limit S_∞.

The Hamiltonian of the central spin model without external magnetic field is given by

$$H_0 = \sum_{i=1}^{N} J_i \vec{S}_0 \cdot \vec{S}_i \,. \quad (6.2)$$

Exploiting the integrability of the central spin model does not yield a tight lower bound. Therefore, Seifert et al. [23] identified relevant combinations of known constants of motion to obtain an improvement. Yet again, the calculated lower bounds are still not good enough to describe the *full* persisting part S_∞ of the autocorrelation function $S(t)$.

Since only a lower bound can be calculated by this method, information is lost within this process. The new approach consists of calculating an estimate for the autocorrelation

function, based on an approximation of the generalized Gibbs ensemble [52]. The main idea is to include information which is lost during the process of calculating a rigorous lower bound by referring to an appropriate equilibrium state.

6.1 Derivation of estimates for persisting correlations

The autocorrelation function of the operator $S_0^z(t)$ can be written as

$$S(t) = \langle S_0^z(t) S_0^z(0) \rangle = \langle U^\dagger(t) S_0^z U(t) S_0^z \rangle = \operatorname{Tr}\left(U^\dagger(t) S_0^z U(t) S_0^z \rho_0 \right) , \tag{6.3}$$

with the unitary time evolution operator $U(t)$.

The hyperfine couplings J_i in the central spin model are in the range of μeV[16, 55, 56], corresponding to temperatures of about 10 mK which is small in comparison to the experimentally relevant temperature [13]. Therefore, the spin system is assumed to be completely disordered so that $\rho_0 = \frac{1}{2^{N+1}} \mathbb{1}$ is a valid approximation. [22]

In this case, the autocorrelation function $\langle S_0^z(t) S_0^z(0) \rangle$ is equivalent to $\langle S_0^z(t) P_\uparrow(0) \rangle$, with the projector on the up-state $|\uparrow\rangle$ of the central spin $P_\uparrow(0) = P_\uparrow = S_0^z + \frac{1}{2}\mathbb{1}$. Now making use of the invariance of the trace under cyclic permutation yields

$$\langle S_0^z(t) P_\uparrow \rangle = \frac{1}{2^{N+1}} \operatorname{Tr}\left(S_0^z U(t) P_\uparrow U^\dagger(t) \right) . \tag{6.4}$$

Note that $\frac{1}{2^N} U(t) P_\uparrow U^\dagger(t) =: \rho(t)$ fulfills the criteria of a density matrix. Thus, the autocorrelation function can be rewritten as

$$\langle S_0^z(t) P_\uparrow \rangle = \frac{1}{2} \operatorname{Tr}\left(S_0^z \rho(t) \right) = \frac{1}{2} \langle S_0^z \rangle_{\rho(t)} . \tag{6.5}$$

It describes the expectation value of the Schrödinger picture operator S_0^z with respect to the density matrix $\rho(t)$.

Since it is known that persisting correlations of the central spin operator S_0^z exist, this density matrix has to be constant on average for infinite times $t \to \infty$. This means that an equilibrium state exists. It is not clear, though, how this equilibrium state is reached dynamically. The long-time equilibrium state has to be equal to the time average, meaning

$$\rho_\infty := \lim_{t \to \infty} \frac{1}{t} \int_0^t \rho(t') \, \mathrm{d}t' . \tag{6.6}$$

This state is the maximum entropy state which keeps all conserved quantities X_i of the system fixed [52]. Note that if a quantum system is integrable, for example the central spin model [53, 54], the system should not be expected to fully thermalize. This is because the constants of motion prohibit thermalization to the canonical ensemble. However, the system can still be expected to equilibrate to the maximum entropy state, given the constants of motion X_i. This state is the so-called *generalized Gibbs ensemble* (GGE)

$$\rho_\infty = \frac{1}{Z\left(\vec{\lambda}\right)} \exp\left(\sum_i \lambda_i X_i \right) , \tag{6.7}$$

with the partition function $Z\left(\vec{\lambda}\right) = \mathrm{Tr}\left[\exp\left(\sum_i \lambda_i X_i\right)\right]$ and the real Lagrange multipliers λ_i. [52]

In general, the index i runs through the full set of constants of motions X_i of the integrable system. However, not all conserved quantities of the central spin model can be taken into account for this approach. Therefore, the index i runs through a finite number of considered constants of motion X_i. By taking the most important X_i into account, the intention is to approximately describe the complete GGE (6.7). In the following, this ansatz for the equilibrium state is denoted as $\tilde{\rho}_\infty$ to distinguish from the complete GGE in equation 6.7. Note that there are non-integrable systems where the GGE fails to describe the equilibrium state correctly when using all known constants of motion [52, 62, 63]. Therefore, it is not clear a priori if this approach allows for calculating the full persisting part of the central spin autocorrelation function when only a finite number of conserved quantities is considered.

When using this ansatz, the main task consists of obtaining the Lagrange multipliers λ_i. The scalar product $(A|B) := \langle A^\dagger B\rangle = \mathrm{Tr}\left(A^\dagger B\rho\right)$ used by Uhrig et al. [22] and Seifert et al. [23] can be rewritten according to

$$x_i := \left(X_i|P_\uparrow\right) = \mathrm{Tr}\left(X_i P_\uparrow \rho_0\right) = \mathrm{Tr}\left(U^\dagger(t) X_i U(t) P_\uparrow \rho_0\right) \tag{6.8a}$$

$$= \mathrm{Tr}\left(X_i U(t) P_\uparrow \rho_0 U^\dagger(t)\right) = \frac{1}{2}\mathrm{Tr}\left(X_i \tilde{\rho}(t)\right) = \frac{1}{2}\mathrm{Tr}\left(X_i \tilde{\rho}_\infty\right) . \tag{6.8b}$$

Here, the trick is to use the relation $U^\dagger(t) X_i U(t) = X_i(t) = X_i$, which holds for any constant of motion because they are obviously constant in time. The unitary time evolution operator is applied to $P_\uparrow\rho_0$ by making use of the invariance of the trace under cyclic permutation. Moreover, the scalar product $x_i = \left(X_i|P_\uparrow\right)$ is constant for all times t in this completely disordered system with $\rho_0 = \frac{1}{2^{N+1}}\mathbb{1}$.

Now calculating the derivative

$$\frac{\partial}{\partial\lambda_i}\ln Z\left(\vec{\lambda}\right) = \frac{1}{Z\left(\vec{\lambda}\right)}\mathrm{Tr}\left[X_i \exp\left(\sum_i \lambda_i X_i\right)\right] = \mathrm{Tr}\left[X_i\tilde{\rho}_\infty\right] = 2x_i \tag{6.9}$$

leads to the system of equations

$$\frac{1}{Z\left(\vec{\lambda}\right)}\mathrm{Tr}\left[X_i \exp\left(\sum_i \lambda_i X_i\right)\right] - 2\left(X_i|P_\uparrow\right) = 0 \qquad \forall\, i\,. \tag{6.10}$$

This system of equations fixes the Lagrange multipliers λ_i which are required to calculate $\tilde{\rho}_\infty$. The scalar products $x_i = \left(X_i|P_\uparrow\right)$ can be calculated analytically as shown in Reference [23]. Then, the system is solved numerically by using the *fzero*-solver provided by GNU Octave [64].

The estimate for the persisting part of the autocorrelation function is given by

$$S_{\mathrm{est}} = \frac{1}{2}\mathrm{Tr}\left(S_0^z\tilde{\rho}_\infty\right) . \tag{6.11}$$

Yet, this system of equations requires heavy numerical effort for large bath sizes N due to the exponentially growing Hilbert space, similar to exact diagonalization of the Hamiltonian H_0.

6.2 Choice of constants of motion

By taking more conserved quantities X_i into account, the complete GGE (6.7) is approximated better, leading to a more precise description of the equilibrium state. Therefore, the choice and number of constants of motions should increase the value of the estimate S_{est}, similar to calculating the rigorous lower bounds. Calculating the lower bounds does not benefit from using constants of motions that have a vanishing overlap $(X_i|S_0^z)$. Nevertheless, they may have an overlap with $P_\uparrow$, meaning $\left(X_i|P_\uparrow\right) \neq 0$. This is due to the fact that $P_\uparrow = S_0^z + \frac{1}{2}\mathbb{1}$ and hence, in case of a vanishing overlap with S_0^z, an overlap with the unity operator $\mathbb{1}$ may exist.

Seifert et al. [23] identified the three constants of motion $I^z H_0$, $I^z H_0^3$ and $I^z I^2 H_0$ as the most relevant conserved quantities to calculate the lower bound in the thermodynamical limit $N \to \infty$. In this limit, constants of motion with an *odd* number of summed spin operators, for example I^z, yield a vanishing contribution to the lower bound. Here, the notation $I^z := \sum_{i=0}^{N} S_i^z$ and $I^2 := \vec{I}^2 = \left(\sum_{i=0}^{N} \vec{S}_i\right)^2$ is introduced.

An advantage of the new approach can be noticed when looking at the series expansion of the density matrix

$$\tilde{\rho}_\infty = \frac{1}{Z\left(\vec{\lambda}\right)} \exp\left(\sum_i \lambda_i X_i\right) = \frac{1}{Z\left(\vec{\lambda}\right)} \sum_{k=0}^{\infty} \frac{1}{k!} \left(\sum_i \lambda_i X_i\right)^k . \tag{6.12}$$

Now imagine the case $X_1 = H_0$ and $X_2 = I^z$. Even though $I^z H_0$ is not used, this conserved quantity appears in second order of the series expansion (6.12) This means that a constant of motion which is not explicitly used might appear in the series expansion and thus, leads to additional information and therefore a better estimate S_{est}. This leads to the idea of using the main ingredients to build most combinations of constants of motions, i. e. H_0, I^z, $I^z H_0$, H_0^2, $(I^z)^2$ and I^2. In addition, $I^z H_0^3$ and $I^z I^2 H_0$ are used because they lead to an noticeable improvement of the rigorous lower bound.

For constants of motions $X_i \propto I^z$, the relation

$$(X_i|S_0^z) = \frac{1}{2}\left(X_i|P_\uparrow - P_\downarrow\right) = \frac{1}{2}\left(X_i|P_\uparrow\right) + \frac{1}{2}\left(X_i|P_\uparrow\right) = \left(P_\uparrow|X_i\right) \tag{6.13}$$

holds. Hence, the required scalar products $(X_i|S_0^z)$ that were already calculated in the previous works by Uhrig et al. [22] and Seifert et al. [23] can be used. Note that the notation $\Sigma_m := \sum_{i=1}^{N} J_i^m$ is used for the moments of the couplings J_i which appear in the following terms.

$$\left(I^z H_0|P_\uparrow\right) = \frac{\Sigma_1}{16} \tag{6.14a}$$

$$\left(I^z H_0^3|P_\uparrow\right) = \frac{1}{256}\left(5\Sigma_1\Sigma_2 - 4\Sigma_3\right) \tag{6.14b}$$

$$\left(I^z I^2 H_0|P_\uparrow\right) = \frac{1}{64}\left(\left(5N+3\right)\Sigma_1\right) \tag{6.14c}$$

The remaining scalar products are calculated by exploiting $\rho_0 = \frac{1}{2^{N+1}}\mathbb{1}$.

$$\left(H_0|P_\uparrow\right) = \mathrm{Tr}\left(H_0 P_\uparrow \rho_0\right) = \frac{1}{2^{N+1}}\,\mathrm{Tr}\left(H_0\left(S_0^z + \frac{1}{2}\mathbb{1}\right)\right) = 0 \tag{6.15a}$$

$$\left(I^z|P_\uparrow\right) = \frac{1}{2^{N+1}}\,\mathrm{Tr}\left(I^z P_\uparrow\right) = \frac{1}{2^{N+1}}\,\mathrm{Tr}\left(I^z\left(S_0^z + \frac{1}{2}\mathbb{1}\right)\right) = \frac{1}{4} \tag{6.15b}$$

$$\left(H_0^2|P_\uparrow\right) = \frac{1}{2^{N+1}}\,\mathrm{Tr}\left(\left(\sum_{i=1}^{N} J_i \vec{S}_0 \cdot \vec{S}_i\right)^2\left(S_0^z + \frac{1}{2}\mathbb{1}\right)\right) \tag{6.15c}$$

$$= \frac{1}{2^{N+1}}\,\mathrm{Tr}\left(\frac{1}{2}\sum_{i,j=1}^{N}\sum_{\alpha,\beta=x,y,z} J_i J_j S_0^\alpha S_0^\beta S_i^\alpha S_j^\beta\right) = \frac{3}{32}\Sigma_2 \tag{6.15d}$$

$$\left(\left(I^z\right)^2|P_\uparrow\right) = \frac{1}{2^{N+1}}\,\mathrm{Tr}\left(\sum_{i,j=0}^{N} S_i^z S_j^z\left(S_0^z + \frac{1}{2}\mathbb{1}\right)\right) = \frac{1}{8}\left(N+1\right) \tag{6.15e}$$

$$\left(I^2|P_\uparrow\right) = 3\left(\left(I^z\right)^2|P_\uparrow\right) = \frac{3}{8}\left(N+1\right) \tag{6.15f}$$

6.3 Results and comparison to exact diagonalization and rigorous lower bounds

For small bath sizes N, it is feasible to calculate the exact persisting part S_∞ autocorrelation function $\langle S_0^z(t)S_0^z(0)\rangle$. In the case of an completely disordered system, the density operator $\rho = \frac{1}{2^{N+1}}\mathbb{1}$ commutes with the CSM Hamiltonian H_0, meaning $[\rho, H_0] = 0$, and hence they have a complete common eigenbasis $|j\rangle$. Their spectra are $\{\rho_j = \frac{1}{2^{N+1}}\}$ and $\{E_j\}$, respectively. Then, using the Lehmann representation, the autocorrelation function takes the form

$$S(t) = \langle S_0^z(t)S_0^z(0)\rangle = \mathrm{Tr}\left(S_0^z(t)S_0^z\rho\right) \tag{6.16a}$$

$$= \sum_{j,m=1}^{N+1} \rho_j |\langle j|S_0^z|m\rangle|^2 \exp\left[i\left(E_j - E_m\right)t\right] \tag{6.16b}$$

$$= \frac{1}{2^{N+1}}\sum_{j,m=1}^{N+1} |\langle j|S_0^z|m\rangle|^2 \exp\left[i\left(E_j - E_m\right)t\right]\,. \tag{6.16c}$$

In case the limit $S_\infty = \lim_{t\to\infty} S(t)$ exists (compare Figure 6.1), it is given by

$$S_\infty = \frac{1}{2^{N+1}}\sum_{j,m=1}^{N+1} |\langle j|S_0^z|m\rangle|^2 \delta_{E_j,E_m} \geq 0\,. \tag{6.17}$$

This exact calculation of the persisting part S_∞ requires the exact diagonalization of the Hamiltonian H_0 in order to obtain its spectrum $\{E_j\}$ and eigenstates $|j\rangle$. However, this also requires exponentially growing computation times and memory space and hence limits the bath size to around ten spins. Then, testing for the degeneracy of the spectrum $\{E_j\}$ is required to calculate the exact persisting part S_∞ by resorting to equation (6.17). The

exact values S_∞ function as a reference for the estimates S_{est}. Note that due to small numerical inaccuracies occurring during the exact diagonalization of the Hamiltonian H_0, a small tolerance of 10^{-11} has to be taken into account for the eigenvalues when testing their degeneracy. It has to be ensured that this tolerance is not too large because otherwise, a false degeneracy might be detected. This would lead to too large results for the exact persisting part S_∞. [22]

The rigorous lower bound $S_{\text{low},3}$ is calculated by using the constants of motion $I^z H_0$, $I^z H_0^3$ and $I^z I^2 H_0$. The data is taken from Reference [23]. The estimate $S_{\text{est},3}$ is calculated by using the same three constants of motions as for $S_{\text{low},3}$. Resorting to all eight constants of motions listed in section 6.2 yields the estimate $S_{\text{est},8}$. While the rigorous lower bounds are basically available for large bath sizes of $\mathcal{O}(1000)$ spins, the new approach can be evaluated only for bath sizes of about nine spins.

The couplings are chosen to be exponentially distributed, meaning

$$J_i = \mathcal{N} \exp\left[-i\frac{x}{N}\right] , \qquad i \in \{1, \dots, N\} . \tag{6.18}$$

This distribution is normalized by choosing $\mathcal{N}$ such that $J_Q^2 = \Sigma_2 = 1$ holds numerically. The parameter x is chosen as $x = 1$ and $x = 4$ so that the influence of weakly coupling bath spins can be studied as well. The calculations are performed numerically using GNU Octave.

Seifert et al. [23] calculated the values S_{BB} and S_{BA} for the persisting part of the autocorrelation function in the thermodynamical limit $N \to \infty$ by using extrapolations. The values $S_{\text{BB}}(N)$ are obtained by using an estimate based on the autocorrelation function of the Overhauser field operator $\vec{B} := \sum_{i=1}^{N} J_i \vec{S}_i$. This approach is justified by the separation of timescales for large bath sizes. Note that here, the notation for the Overhauser field operator is taken from Reference [23], meaning $\vec{B}$ does not represent an external magnetic field as in the previous chapters. The values $S_{\text{BA}}(N)$ are obtained by evaluating the available Bethe ansatz equations using Monte Carlo sampling [32, 33] and calculating the long-time average for different bath sizes N. Then, these values for finite bath sizes are used for an extrapolation [23] to infinite baths $N \to \infty$ which leads to the here shown values S_{BB} and S_{BA}. Studying the thermodynamical limit $N \to \infty$ is reasonable because the physical relevant bath sizes correspond to $10^4 - 10^6$ bath spins. In this thesis, the interval $[S_{\text{BA}}, S_{\text{BB}}]$ shall indicate the range in which the exact persisting part of the autocorrelation function is expected for an infinite bath size. It is used to get an idea for the exact solution in the thermodynamical limit $N \to \infty$ which cannot be calculated exactly anymore.

The estimates $S_{\text{est},3/8}$, the rigorous lower bounds $S_{\text{low},3}$, and the exact persisting part S_∞ are plotted in Figure 6.2 for up to $N = 9$ bath spins. Overall, the persisting part S_∞ of the autocorrelation function decreases for larger baths which is due to the increasing amount of weakly coupled bath spins that are responsible for the long-time behavior of the central spin dynamic. The lower bound $S_{\text{low},3}$ is not sufficiently large to describe the full persisting part S_∞ of the autocorrelation function. Looking at the estimate $S_{\text{est},3}$, the new approach results in an improvement when using the same constants of motions as for $S_{\text{low},3}$. This improvement decreases for larger N, though. Resorting to all eight constants of motions to calculate $S_{\text{est},8}$ results in an additional improvement. This is an expected observation

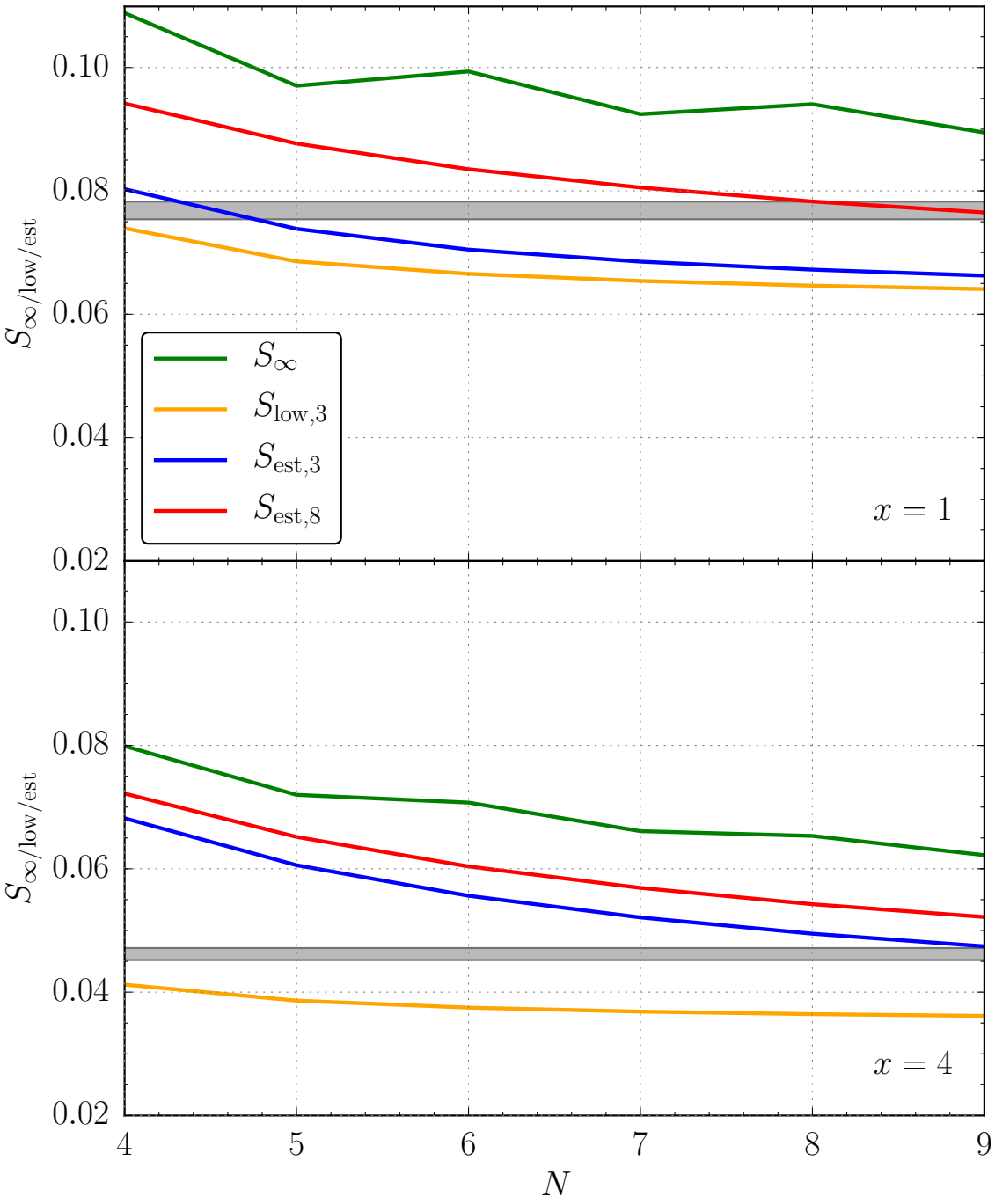

Figure 6.2: Comparison between the rigorous lower bounds $S_{\mathrm{low},3}$ and the estimates $S_{\mathrm{est},3}$ and $S_{\mathrm{est},8}$. In addition, the exact persisting part S_∞ of the autocorrelation function is shown. The gray area indicates the interval $[S_{\mathrm{BA}}, S_{\mathrm{BB}}]$ in which the exact persisting part S_∞ is expected in the thermodynamical limit $N \to \infty$.

because by resorting to more constants of motions, the complete GGE (6.7) is approximated better. While the estimates $S_{\mathrm{est},8}$ get significantly closer to the exact result S_∞, they are yet again not sufficiently large to describe the full persisting part S_∞.

Not all constants of motion X_i by themselves yield a significant improvement of the estimate. This is mainly the case for H_0 which does not have an overlap with neither $P_\uparrow$ nor S_0^z. In contrast, I^z yields a large improvement for these small bath sizes. Nevertheless, it is unclear what happens exactly in the thermodynamical limit $N \to \infty$.

The improvements also depend on the parameter x and seem to become better for larger x. This parameter appears in the exponential coupling distribution (6.18) and fixes the amount of bath spins with a small hyperfine coupling J_i. For a larger x, the dephasing of the central spin becomes more dominant, leading to a smaller persisting part of the autocorrelation function. This is because the amount of weakly coupled bath spins is mainly responsible for the long-time behavior of the central spin [18, 20, 23]. The degeneracy of the eigenvalues $\{E_j\}$, required for the exact calculation of S_∞ using (6.17), depends noticeably on the parameter x. Since the degeneracy decreases for larger x, the value of S_∞ decreases as well, meaning the persisting fraction of the autocorrelation function depends on the amount of weakly coupled bath spins. Note that the observed behavior is indeed in agreement with the calculations for the exact persisting part S_∞, the estimates S_{est}, and the rigorous lower bounds S_{low} shown in Figure 6.2.

Bath sizes of up to nine spins as shown in figure 6.2 do not describe the physical systems of interest. Extrapolating to larger bath sizes as done in reference [23] requires data for at least bath sizes of $\mathcal{O}(100)$ spins for reliable results. Hence, it can only presumed what happens for larger N. Unfortunately, since the estimates are already quite close to or even within the interval $[S_{\mathrm{BA}}, S_{\mathrm{BB}}]$, it has to be expected that an extrapolation would still lead to too small values for infinite bath sizes $N \to \infty$. This must be the case because not all relevant constants of motions X_i are taken into account, meaning not the complete GGE (6.7) but the approximation $\tilde{\rho}_\infty$ is used to describe the equilibrium state. The improvements gained through higher order combinations of conserved quantities in the series expansion (6.12) seem to be too small to make up for not including all possible combinations of conserved quantities directly in first order. This is in agreement with the observed improvements gained by considering more constants of motion directly, meaning $S_{\mathrm{est},8} > S_{\mathrm{est},3}$.

To study the present approach in the thermodynamical limit of an infinite bath size $N \to \infty$, a route based on calculating the leading orders of the individual contributions using Gaussian integrals to evaluate traces analytically can be considered, similar to the calculations by Seifert et al. [23] to obtain the leading orders for the rigorous lower bounds. It is a valid method to obtain the leading order contributions because the central spin model is expected to behave classically in the thermodynamical limit $N \to \infty$.

7 Conclusion

In this thesis, spin dynamics in the central spin model were studied by employing the Born approximation to derive the first quantum mechanical corrections to the classical equations of motion. In an experimental context, the central spin model describes the decoherence of a single electron spin (qubit) which is confined in a quantum dot. The decoherence occurs mainly due to the hyperfine interaction between the electron and the surrounding nuclear spins. Theoretical analyses on this field are relevant for spin noise measurements.

The intention of this thesis consisted of improving the classical simulation by taking first quantum mechanical corrections into account. By splitting the Hamiltonian of the central spin model into two parts, the classical equations of motion are still contained within the derived DEQ system. Then, the second order correction is obtained by treating the interacting part of the split Hamiltonian within Born approximation. This leads to a DEQ system which scales linearly with the amount of bath spins, rendering a treatment of large bath sizes feasible.

The numerical analysis of the derived DEQ system shows an improvement over the classical equations of motion on a small timescale. Various errors show the correct power law so that the DEQ system has to be considered as correct. Because of this, it also seems like the weak-coupling approximation is valid, at least on this small timescale. By comparing the results to exact and DMRG data, it can be concluded that the approach is not capable of describing the long-time behavior of the central spin dynamic, though. Mainly, the dephasing for longer times is missing. Because the Markov-approximation is not justified for the central spin model, treating it within Born approximation only yields an improvement for short times. This timescale could be extended by gradually including higher order corrections. However, this is not an easy task which will most likely lead to only a small improvement. The required computation times to solve the related DEQ systems would also grow accordingly due to the additional complexity. Another improvement is gained when applying an external magnetic field to the central spin because this interaction is included exactly within this approach. This leads to an overall smaller error. Yet, dephasing is still missing or too slow within the solution.

The missing feature of dephasing can be partly included by taking a route based on calculating averages of Gaussian bath ensembles, just as used for classical simulations. However, trying to improve the classical simulations by including the Born corrections leads to the challenge of finding a valid sampling method for the Gaussian distributed Overhauser field. Because the spin length has to be treated in a quantum mechanical manner, it is not possible to use the full classical simulation (FCS) as a basis for a simulation including the Born corrections. The approach using quantum mechanical sampling (QMS) leads to problems with the scaling of the second order correction for larger bath sizes because the sampled bath spin length depends on the bath size. Hence, since the Born corrections already yield a too large

contribution for small baths, no improvement is gained when dealing with a much larger bath. Alternative sampling approaches yield a wrong variance, but they also indicate that the scaling of the sampled bath spin length is not the only problem of the present approach. The Born corrections seem to be simply too large for all times, almost independently of the considered bath size.

In a final approach to make use of the derived Born corrections, a semiclassical approach is studied. Here, the central spin only precesses around the Overhauser field, meaning its problematic second order correction is simply neglected. They are still taken into account for the individual bath spins. Yet, this semiclassical simulation leads to an unpredictable behavior for the central spin dynamics after the first characteristic minimum, which is very hard to analyze any further. This must be the case because the Born approximation leads to a second order correction of classical equations of motion. This correction yields an improvement over the simple classical precession, but only on a small timescale. For longer times, this approach is not controllable anymore so that an unpredictable behavior might occur. Thus, the approach of improving the classical simulation by the first quantum mechanical corrections concludes unsuccessfully.

Further studies could analyze the impact of the inclusion of a strong external magnetic field on the developed approaches. Since the inclusion already yields an improvement for a single simulation as discussed in chapter 4, it should also yield an improvement when averaging over an ensemble of individual calculations. Yet, other approaches already focus directly on including a strong magnetic field, allowing them to deal with this particular case quite well. Remember that the main intention of this thesis was describing the vanishing or low field limit which is important for spin noise measurements which has failed. As mentioned before, the discussed approaches did not yield the anticipated results.

For further studies on this field, the full classical simulation should be considered. In a recent master thesis by Hüdepohl [20], it has been shown that the full classical simulation is a very efficient approach to study the behavior of the central spin for long times and in the thermodynamical limit of an infinite bath size. Later, other semiclassical approaches could be studied, for example to deal with the spin length in a quantum mechanical manner.

In the last chapter, a new approach is presented which allows for calculating estimates for persisting correlations in the central spin model. The intention is to obtain an improvement of the rigorous lower bounds which were recently calculated by Seifert et al. [23]. The approach is based on the generalized Gibbs ensemble, using a limited amount of constants of motions to approximately describe the density operator which describes the equilibrium state for infinite times. While this approach leads to an improvement over rigorous lower bounds for very small bath sizes, it is still not close enough to the exact solution. It can only be presumed what happens for a much larger bath, but it seems like this would still be the observation in the thermodynamical limit.

It may be possible to further improve the estimates by taking other conserved quantities into account. This should lead to an improvement due to approximating the complete generalized Gibbs ensemble better. However, those constants of motion that have been identified to be the most relevant ones for the rigorous lower bounds by Seifert et al. [23] are already

considered in the present thesis. Therefore, improving the new estimates significantly by only a small number of additional conserved quantities seems to be a hard task.

Until now, it is unclear if the improvements for small bath sizes also translate to an improvement in the thermodynamical limit. Hence, another route for further studies could consist of looking at the leading orders of the individual contributions, obtained by using Gaussian integrals to evaluate traces analytically, similar to calculations in Reference [23]. Through this, it should be possible to obtain results for infinite bath sizes which is the physical limit of interest.

A Spin and vector algebra

Note that throughout this thesis, natural units ($\hbar = 1$) are used.

Pauli matrices:

$$\sigma^x = \begin{pmatrix} 0 & 1 \\ 1 & 0 \end{pmatrix}, \qquad \sigma^y = \begin{pmatrix} 0 & -i \\ i & 0 \end{pmatrix}, \qquad \sigma^z = \begin{pmatrix} 1 & 0 \\ 0 & -1 \end{pmatrix} \tag{A.1}$$

$$\sigma^\alpha \sigma^\beta = \delta_{\alpha\beta}\mathbb{1} + i\sum_\gamma \sigma^\gamma \epsilon_{\alpha\beta\gamma} \tag{A.2}$$

$$\left[\sigma^\alpha, \sigma^\beta\right] = 2i\sum_\gamma \sigma^\gamma \epsilon_{\alpha\beta\gamma} \tag{A.3}$$

$$\left\{\sigma^\alpha, \sigma^\beta\right\} = 2\delta_{\alpha\beta}\mathbb{1} \tag{A.4}$$

$$\mathrm{Tr}\left\{\sigma^\alpha\right\} = 0 \tag{A.5}$$

Spin operators:

$$s^\alpha = \sigma^\alpha/2 \tag{A.6}$$

$$S_i^\alpha = \mathbb{1} \otimes \cdots \otimes \underbrace{\sigma^\alpha/2}_{i\text{th place}} \otimes \cdots \otimes \mathbb{1} \tag{A.7}$$

$$S_i^\alpha S_i^\beta = \frac{\delta_{\alpha\beta}}{4}\mathbb{1} + \frac{i}{2}\sum_\gamma S_i^\gamma \epsilon_{\alpha\beta\gamma} \tag{A.8}$$

$$\left[S_i^\alpha, S_i^\beta\right] = i\sum_\gamma S_i^\gamma \epsilon_{\alpha\beta\gamma} \tag{A.9}$$

$$\left[S_i^\alpha S_j^\beta, S_j^\gamma S_i^\delta\right] = \frac{i}{4}\sum_\kappa \left(S_j^\kappa \epsilon_{\beta\gamma\kappa}\delta_{\alpha\delta} + S_i^\kappa \epsilon_{\alpha\delta\kappa}\delta_{\gamma\beta}\right) \tag{A.10}$$

$$\left\{S_i^\alpha, S_i^\beta\right\} = \frac{\delta_{\alpha\beta}}{2}\mathbb{1} \tag{A.11}$$

Rotation matrix D ($\det D = +1$):

$$D^T D = \mathbb{1} \tag{A.12}$$

$$D\left(\vec{a} \times \vec{b}\right) = \det D\left[(D\vec{a}) \times (D\vec{b})\right] = (D\vec{a}) \times (D\vec{b}) \tag{A.13}$$

Scalar product:

$$\vec{a} \cdot \vec{b} = \vec{b} \cdot \vec{a} = \vec{a}^T\vec{b} = \sum_\alpha a^\alpha b^\alpha \tag{A.14}$$

Cross product:

$$\vec{a} \times \vec{b} = \sum_{\alpha\beta\gamma} \vec{e}_\alpha a^\beta b^\gamma \epsilon_{\alpha\beta\gamma} \tag{A.15}$$

$$\vec{v}_0 \times \vec{v}_i = V_0 \vec{v}_i \tag{A.16}$$

$$V_0^T = -V_0 \qquad \text{(skew-symmetric)} \tag{A.17}$$

Matrix-vector product:

$$M\vec{a} = \sum_{\alpha\beta} M^{\alpha\beta} a^\beta \vec{e}_\alpha \tag{A.18}$$

Matrix multiplication:

$$(AB)^{\alpha\beta} = \sum_\gamma A^{\alpha\gamma} B^{\gamma\beta} \tag{A.19}$$

Scalar triple product:

$$\vec{a} \cdot \left(\vec{b} \times \vec{c}\right) = \vec{c} \cdot \left(\vec{a} \times \vec{b}\right) = \vec{b} \cdot (\vec{c} \times \vec{a}) \tag{A.20}$$

$$\left(\vec{a} \times \vec{b}\right) \cdot \vec{c} = \sum_{\alpha\beta\gamma} a^\alpha b^\beta c^\gamma \epsilon_{\alpha\beta\gamma} \tag{A.21}$$

Product of two scalar-products:

$$\left(\vec{a} \cdot \vec{S}_i\right)\left(\vec{b} \cdot \vec{S}_0\right) = \left[\left(\vec{b}\vec{a}^T\right)\vec{S}_i\right] \cdot \vec{S}_0 \tag{A.22}$$

Bibliography

[1] P. Shor, "Algorithms for quantum computation: Discrete logarithms and factoring", 35th Annual Symposium on Foundations of Computer Science, 1994 Proceedings, 124 (1994).

[2] P. Shor, "Polynomial-Time Algorithms for Prime Factorization and Discrete Logarithms on a Quantum Computer", SIAM J. Comput. **26**, 1484 (1997).

[3] L. K. Grover, "Quantum Mechanics Helps in Searching for a Needle in a Haystack", Phys. Rev. Lett. **79**, 325 (1997).

[4] D. P. DiVincenzo, "The Physical Implementation of Quantum Computation", Fortschr. Phys. **48**, 771 (2000).

[5] D. Loss and D. P. DiVincenzo, "Quantum computation with quantum dots", Phys. Rev. A **57**, 120 (1998).

[6] J. Schliemann, A. Khaetskii, and D. Loss, "Electron spin dynamics in quantum dots and related nanostructures due to hyperfine interaction with nuclei", J. Phys. Condens. Matter **15**, R1809 (2003).

[7] A. V. Khaetskii, D. Loss, and L. Glazman, "Electron Spin Decoherence in Quantum Dots due to Interaction with Nuclei", Phys. Rev. Lett. **88**, 186802 (2002).

[8] J. M. Kikkawa and D. D. Awschalom, "Resonant Spin Amplification in n-Type GaAs", Phys. Rev. Lett. **80**, 4313 (1998).

[9] A. Greilich, R. Oulton, E. A. Zhukov, I. A. Yugova, D. R. Yakovlev, M. Bayer, A. Shabaev, A. L. Efros, I. A. Merkulov, V. Stavarache, D. Reuter, and A. Wieck, "Optical Control of Spin Coherence in Singly Charged (In, Ga)As/GaAs Quantum Dots", Phys. Rev. Lett. **96**, 227401 (2006).

[10] R. Hanson, L. P. Kouwenhoven, J. R. Petta, S. Tarucha, and L. M. K. Vandersypen, "Spins in few-electron quantum dots", Rev. Mod. Phys. **79**, 1217 (2007).

[11] F. Jelezko and J. Wrachtrup, "Single defect centres in diamond: A review", Phys. Status Solidi A **203**, 3207 (2006).

[12] G. A. Álvarez, A. Ajoy, X. Peng, and D. Suter, "Performance comparison of dynamical decoupling sequences for a qubit in a rapidly fluctuating spin bath", Phys. Rev. A **82**, 042306 (2010).

[13] B. Urbaszek, X. Marie, T. Amand, O. Krebs, P. Voisin, P. Maletinsky, A. Högele, and A. Imamoglu, "Nuclear spin physics in quantum dots: An optical investigation", Rev. Mod. Phys. **85**, 79 (2013).

[14] J. R. Maze, J. M. Taylor, and M. D. Lukin, "Electron spin decoherence of single nitrogen-vacancy defects in diamond", Phys. Rev. B **78**, 094303 (2008).

[15] G. S. Uhrig, "Keeping a Quantum Bit Alive by Optimized π-Pulse Sequences", Phys. Rev. Lett. **98**, 100504 (2007).

[16] I. A. Merkulov, A. L. Efros, and M. Rosen, "Electron spin relaxation by nuclei in semiconductor quantum dots", Phys. Rev. B **65**, 205309 (2002).

[17] S. I. Erlingsson and Y. V. Nazarov, "Evolution of localized electron spin in a nuclear spin environment", Phys. Rev. B **70**, 205327 (2004).

[18] G. Chen, D. L. Bergman, and L. Balents, "Semiclassical dynamics and long-time asymptotics of the central-spin problem in a quantum dot", Phys. Rev. B **76**, 045312 (2007).

[19] D. Stanek, C. Raas, and G. S. Uhrig, "From quantum-mechanical to classical dynamics in the central-spin model", Phys. Rev. B **90**, 064301 (2014).

[20] J. Hüdepohl, "Effiziente Algorithmen zur Berechnung von Autokorrelationsfunktionen im klassischen Zentralspinmodell mit unendlich vielen Badspins", Master thesis (TU Dortmund, 2016).

[21] K. A. Al-Hassanieh, V. V. Dobrovitski, E. Dagotto, and B. N. Harmon, "Numerical Modeling of the Central Spin Problem Using the Spin-Coherent-State P Representation", Phys. Rev. Lett. **97**, 037204 (2006).

[22] G. Uhrig, J. Hackmann, S. Stanek, J. Stolze, and F. B. Anders, "Conservation laws protect dynamic spin correlations from decay: Limited role of integrability in the central spin model", Phys. Rev. B **90**, 060301 (2014).

[23] U. Seifert, P. Bleicker, P. Schering, A. Faribault, and G. S. Uhrig, "Persisting correlations of a central spin coupled to large spin baths", Phys. Rev. B **94**, 094308 (2016).

[24] H. Tal-Ezer and R. Kosloff, "An accurate and efficient scheme for propagating the time dependent Schrödinger equation", J. Chem. Phys **81**, 3967 (1984).

[25] V. V. Dobrovitski, H. A. De Raedt, M. I. Katsnelson, and B. N. Harmon, "Quantum Oscillations without Quantum Coherence", Phys. Rev. Lett. **90**, 210401 (2003).

[26] V. V. Dobrovitski and H. A. De Raedt, "Efficient scheme for numerical simulations of the spin-bath decoherence", Phys. Rev. E **67**, 056702 (2003).

[27] J. Hackmann and F. B. Anders, "Spin noise in the anisotropic central spin model", Phys. Rev. B **89**, 045317 (2014).

[28] D. Stanek, C. Raas, and G. S. Uhrig, "Dynamics and decoherence in the central spin model in the low-field limit", Phys. Rev. B **88**, 155305 (2013).

[29] L. B. Gravert, P. Lorenz, C. Nase, J. Stolze, and G. S. Uhrig, "Increased coherence time in narrowed bath states in quantum dots", Phys. Rev. B **94**, 094416 (2016).

[30] M. Bortz, S. Eggert, C. Schneider, R. Stübner, and J. Stolze, "Dynamics and decoherence in the central spin model using exact methods", Phys. Rev. B **82**, 161308 (2010).

[31] M. Bortz and J. Stolze, "Exact dynamics in the inhomogeneous central-spin model", Phys. Rev. B **76**, 014304 (2007).

[32] A. Faribault and D. Schuricht, "Integrability-Based Analysis of the Hyperfine-Interaction-Induced Decoherence in Quantum Dots", Phys. Rev. Lett. **110**, 040405 (2013).

[33] A. Faribault and D. Schuricht, "Spin decoherence due to a randomly fluctuating spin bath", Phys. Rev. B **88**, 085323 (2013).

[34] A. Khaetskii, D. Loss, and L. Glazman, "Electron spin evolution induced by interaction with nuclei in a quantum dot", Phys. Rev. B **67**, 195329 (2003).

[35] W. A. Coish and D. Loss, "Hyperfine interaction in a quantum dot: Non-Markovian electron spin dynamics", Phys. Rev. B **70**, 195340 (2004).

[36] J. Fischer and H.-P. Breuer, "Correlated projection operator approach to non-Markovian dynamics in spin baths", Phys. Rev. A **76**, 052119 (2007).

[37] E. Ferraro, H.-P. Breuer, A. Napoli, M. A. Jivulescu, and A. Messina, "Non-Markovian dynamics of a single electron spin coupled to a nuclear spin bath", Phys. Rev. B **78**, 064309 (2008).

[38] W. A. Coish, J. Fischer, and D. Loss, "Free-induction decay and envelope modulations in a narrowed nuclear spin bath", Phys. Rev. B **81**, 165315 (2010).

[39] E. Barnes and S. E. Economou, "Electron-Nuclear Dynamics in a Quantum Dot under Nonunitary Electron Control", Phys. Rev. Lett. **107**, 047601 (2011).

[40] E. Barnes, Ł. Cywiński, and S. Das Sarma, "Nonperturbative Master Equation Solution of Central Spin Dephasing Dynamics", Phys. Rev. Lett. **109**, 140403 (2012).

[41] W. Beugeling, G. S. Uhrig, and F. B. Anders, "Quantum model for mode locking in pulsed semiconductor quantum dot", arXiv:1609.06528 (2016).

[42] N. Wu, N. Fröhling, X. Xing, J. Hackmann, A. Nanduri, F. B. Anders, and H. Rabitz, "Decoherence of a single spin coupled to an interacting spin bath", Phys. Rev. B **93**, 035430 (2016).

[43] Ł. Cywiński, W. M. Witzel, and S. Das Sarma, "Electron Spin Dephasing due to Hyperfine Interactions with a Nuclear Spin Bath", Phys. Rev. Lett. **102**, 057601 (2009).

[44] Ł. Cywiński, W. M. Witzel, and S. Das Sarma, "Pure quantum dephasing of a solid-state electron spin qubit in a large nuclear spin bath coupled by long-range hyperfine-mediated interactions", Phys. Rev. B **79**, 245314 (2009).

[45] W. M. Witzel, R. de Sousa, and S. Das Sarma, "Quantum theory of spectral-diffusion-induced electron spin decoherence", Phys. Rev. B **72**, 161306 (2005).

[46] W. Yang and R.-B. Liu, "Quantum many-body theory of qubit decoherence in a finite-size spin bath", Phys. Rev. B **78**, 085315 (2008).

[47] Y. Li, N. Sinitsyn, D. L. Smith, D. Reuter, A. D. Wieck, D. R. Yakovlev, M. Bayer, and S. A. Crooker, "Intrinsic Spin Fluctuations Reveal the Dynamical Response Function of Holes Coupled to Nuclear Spin Baths in (In, Ga)As Quantum Dots", Phys. Rev. Lett. **108**, 186603 (2012).

[48] A. V. Kuhlmann, J. Houel, L. Ludwig Arne and Greuter, D. Reuter, A. D. Wieck, M. Poggio, and R. J. Warburton, "Charge noise and spin noise in a semiconductor quantum device", Nat. Phys. **9**, 570 (2013).

[49] R. Dahbashi, J. Hübner, F. Berski, K. Pierz, and M. Oestreich, "Optical Spin Noise of a Single Hole Spin Localized in an (InGa)As Quantum Dot", Phys. Rev. Lett. **112**, 156601 (2014).

[50] P. Glasenapp, D. S. Smirnov, A. Greilich, J. Hackmann, M. M. Glazov, F. B. Anders, and M. Bayer, "Spin noise of electrons and holes in (In, Ga)As quantum dots: Experiment and theory", Phys. Rev. B **93**, 205429 (2016).

[51] H.-P. Breuer and F. Petruccione, *The Theory of Open Quantum Systems* (Oxford University Press, 2006), p. 131.

[52] J. Eisert, M. Friesdorf, and C. Gogolin, "Quantum many-body systems out of equilibrium", Nat. Phys. **11**, 124 (2015).

[53] M. Gaudin, "Diagonalisation d'une classe d'hamiltoniens de spin", J. Phys. France **37**, 1087 (1976).

[54] M. Gaudin, *La Fonction d'Onde de Bethe* (Masson, Paris, 1983).

[55] S. Lee, P. von Allmen, F. Oyafuso, G. Klimeck, and K. B. Whaley, "Effect of electron-nuclear spin interactions for electron-spin qubits localized in InGaAs self-assembled quantum dots", J. Appl. Phys. **97**, 043706 (2005).

[56] M. Y. Petrov, I. V. Ignatiev, S. V. Poltavtsev, A. Greilich, A. Bauschulte, D. R. Yakovlev, and M. Bayer, "Effect of thermal annealing on the hyperfine interaction in InAs/GaAs quantum dots", Phys. Rev. B **78**, 045315 (2008).

[57] D. Stanek, "Dynamics and Decoherence in the Central Spin Model: From a Quantum Mechanical to a Classical Description", PhD thesis (TU Dortmund, 2013).

[58] R. V. Pound, "Nuclear Electric Quadrupole Interactions in Crystals", Phys. Rev. **79**, 685 (1950).

[59] J. Hackmann, P. Glasenapp, A. Greilich, M. Bayer, and F. B. Anders, "Influence of the Nuclear Electric Quadrupolar Interaction on the Coherence Time of Hole and Electron Spins Confined in Semiconductor Quantum Dots", Phys. Rev. Lett. **115**, 207401 (2015).

[60] H.-P. Breuer, D. Burgarth, and F. Petruccione, "Non-markovian dynamics in a spin star system: exact solution and approximation techniques", Phys. Rev. B **70**, 045323 (2004).

[61] L. Gravert, *private communication* (2016).

[62] B. Wouters, J. De Nardis, M. Brockmann, D. Fioretto, M. Rigol, and J.-S. Caux, "Quenching the anisotropic heisenberg chain: exact solution and generalized gibbs ensemble predictions", Phys. Rev. Lett. **113**, 117202 (2014).

[63] B. Pozsgay, M. Mestyán, M. A. Werner, M. Kormos, G. Zaránd, and G. Takács, "Correlations after quantum quenches in the xxz spin chain: failure of the generalized gibbs ensemble", Phys. Rev. Lett. **113**, 117203 (2014).

[64] J. W. Eaton, D. Bateman, S. Hauberg, and R. Wehbring, *GNU Octave version 4.0.0 manual: a high-level interactive language for numerical computations* (2015).

Danksagung

Ich möchte mich zunächst bei Herrn Prof. Dr. Götz S. Uhrig für die Vergabe des Themas und insbesondere für die intensive Betreuung bedanken. Dadurch war stets eine sehr gute Zusammenarbeit möglich. Herrn Prof. Dr. Frithjof B. Anders danke ich für die Übernahme der Zweitkorrektur. Meinen Bürokollegen Fabian Köhler und Frederik Keim möchte ich für die stetige Hilfe bei technischen Problemen meinen Dank aussprechen. Lars Gravert danke ich für die Bereitstellung der exakten Daten für homogen verteilte Kopplungen und für die DMRG Daten für exponentiell verteilte Kopplungen. Ebenfalls möchte ich mich bei ihm und Philip Bleicker für das Korrekturlesen der Arbeit bedanken.

Ein besonderer Dank gebührt meinen Eltern, die mich während meines Studiums finanziell unterstützt haben. Erst dadurch war es mir möglich, meinen Fokus allein auf das Studium zu richten. Zuletzt möchte ich mich ausdrücklich bei meiner Lebensgefährtin Jacqueline Nakath bedanken, die mir stets mit Zuversicht und Rat auch in schwierigen Phasen beigestanden und mir jederzeit den nötigen Rückhalt gegeben hat.

Eidesstattliche Versicherung

Ich versichere hiermit an Eides statt, dass ich die vorliegende Abschlussarbeit mit dem Titel "Dynamics in the central spin model employing the Born approximation" selbstständig und ohne unzulässige fremde Hilfe erbracht habe. Ich habe keine anderen als die angegebenen Quellen und Hilfsmittel benutzt, sowie wörtliche und sinngemäße Zitate kenntlich gemacht. Die Arbeit hat in gleicher oder ähnlicher Form noch keiner Prüfungsbehörde vorgelegen.

Ort, Datum	Unterschrift

Belehrung

Wer vorsätzlich gegen eine die Täuschung über Prüfungsleistungen betreffende Regelung einer Hochschulprüfungsordnung verstößt, handelt ordnungswidrig. Die Ordnungswidrigkeit kann mit einer Geldbuße von bis zu 50 000 € geahndet werden. Zuständige Verwaltungsbehörde für die Verfolgung und Ahndung von Ordnungswidrigkeiten ist der Kanzler/die Kanzlerin der Technischen Universität Dortmund. Im Falle eines mehrfachen oder sonstigen schwerwiegenden Täuschungsversuches kann der Prüfling zudem exmatrikuliert werden (§ 63 Abs. 5 Hochschulgesetz –HG–).

Die Abgabe einer falschen Versicherung an Eides statt wird mit Freiheitsstrafe bis zu 3 Jahren oder mit Geldstrafe bestraft.

Die Technische Universität Dortmund wird ggf. elektronische Vergleichswerkzeuge (wie z. B. die Software "turnitin") zur Überprüfung von Ordnungswidrigkeiten in Prüfungsverfahren nutzen.

Die oben stehende Belehrung habe ich zur Kenntnis genommen.

Ort, Datum	Unterschrift